KINETICS AND REGULATION OF THE INITIAL STAGES OF CADHERIN-MEDIATED ADHESION

BY

MATTHEW DOUGLAS LANGER

DISSERTATION

Submitted in partial fulfillment of the requirements
for the degree of Doctor of Philosophy in Chemical Engineering
in the Graduate College of the
University of Illinois at Urbana-Champaign, 2011

Urbana, Illinois

Doctoral Committee:

Professor Deborah Leckband, Chair and Director of Research
Professor Jonathan Higdon
Assistant Professor Hyunjoon Kong
Assistant Professor Peter Yingxiao Wang

Abstract

Cell adhesion plays a critical role in development, and in the maintenance of tissue integrity. Cadherins are calcium-dependent adhesion proteins which mediate cell adhesion in soft tissues. Several theories have been offered to explain the mechanism of cadherin adhesion. The first proposed mechanism put forth held that cadherins mediated binding through exchange of a tryptophan containing strand at the N-terminal domain. Another theory holds that there is an initial equilibrium which then is converted to the strand exchange form. These theories do not fully account for the range of observed experimental data, which demonstrates that there appear to be multiple binding conformations, and that lateral interactions may play a critical role in cadherin kinetics.

This dissertation looks at kinetic measurements of cadherin binding which are done in the context of the cell membrane, and quantifies the affinity of the tryptophan strand exchange for three classical cadherins. Both the interactions between cadherins of the same type (homophilic), and cadherins of different types (heterophilic) are quantified. The affinity changes are then correlated with cell aggregation results, demonstrating the threshold of affinity change required to see cells segregate.

Multiple cell types which express cadherin were characterized. This allowed for investigation of whether there are other factors which would be cell-line specific to alter the intrinsic affinity of the cadherin bond. To further test the ability of cadherin to mediate binding independent of other factors, the soluble portion of the protein was immobilized on the surface of a red blood cell, and the binding kinetics were observed.

When cadherins are produced by the cell, carbohydrates are added to the protein backbone in a process called glycosylation. The effect that one type of glycosylation, N-glycosylation, has on cadherin kinetics was investigated. It was determined that the loss of N-glycosylation on regions of the protein not associated with the Tryptophan strand exchange can have a qualitative effect on the cadherin binding kinetics. Based upon data available in the field, this dissertation proposes a new model for cadherin binding which accounts for this finding.

To Fred, Jan, Greg, and Amy

ACKNOWLEDGEMENTS

During the course of my graduate studies, there are many people who contributed to my success and completion of my Ph.D. First of all, I would like to thank Dr. Deborah Leckband for giving me the opportunity to study in her lab, for being my advisor, and for supporting me throughout this scientific endeavor. Her attention to detail and the rigor with which she directs her research projects are traits I admire, and I will take these learning experiences forward and they will help guide my scientific career. I would also like to thank my dissertation committee for their valuable feedback on my preliminary exam and their support.

I would also like to thank all of my co-workers during my graduate studies, for their assistance, and for their camaraderie as we all tackled scientific challenges. I thank Saiko and Sandy for their work and training on protein purification and cell culture, respectively. I thank Chun Yan and Marco Bayas for teaching me to use the SPR and the vacuum evaporator. I thank Anil, Venkat, Kenny, and Sindhu for training me on the SFA. I thank Yuan-Hung and Quanming for their work on the Micropipette Apparatus, and I thank Nitesh for his assistance in completing the experiments and controls required to make my studies successful. And I thank the rest of my colleagues, Colin, Julie, Rico, Beth, Robyn, Zhu Xi, Tor, Myongsin, Catherine, Fang, Keng Jin, Jon, Cynthia, Hamid, Changying, Paula, Adrienne, Johana, Sangwook, Byung-Chan, QJ, Ismaeel, Jillian, and Sam for making the lab an unforgettable place to work over the past few years. And when things did not go quite to plan, I thank Jim Wentz of the Electrical Shop, Bill Knight of the Machine Shop, and Mike Harland of the Machine Shop for making sure things were set straight as soon as possible.

I would also like to thank the collaborators from other institutions who contributed to this work. I thank Dr. Barry Gumbiner at the University of Virginia for the C-cadherin, Dr. James Nelson at Stanford for the E-cadherin, and Dr. Rene-Marc Mege at INSERM in France for the N-cadherin constructs. In addition, I'd like to thank Dr. Gumbiner for the CHO cells expressing C-cadherin on the surface, and Dr. Huabei Guo and Dr. Michael Pierce at the University of Georgia for the CHO cells expressing N-cadherin and its glycosylation mutants. Finally, I'd like to thank Dr. Cheng Zhu at Georgia Tech for developing the micropipette technique which was used in these studies.

I would also like to thank Ben, Ryan, Matt, Everett, Sarah, Paula, and Shuyi for being great friends and a strong support system. I'd like to thank Carol Baxter for providing valuable insight on the graduate student experience, and Linda Miller for her assistance in keeping a positive outlook on my studies.

Finally, I'd like to thank my loved ones: my mother, father, brother, and Amy. Each of you makes an essential contribution to the person I am, and to all the things I do. My life is a brighter place for having each of you, and you all helped support and foster the creativity, the persistence, and the effort which made this dissertation happen. I thank each of you for the role you played in making sure this dissertation came to fruition.

TABLE OF CONTENTS

Chapter 1

Introduction

1.1 Overview

Multicellular life develops through the differentiation of cells into lineages, and the subsequent organization of cells by lineage into compact tissues. These morphogenetic processes require signaling and adhesion in a spatio-temporally regulated manner [1, 2]. Cell adhesion molecules mediate the contacts that each of the trillion cells of an organism has with its surroundings. Cell adhesion proteins are membrane-bound and mediate adhesion either between the cell and the substratum or between adjacent cells. Adhesive interactions between the cell and its surrounding extracellular matrix are mediated by integrins. Adhesive interactions between cells are mediated by cadherins and by immunoglobulin-type adhesion molecules [1-3]. The exact mechanisms that drive large scale cell movements and tissue organizations during morphogenesis are still not topics of intense research.

The first model proposed to explain cell positioning during morphogenesis was the chemoaffinity hypothesis, which postulated that different tissues express different adhesion proteins, and these interacted in a highly specific manner to drive cell sorting into distinct tissues [4]. However, different cell types do form transient intercellular contacts during development, so that this initial hypothesis was broadened to propose that differential adhesion leads to cell

sorting [5]. However, subsequent studies found that factors independent of cell adhesion molecules, such as the membrane and cortical tension, can also influence large-scale cell movements [6-8]. Importantly, many adhesion proteins not only determine the intercellular adhesion, but also regulate the cytoskeleton through GTPases.

Cadherins are calcium dependent adhesion proteins that are essential for cohesive interactions between cells in all soft tissues [1, 2, 9]. In mature organisms, cadherins maintain the barrier properties of cell linings in, for example, the cardiovascular system and the digestive tract [10, 11]. Cadherins are a large superfamily of proteins of over 100 proteins that are divided into five groups: type I classical cadherins, type II classical cadherins, desmosomal cadherins, protocadherins, and cadherin-related proteins [1, 2]. The type I classical cadherins have been studied most extensively, and are essential for development and the maintenance of mature tissue structure. Individual cadherins in this class are named after the tissues from which they were first isolated, such as neural (N), epithelial (E), cleavage stage (C), and placental (P) cadherins. Cells of a given tissue type may express more than one cadherin, and cadherins are expressed in tissue-specific combinations [1, 2].

1.2 Biological Significance of Cadherins

There are multiple biological contexts in which classical cadherins are critically important. During embryonic development, large scale cellular rearrangements are associated with spatio-temporal changes in cadherin expression [12]. Altering cadherin expression in embryonic cells or expressing a non-adhesive mutant of cadherin leads to serious morphological defects and the loss of tissue structure [13-16]. This loss of cell-cell cohesion results in the dispersion of

embryonic cells. Blocking cadherin function with inhibitory antibodies that bind to the extracellular region have similar effects [17].

Cadherins maintain the barrier functions of several organ systems. Vascular endothelial (VE-) cadherin regulates the exchange of oxygen and carbon dioxide across the endothelial lining of pulmonary alveolae, and VE-cadherin also regulates transendothelial transport of fluid and proteins. E-cadherin similarly maintains the barrier properties of epithelial cell monolayers.

In diseases such as cancer, genetic switching that results in changes in cadherin expression frequently mark the metastatic transition in several types of cancers [18]. E-cadherin expression is commonly altered during the onset of metastasis. In addition, cadherin mutations or aberrant cadherin expression are frequently associated with the onset of esophageal, gastric, and colon cancers [19].

Understanding the processes by which cadherin junctions are formed and maintained has motivated much of the research in this area. From these studies, it is apparent that cadherins influence signaling by Rho family of GTPases, ERK, and Wnt signaling pathways. In addition, cadherin clustering and long term junction maintenance requires the remodeling of the actin cytoskeleton. What is not completely understood is the molecular mechanism by which cadherin bonds initially form, and how the associated binding information is transduced across the cell membrane into signals that respond to ligand and trigger junction remodeling. To understand the underlying molecular mechanisms require consideration of the architecture of classical cadherins.

1.3 Cadherin Structure

Type I classical cadherins have a cytoplasmic domain, which binds the cytoplasmic protein β-catenin and α-catenin, the attachment of cadherin to the actin cytoskeleton. Classical cadherins have a single pass trans-membrane domain (Figure 1.1). The extracellular region of type I classical cadherins is comprised of 5 cadherin domains, typically numbered one through five, with extracellular domain 1 (EC1) at the N-terminus, and EC5 being adjacent to the membrane. At the junctions between each of the five domains, there are three calcium ion binding-sites. Calcium binding stabilizes the structure of the extracellular region, and is critical for proper cadherin function. Typical observation of cadherin adhesion indicated a loss of cadherin function when the Ca^{2+} concentration was below 0.5 mM [20]. However, observations of the backbone stiffness by electron microscopy and NMR indicated that substantial changes in backbone properties occur at Ca^{2+} concentration is below 40 μM [20, 21].

1.4 N-Glycosylation in Cadherin Binding

Cadherins are also glyco-proteins, with a number of N-linked and O-linked glycosylation sites along the extracellular region. Glycans comprise about 20% of the molecular weight of the mature protein [22, 23]. The extent of glycosylation has been characterized for human N-cadherin, and mouse E-cadherin [24, 25].

Because of the difficulties in crystallizing glycosylated proteins, cadherin structures were obtained for the deglycosylated extracellular regions of the full extracellular domains of C-cadherin, E-cadherin, and N-cadherin [22, 26], as well as of fragments of the extracellular region. The crystal structures of *Xenopus* C-cadherin identified a bond formed through the exchange of

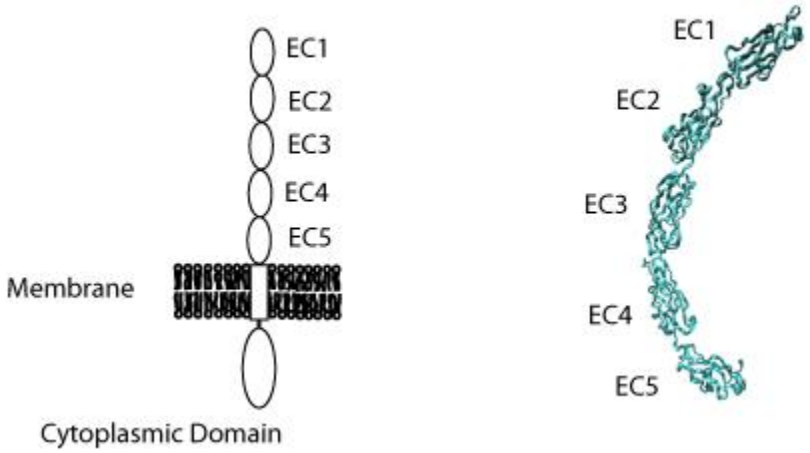

Figure 1.1: Left: A cartoon structure of cadherin, showing the extracellular region, with domains numbered EC1 to EC5 starting at the N-terminus, a single pass trans-membrane domain, and a cytoplasmic domain. Right: The crystal structure of the extracellular region of xenopus C-cadherin (pdb id: 1L3W)

tryptophan (W2) at the N-terminal β-strand of EC1 with a binding pocket on the EC1 domain of an adjacent cadherin (Figure 1.2) [22]. From the crystal structures of multiple cadherin subtypes [27, 28], it was also theorized that there is a binding region at the EC1/2 interface [28]. This structure has been named the X-dimer, and is thought to be an intermediate prior to the formation of the strand-swapped dimer. One potential problem with these structures is that when these studies produced the soluble ectodomain fragment that was crystallized, they were expressed in cell lines that minimize glycosylation. Despite this, the crystal structures have provided important insight into the mechanism of cadherin binding.

The position and type of cadherin glycosylation also affects the cadherin function. Cadherins feature several N-glycosylation sites along the ectodomain backbone, and glycosylation is frequently involved in trafficking to the membrane. Additionally, excessive cadherin glycosylation is a hallmark of several varieties of cancer [29-31]. Aberrant glycosylation of E-cadherin has also been linked to morphological defects in *Drosophila* embryos [32].

The N-glycosylation of N-cadherin was also recently shown to play a critical regulatory role in the stability of junctions. Upon the removal of all 8 N-glycosylation sites from the extracellular region of N-cadherin, intercellular junction stability increased [24]. The cells also demonstrated reduced motility in a wound-healing assay. Finally, chemical cross-linking studies demonstrated that there were more cadherin dimers on the surface of the cell in the case of glycosylation removal [24].

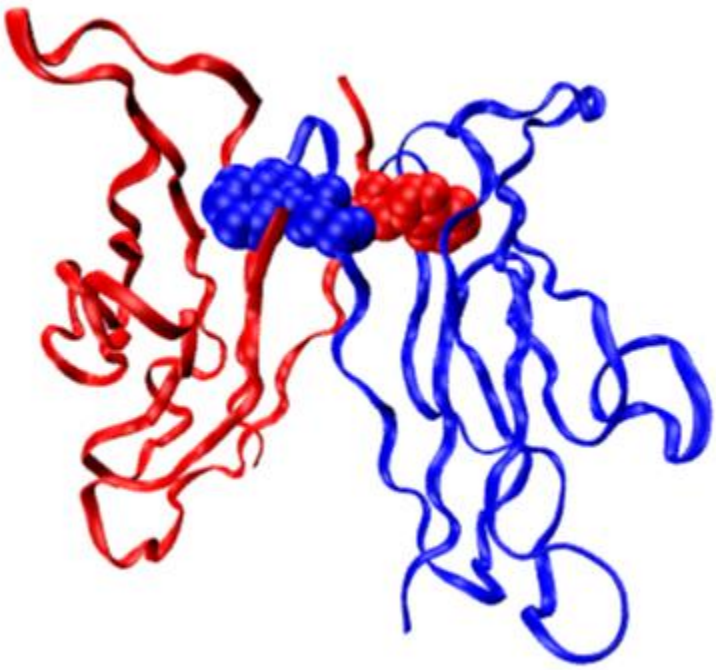

Figure 1.2: Structure of the EC1 domain of two adjacent cadherins, demonstrating the tryptophan-containing strand exchange (pdb ID: 1NCI)

1.5 Studies of Cadherin Binding

The first studies of the adhesive function of classical cadherins demonstrated that they would mediate the aggregation of non-adhesive cells when expressed on the cell surface [33]. Initial findings also suggested that cadherins selectively bind to specific cadherin subtypes, so that cadherins of a given type would only adhere to a cadherin of the same type. This view was reinforced by a study which the EC1 domain of E-cadherin was exchanged with the EC1 domain of P-cadherin. This altered the binding specificity of cells expressing the E-cadherin chimera [34]. In addition, surfaces that had been coated with only the EC1 and EC2 domains of cadherin could support cell adhesion, and that these fragments could aggregate cells [35, 36]. This evidence, combined with the interest in determining the mechanism for cell sorting during development, focused the majority of research on cadherin dependent cell sorting on EC1.

The predominant theory is that differences in cadherin binding affinity were responsible for the functional cell sorting that is observed [5, 37, 38]. Therefore, much of the research in the field has focused on characterizing the binding affinities of the EC1 domains. Several techniques have been used to quantify the binding properties of the soluble extracellular fragment, including nuclear magnetic resonance (NMR), Analytical Ultra-Centrifugation (AUC), and Surface Plasmon Resonance (SPR).

In NMR experiments, soluble cadherin ectodomains expressed by mammalian cells were purified and then allowed to freely interact in solution [21]. There was a shift observed in the NMR signature that corresponded with tryptophan exchange on the EC1 residue. Because of the orientation-specific nature of resonance shifts, it was further determined that the bound proteins were oriented in a manner consistent with an antiparallel *trans*, or adhesive, interaction.

AUC measurements quantify intermolecular dissociation constant by balancing the sedimentation rate from centrifugation with diffusion. This technique has been used to measure the dissociation constant of the full extracellular region of C-cadherin (64 μM), along with the EC1-2 fragments of N-cadherin and E-cadherin [35, 39]. Mutating the W2 residue to alanine (A) resulted in a several order of magnitude increase in the dissociation constant [28].

SPR measures the binding between a soluble ligand and an immobilized receptor on the sensor surface. In the absence of competing interactions in solution, it is possible to measure the interaction affinity and dissociation rate for a given interaction. If the soluble ligand self-associates, however, this additional interaction complicates the data analysis such that it is only possible to determine relative binding affinities. This is the case for cadherins, so that only relative affinities were determined for heterophilic binding by N-cadherin, E-cadherin, and a heterophilic interaction between N-cadherin and E-cadherin [39]. These measurements were exclusively conducted with the fragment of the ectodomain including EC1 and EC2 only. SPR studies using the full ectodomain of E-cadherin were complicated by significant non-specific binding [40].

Although the AUC measurements quantified homophilic binding that depends on the W2 strand exchange, it is impossible to determine, strictly from solution data, whether the measured interaction reflects a *cis* bond (between cadherins on the same surface) or a *trans* bond (between cadherins on opposite surfaces). To determine the conformation of cadherins in the strand exchanged complex, Fluorescence Resonance Energy Transfer (FRET) was used [41]. Cadherin ectodomains were immobilized on a surface in close contact, and the molecules were fluorescently labeled such that, if there were *cis*-dimerization mediated by the W2 residue, then

the resultant emitted wavelength would be longer than if there were no *cis*-dimerization. The observed result demonstrated no significant *cis*-interactions involving the W2 interface.

To determine the significance of the X-dimer, in addition to the strand swapped dimer, the FRET technique was also used [42] with the W2A mutant, which cannot form the strand swapped dimer. In this case, the cadherins did form a close, initial encounter complex. Other SPR and AUC studies suggested that this initial complex is an intermediate that subsequently forms the strand swap dimer. Without the W2 residue, the encounter complex was kinetically trapped. It is likely that this initial encounter complex is the X-dimer.

It should be noted that all of these previous techniques focused primarily on dimerization via EC1 strand swapping. No solution binding experiment has recorded evidence of other domains being directly involved in cadherin-mediated adhesion. From the solution experiments, it appears as if only strand-swapped EC1 dimers form between soluble ectodomains.

A second set of experimental approaches interrogate the interactions of cadherins bound on a surface. These can broadly be called adhesion measurements, since they generally measure the response of cadherin bonds to an applied force. The first measurement of cadherin adhesion was done by mixing cells expressing cadherins at a given shaking rate, and observing the distributions of cells in the aggregates that formed. The original measurements of this type suggested that cadherins sorted exclusively by subtype, and suggested that heterophilic interactions are minimal [33]. This work was revisited once the capacity to control surface expression levels was developed [43]. In that work, cadherin density appeared to also play a significant role in cell sorting, and the same cadherins that had formed separate aggregates in the earlier work formed intermixed aggregates when the expression levels were similar [43].

At similar, controlled expression levels, some cadherin subtypes could induce cell segregation [44]. Specifically, *Xenopus* E-cadherin expressing cells and human E-cadherin expressing cells formed separate aggregates, as did cells transfected with human E-cadherin and human N-cadherin. These proteins were also compared with cells expressing *Xenopus* C-cadherin, but all of the mixed pairings, aside from the two outlined above, did not trigger cell segregation. To determine whether cell adhesion strength governed this behavior, studies assessed the relative capacity of cells adhered to immobilized cadherin to resist shear [44]. In these studies, cells attached to cadherin-ectodomain-coated capillaries and formed adhesive contacts. The cells were sheared by flowing liquid through the capillaries at a controlled flow rate. As the flow rate was increased, along with the corresponding shear stress on the cells, the number of cells that remained attached was documented. In this case, all of the cadherins appeared to support similar cell adhesion, suggesting that cell sorting specificity was independent of cell adhesion strength. It was postulated that cadherin binding may occur through an initial, specificity determining step, which was followed by further junction remodeling to determine the final adhesive strength.

Further studies of cadherin adhesion energies used the Surface Force Apparatus (SFA). This approach quantifies the interaction energy between two surfaces as function of the separation distance. The SFA technique uses interferometry to measure the absolute distance between two surfaces, with ±0.1 nm resolution [45], and quantifies the normalized force between the two surfaces using a sensitive force-measuring spring (±1nN). Surface force measurements of adhesion between immobilized, oriented cadherin monolayers on two apposed surfaces identified binding at three distinct surface separations (39 nm, 32 nm, and 26 nm) [46-48]. When only the outer 2 extracellular domains were used, only 2 bound states were observed, and a mutant lacking domain 3 also lacked the strongest adhesion at 26nm [47]. This suggests that EC3 is

critical for the strongest bond detected in these measurements. The other two bonds were at distances consistent with the strand-swap dimer (39nm) and with the X-dimer (32nm), when positions of adhesion were compared with crystal structures.

To independently test the results of the surface force measurements, AFM measurements were used to quantify the force required to break a single cadherin bond. These measurements can determine either the most probable force to rupture a bond as a function of the loading rate or the lifetime of a single bond under force [49-51]. Analyses of these single bond measurements determined the number of bound states, the strength of each bond, and the dissociation rate for each bond. Studies of binding between the outer two EC domains of cadherin (EC12) detected two bound states, while a third, stronger bond required EC3 [50-52]. One of the two EC12-dependent bonds appeared to require W2, but the other was W2 independent [52]. The W2 independent bond was weaker, consistent with other measurements of the X-dimer [42].

Through all of these previous studies, one difficulty in making comparisons was that the solution binding studies measure force-independent properties, while the adhesion measurements were made by applying force to the bonds. In an attempt to resolve these issues, micropipette manipulation was used. Micropipette manipulation is a technique that measures the intercellular binding probability as a function of cell-cell contact time. It has been used successfully to characterize several membrane protein interactions, such as selectins [53-57]. Investigations of cadherin-mediated intercellular adhesion with the micropipette technique demonstrated that the kinetics are biphasic [58]. That is to say, there was an initial increase in binding probability, followed by a lag, followed by a second increase. This type of kinetic profile had not been seen in other micropipette measurements.

Studies with domain deletions of the C-cadherin extracellular domain showed that the first binding phase requires EC12 domains. Additionally, the EC3 domain was required for the lag phase and subsequent second rise to the final, higher binding probability. In cases where the tested cadherin was lacking the EC3 domain, a single phase kinetic response was observed [58]. This rise corresponded with the equation for a simple ligand-receptor interaction (Equation 2.4). From the accrued experimental data, several theories of cadherin binding have been proposed.

1.6 Models of Cadherin Binding

When cadherins were first characterized, experiments primarily focused on the effects of altering cadherin on cell aggregation, or on the aggregation of beads coated with cadherin ectodomains. From those studies, it was claimed that *cis*-dimerization, which is lateral dimerization between two cadherin molecules on the same cell membrane, is essential for proper cadherin function [23, 59, 60]. When dimerization was forced by use of an Fc-tag, cadherin coated beads formed larger aggregates. However, as the structures of the ectodomains have been determined, there is no consensus regarding where this *cis*-interface would be. The crystal structures of C-cadherin, E-cadherin, and N-cadherin suggest that there may be a *cis*-interface between the EC1 domain of one protein and the EC2 domain of an adjacent cadherin [26]. Further, simulations suggest that this *cis*-interface leads to the formation of large cadherin clusters on the cell membrane. NMR studies of E-cadherin, however, showed no shifts that would correspond with this putative *cis* interaction [21]. It has been proposed that the confinement of the cadherin in the cell membrane will make this interaction more favorable than in solution, possibly explaining the lack of NMR data [61]. This study was limited in that it only considered entropic effects of confinement, although other factors such as the membrane microtopology, lateral diffusivity, and clustering

could also influence two-dimensional affinities [62]. One study suggested that the adhesive and lateral bonds share the same W2 interface [60]. So the existence and location of a *cis*-binding interface in the extracellular domain has yet to be identified.

There is substantial experimental evidence that the swapping of the W2 strands is essential for cadherin function. In experiments performed in solution as well as those performed in the context of a membrane, W2A mutations abolished adhesion [28, 52, 63]. The best evidence that the W2 interaction mediates a *trans*-interaction exclusively comes from FRET data described earlier [41]. In that case, even when cadherin ectodomains were held in close proximity on the same surface, *cis*-interactions mediated by W2 were not observed, indicating that the proteins only form *trans* bonds in solution.

Biophysical measurements of cadherin bond energies found that cadherins form multiple adhesive bonds, and the strongest adhesion detected required the third extracellular domain (EC3) [48]. Additionally, studies of cadherin bond rupture forces suggest the existence of 3-4 bound states, only 2 of which are attributable to EC1 and EC2 [50]. Assays determining the shear stress required to break bonds as well as the ability of cadherin to aggregate cells, determined that beads coated with EC12 fragments support weaker adhesion than the full length protein [36]. To further explore this result, subsequent experiments were tested where beads coated with EC1-2 fragments mixed with beads with all five extracellular domains [64]. A parallel set of experiments involved mixing cells expressing solely EC1-2 with cells that had EC1-2 fragments attached to two spacer domains [65]. In the case where cells expressing EC1-2 were mixed with cells expressing the full extracellular region, the cells completely intermixed and demonstrated standard cell adhesion properties. In the case where the domains proximal to the membrane were

replaced with a spacer, the same weak adhesion was observed as seen with cells that expressed EC1-2 exclusively.

Further evidence for the involvement of multiple EC domains in cadherin adhesion came from initial characterizations of *Xenopus* C-cadherin kinetics in the context of the cell membrane [58]. Micropipette manipulation measurements detected cadherin-mediated intercellular adhesion events by visualizing the deformation of a red blood cell (RBC) coated with cadherin extracellular domains during bond formation and rupture. Cadherin-dependent cell-cell adhesion kinetics exhibited biphasic kinetics in which fast initial binding was followed by a short lag phase and then subsequent increase to a higher limiting binding probability. These kinetics were inconsistent with simple EC1-EC1 strand exchange. Furthermore, deleting EC3 abolished the lag phase and slow second rise to the limiting binding probability. Despite this growing body of evidence, there is no binding model that explains all of the existing experimental data.

1.7 Questions Addressed in this Thesis

The goal of the research described in this thesis is to (i) establish a methodology for the analysis of binding affinity from the first phase of two phase kinetics, (ii) to study the impact of cell context on cadherin affinity, and (iii) to identify key structural players in cadherin adhesion, for the purpose of building towards a complete mechanistic model for cadherin interactions. This dissertation investigates the kinetics of both homophilic and heterophilic binding by C-cadherin, E-cadherin, and N-cadherin. From the kinetic data, a methodology for determining the affinity of the first stage of binding was developed. Then, the influence of the cell surface environment on cadherin binding affinities is tested. Subsequently, structural components in the ectodomains are analyzed to determine their effect on fundamental cadherin affinity. The effects of mutations

of key points on EC1 are characterized, and glycosylation is studied for its impact on cadherin binding.

Chapter 2

Deriving EC1-dependent Binding Affinities from Biphasic Kinetic Time Courses

Note: The majority of micropipette data presented in this chapter was originally collected by Yuan-Hung Chien. On Table 2.4, experiments performed by him are marked with an asterisk.

2.1 Introduction

Cadherins mediate cell-cell adhesion in soft tissue through interaction with cadherins on adjacent cell membranes. As discussed in section 1.3, the mechanism by which cadherins mediate their diverse functions in embryogenesis and in defining tissue boundaries is unknown. The prevailing idea was the Differential Adhesion Hypothesis (DAH), which held that difference in adhesion energy of cadherins would correlate with the free energy change of the cell membrane, and that would be the thermodynamic driving force behind cell sorting [5, 66]. The first biophysical measurements of adhesion bond energies and estimates of the off-rate in the absence of force from single molecule measurements had apparently contradicted these results [48, 67], but there were valid criticisms. These measurements were done outside of the context of the cell membrane, and the analysis methodology to derive a dissociation rate constant from single molecule measurements make significant assumptions regarding the mechanism of adhesion. Additionally, the biophysical measurements raised some questions about which domains of the protein are involved in binding, as discussed in section 1.3.

To address this question further, an approach was selected that would determine adhesion kinetics and affinity in a situation that did not involve imposing an external force on the cadherin bond. The micropipette manipulation technique, which measures binding kinetics of cell surface proteins in the context of the two-dimensional environment of contacts between cell membranes, was the method of choice for these measurements. Micropipette measurements have been used to determine the two-dimensional affinities and dissociation rates of adhesion protein receptors including cadherins and selectins, in the context of the cell membrane [54-56, 58, 62, 68-71]. In this experiment, one cell, expressing a protein of interest on its surface, is partially aspirated into a micropipette (Figure 2.1). A red blood cell (RBC) which has been chemically labeled with the interaction partner of the protein of interest, is partially aspirated into a second micropipette. The two cells are then repeatedly brought into contact and then separated. If the cells adhere, the RBC will deform slightly, which can be seen under magnification. The eventual readout is the binding probability, which is the number of times binding was observed divided by the total number of contact cycles. The contact time between the two cells is controlled, so that the time course of binding probability as contact time is increased can be observed. This method measures intrinsic bond properties in the context of the cell membrane.

The binding time course of the binding probability between *Xenopus* C-cadherin extracellular domains was characterized using the micropipette manipulation method [58]. For the test cell surface, C-cadherin was expressed in CHOK1 cells, and a construct of the C-cadherin extracellular region attached to an Fc tag was immobilized on a RBC. The binding probability curve demonstrated two phases, an initial, fast rise (1-2 s) to a plateau that lasted ~3-5s, and then a second rise to a final binding probability value (5-20 s) (Figure 2.2). While the first plateau

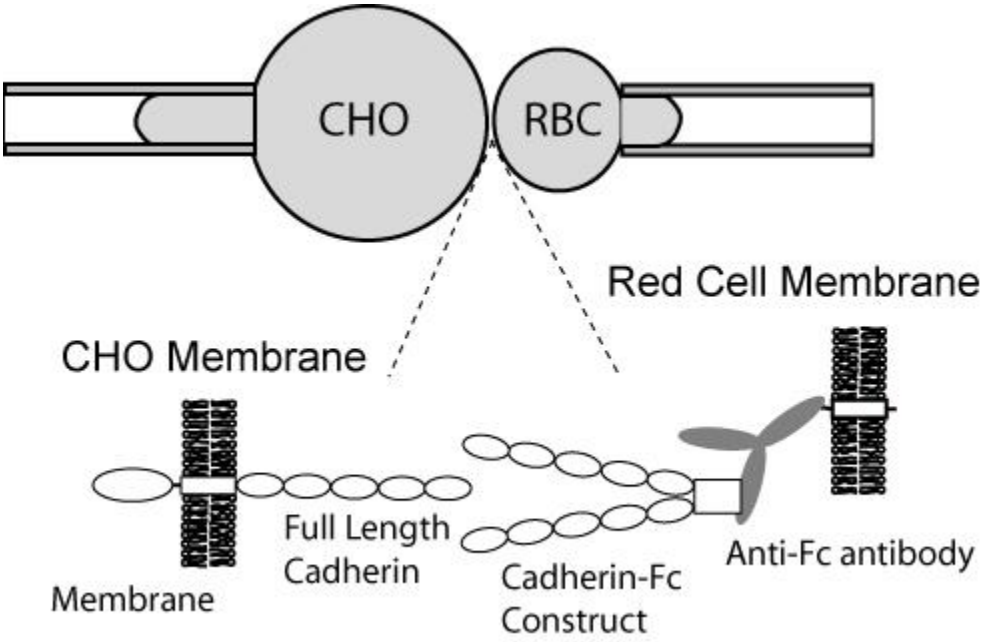

Figure 2.1 Schematic of the micropipette set up. A cadherin-expressing CHO cell is partially aspirated into a micropipette with a diameter of ~7μm. A red blood cell (RBC), which has been chemically modified with Fc-antibody and immobilized, oriented chicken N-cad-Fc is drawn into a micropipette with a 1.5 μm diameter.

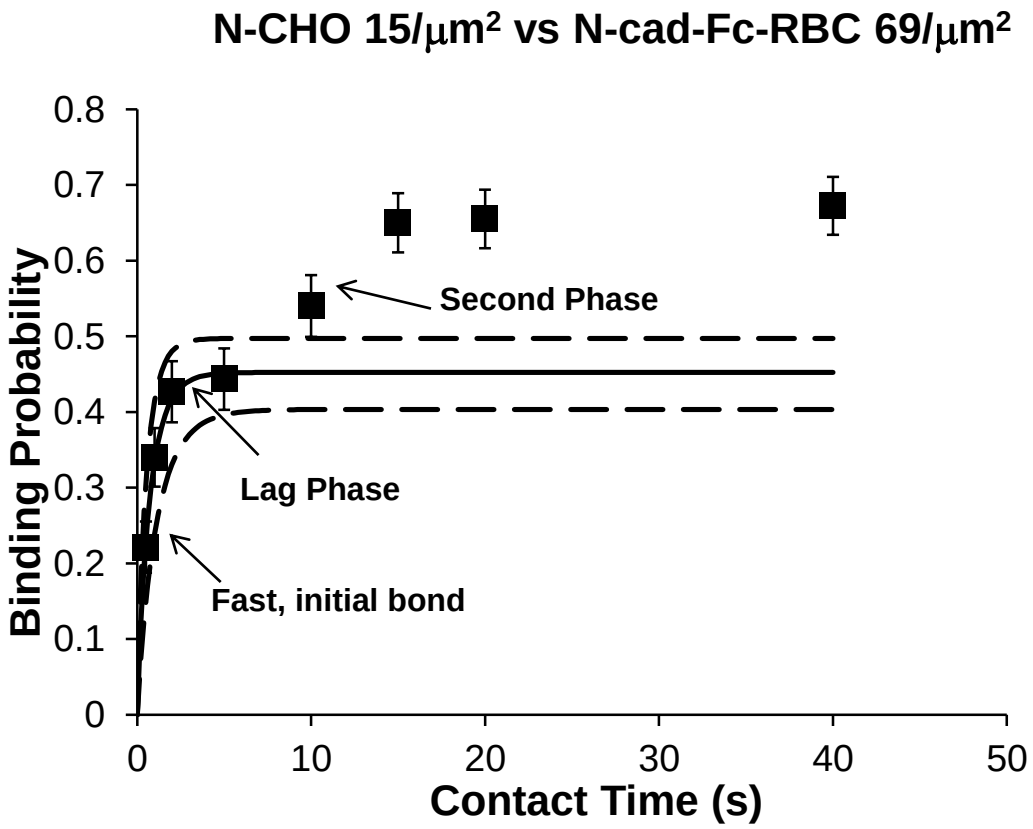

Figure 2.2 Time course showing the typical features observed in micropipette experiments involving cadherins. There is an initial rise in the first two seconds, followed by a lag phase that lasts until five seconds, and then a second increase in the binding probability.

appeared to correlate with a previously tested model for the system, the overall binding probability time course is something that had not been observed.

In addition, the initial increase in the binding probability was directly linked to the EC1 domain, while the second rise required EC3. Previous studies had suggested that EC1 was the specificity-determining region [34, 72, 73], so, in this study, the focus was on modeling the EC1-dependent initial rise. A longer term challenge is to develop a mathematically rigorous approach for analyzing the biphasic kinetic data, and for extracting binding parameters such as affinity. Once the affinity of the cadherin bonds, and by extension, the free energy change associated with cell adhesion, was determined, it would be possible to directly test the DAH in conjunction with published cell sorting data. These data showed that, when other factors such as cell type and expression level were controlled for, *Xenopus* C-cadherin would intermix with canine E-cadherin, but separate from chicken N-cadherin [67]. Meanwhile, canine E-cadherin formed mixed aggregates with both *Xenopus* C-cadherin and chicken N-cadherin [67].

This chapter describes the methodology used to fit the first binding phase, and, in particular, the approach used to parse data contributing to the two phases of the cadherin binding probability time course. I then describe nonlinear-least squares fits of the initial binding data to a simple binding mechanism, and the determination of cadherin-dependent binding parameters. I also tested an alternative proposed mechanism for its ability to describe the biphasic kinetics, as well as its ability to better fit the first phase in the time course. Upon determination of the best model to use, affinities were estimated from fits to the data.

2.2 Materials and Methods

Plasmids and Cell Lines

The cDNAs for the full length *Xenopus* C-cadherin and the C-cadherin W2A mutant in pEE14 plasmids were given by B. Gumbiner (Univ of Virginia, Charlottesville, VA). The cDNA encoding the full-length chicken N-cadherin in the pEGFP-N1 plasmid was contributed by Dr. Andre Sobel (Institut du Fer a Moulin; Gif-sur-Yvette, France). Stable CHO-K1 cells expressing the full length C-cadherin were grown in Glasgow MEM medium containing 10% dialyzed fetal bovine serum (FBS) and 25 μM methionine sulfoximine (Sigma-Aldrich, St Louis, MO) [23]. CHO-K1 cells expressing the full-length chicken N-cadherin were cultured in Dulbecco's Modified Eagle Medium (DMEM) containing 10% FBS and 400 μg/ml G418 (Sigma-Aldrich, St Louis, MO). The G418 selection agent was used for at least four weeks. The cadherin expression levels were determined by quantitative flow cytometry and immuno-blotting. The soluble construct of the protein ectodomain and an Fc-tag was expressed in either CHO K1 cells (C-cadherin) or HEK293 cells (N-cadherin and E-cadherin) and purified as previously described.

Quantification of cadherin surface expression levels of CHO cells

Cadherin surface expression levels were quantified by flow cytometry [53, 58]. CHO-K1 cells stably expressing cadherins were labeled with protein-specific antibodies against the ectodomains. C-cadherin expressing cells were labeled with anti-C-cadherin antibody (C/EP/B-Cadherin (clone xC-12), Santa Cruz Biotechnology, Santa Cruz, CA) followed by the secondary fluorescein isothiocyanate (FITC)-conjugated anti-goat IgG (whole molecule; Sigma-Aldrich, St Louis, MO). Chicken N-cadherin expressing CHO-K1 cells were labeled with monoclonal mouse anti-N-cadherin (Clone GC-4, Sigma-Aldrich, St Louis, MO) and then with fluorescein-

isothiocyanate (FITC)-conjugated anti-mouse IgG (whole molecule; Sigma-Aldrich, St Louis, MO). The antibody labeling was done in phosphate buffered saline (PBS) containing 1w/v% bovine serum albumin (BSA) at pH 7.4. The fluorescence intensities of labeled cells were measured with an LSR II flow cytometer (BD Biosciences) in the Keck Center for Biotechnology (UIUC) [71]. The fluorescence intensity calibration curve was obtained with calibrated FITC-labeled standard beads (Bangs Laboratories, Inc., Fishers, IN) [71].

Surface modification of erythrocytes with oriented cadherin extracellular domains.

Erythrocytes were isolated from human whole blood collected from healthy donors. The whole blood was stored in Vacutainers™, and proper protocols were followed for handling human-derived materials. The erythrocytes were isolated with Histopaque 1119 (Sigma-Aldrich, St Louis, MO), following the manufacturer's protocol. A 12 ml aliquot of Histopaque 1119 was prepared in a 50 ml centrifuge tube. Then 7 ml whole blood and 7 ml of 0.9 w/v% NaCl were mixed, and then slowly transferred to the tube containing Histopaque. The mixture was centrifuged at 800 x g for 20 minutes at room temperature in an Eppendorf 5810R benchtop centrifuge. The supernatant was discarded as biological waste, and the remaining cells were resuspended in 7 ml of 0.9 w/v% NaCl prior to the addition of 1.5 ml of 6 w/v% Dextran. The cells were incubated at room temperature for 45 minutes, during which they settled to the bottom of the tube. After discarding the supernatant, the red blood cells (RBC) were washed twice at room temperature with 0.9 w/v% NaCl, and resuspended in 12 ml EAS45 (2.0 mM Adenine, 110.0 mM dextrose, 55.0 mM Mannitol, 50.0 mM NaCl, 10.0 mM glutamine and 20.0 mM Na_2HPO_4, at pH 8.0) [74]. The purified RBC suspension in EAS45 is stored at 4°C, and can be used for up to 3 weeks, after which the RBCs are treated with bleach and discarded.

Covalently bound anti-Fc antibodies on the RBCs were used to capture the Fc-tagged

cadherin ectodomains. Antibodies were covalently coupled to the RBCs using the $CrCl_3$ coupling method [75, 76]. We used either goat polyclonal anti-human immunoglobin G (IgG) Fc or goat polyclonal anti-mouse IgG Fc antibodies (Sigma-Aldrich, St Louis, MO). Approximately 10^6 RBCs were washed five times with 0.85 w/v% NaCl, and then resuspended in 250 μl of 0.85 % NaCl with 1 μg of the desired antibody. The $CrCl_3$ solution was diluted to concentrations below 0.01 w/v% with 0.02 mM sodium acetate containing 0.85 w/v% NaCl. To chemically activate glycoproteins on RBCs, 250 μl of diluted $CrCl_3$ solution was mixed with 250 μl of the red blood cell/antibody mixture and incubated at room temperature for 5 minutes. The reaction was stopped with 500 μl of "stop solution" (PBS with 0.5 mM EDTA and 1% BSA). The cells were then washed twice with the "stop solution". The concentration of $CrCl_3$ determined the density of antibodies immobilized to the surface of the RBCs, but the antibody density varies. Treating the RBCs with different $CrCl_3$ concentrations was necessary to achieve the desired antibody surface density.

After the antibody immobilization, approximately 20,000 modified RBCs were incubated with 3 μL of 1mg/mL Cadherin-Fc fragments. The resulting cadherin surface densities were then quantified by flow cytometry [53, 58].

Micropipette measurements of cell binding kinetics

The binding probability was determined as a function of contact time with the micropipette manipulation technique [53, 57, 58, 71, 77]. The binding probability P(t) is the ratio of the number of binding events n_b to the total N_T cell-cell touches, n_b/N_T. In these measurements, a cadherin-expressing CHO cell and a RBC modified with Fc-tagged cadherin were partially aspirated into opposing micropipettes (Figure 2.1). The cells were maintained in

the chamber with L15 medium (Invitrogen, Carlsbad, CA) supplemented with 1 w/v% BSA. This is a hypo-osmotic solution for the RBCs, which insures that they remain rounded. Cells were visualized with a 100x oil immersion objective on a Zeiss Axiovert 200 microscope, and images were recorded with a DAGE-MTI CCD100 CCD camera (DAGE-MTI Inc, Michigan City, In) interfaced to a high resolution, flat screen TV monitor. Cells were positioned with automated piezo-electric controllers programmed to cyclically bring the two cells into contact for an operator-defined period. The contact area was controlled at ~3 μm^2 (~1 μm diameter). Adhesion events are identified from the surface deformation of the RBC during separation and recoil at adhesive failure. Contact times are controlled with the programmed piezo-electric actuator. Each cell pair was tested for 50 cell-cell touches ($N_T = 50$), and each contact time represents measurements with at least three different cell pairs ($N > 150$). The reported probabilities P are the mean $\pm$ standard deviation from the mean.

Micropipette Data Format

The data as originally obtained from the micropipette experiment was a series of zeros and ones that corresponded contact cycles where adhesion was or was not observed. There were three sets of zeros and ones for each time point. First, for each data set, the binding probability was calculated by dividing the observed adhesion events by the total number of contacts.

The total probability of observing adhesion can be represented as the sum of the probability of having one bond, two bonds, et cetera. To represent that mathematically in a simplified manner, it is defined as one minus the probability of having zero bonds. From the range of binding probabilities used in the experiments ($0 < P < 0.8$), it can be inferred that the number of bonds present is small, and likely single digits [53]. The Poisson distribution

probability function closely matches the full solution to the master equation under these conditions [53]. With this assumption, the number of bonds that form in the contact site each time cell-cell binding is sampled, and therefore, the number of observed adhesion events, follows a Poisson distribution centered on the mean number of bonds in the contact area. This results in a mathematical expression that relates the average number of bonds in the contact area to the binding probability [53]. For the following system, P is the total binding probability, P_n is the probability of having n number of bonds present, and P0 is the particular case of no bonds, n = 0.

$$P = P_{Total} = \sum_{n=1}^{\infty} P_n$$

$$P = 1 - P_0$$

$$p_n(t) = \frac{\langle n \rangle^n}{n!} \exp(-\langle n \rangle)$$

$$P = 1 - \exp(-\langle n \rangle) \qquad (2.1)$$

Simple Binding Mechanism

The simplest binding mechanism that is also consistent with crystallographic data, is one-step, reversible binding between a receptor and a ligand to form a binary complex. This reaction follows the Equation 2.2 and can be solved analytically (Equation 2.4). Combining this result with Equation 2.1 yields the following expression for the binding probability as a function of time for this type of interaction. The reason that total density of receptors and ligands is used in this derivation is because of the initial assumption that the population of receptors and ligands is

not being depleted during the cell-cell contact. This is required for the distribution of bound states to follow the Poisson distribution.

$$R + L \leftrightarrow RL$$

$$r = k_{on}[R][L] - k_{off}[RL]$$

$$\frac{\partial[RL]}{\partial t} = k_{on}[R][L] - k_{off}[RL] \tag{2.2}$$

$$\langle n \rangle = [RL]A_C = A_C K_a M_R M_L \left(1 - \exp\left(-k_{off} t\right)\right) \tag{2.3}$$

$$P = 1 - \exp(-A_C K_a M_R M_L (1 - \exp\left(-k_{off} t\right))) \tag{2.4}$$

The general form of this equation leads to an exponential rise with a time constant $1/k_{off}$ to a limiting plateau that is determined by the receptor and ligand concentrations mL and MR, contact area Ac, and two dimensional affinity Ka.

Strand Exchange Mechanism

Strand exchange was previously proposed as a mechanism for cadherin-cadherin binding [63]. This model depicts cadherin binding as the exchange of tryptophan containing strands on the EC1 domain with a binding pocket on a neighboring cadherin. This reciprocal exchange of tryptophan residues was observed in contacts in the crystal structure of C-cadherin, E-cadherin, and N-cadherin [22, 78], and there is substantial evidence that the W2 residue on EC domain 1 is essential for cadherin's adhesive function. Another proposed mechanism involved an initial, transient intermediate, called the X-dimer, which would form and then be replaced by the strand dimer [28, 42].

I first sought to determine whether these proposed mechanisms could account for the two-stage cadherin binding kinetics. Figure 2.3 is a schematic of the tested mechanism. If the strand exchange mechanism were going to lead to biphasic kinetics, it would have to be from sequential strand exchanges, as opposed to the simultaneous exchange proposed, so the first and second strand exchanges were assigned independent rate constants. This model reduces to the proposed case of simultaneous strand exchange when k3 is much larger than k1[63].

In this model, the Arabic numerals refer to which of the two surfaces the protein is on, and Greek letters α and β correspond to an occupied cadherin binding pocket on surface 1 and 2, respectively. To describe that system, the following system of differential equations was written.

$$\frac{d(1)}{dt} = -2k_1 *[1]*[2] + k_2 *[12\alpha] + k_2 *[12\beta] - k_3 *[1] + k_2 *[1\alpha] \quad (2.5)$$

$$\frac{d(1\alpha)}{dt} = k_3 *[1] - k_2 *[1\alpha] \quad (2.6)$$

$$\frac{d(2)}{dt} = -2k_1 *[1]*[2] + k_2 *[12\alpha] + k_2 *[12\beta] - k_3 *[2] + k_2 *[2\beta] \quad (2.7)$$

$$\frac{d(1\alpha)}{dt} = k_3 *[2] - k_2 *[2\beta] \quad (2.8)$$

$$\frac{d(12\alpha)}{dt} = k_1 *[1]*[2] - k_2 *[12\alpha] - k_3 *[12\alpha] + k_2 *[12\alpha\beta] \quad (2.9)$$

$$\frac{d(12\beta)}{dt} = k_1 *[1]*[2] - k_2 *[12\beta] - k_3 *[12\beta] + k_2 *[12\alpha\beta] \quad (2.10)$$

$$\frac{d(12\alpha\beta)}{dt} = k_3 *[12\alpha] + k_3 *[12\beta] - 2 * k_2 *[12\alpha\beta] \quad (2.11)$$

For this system, states 12α, 12β, and 12αβ represent adhesive bonds. From Equation 2.1 above, it is possible to relate the total concentration of adhesive bonds to the binding probability.

For the numerical solution of the system of equations 5-11, the overall density of cadherins in the contact region was assumed to be constant. Because cell-cell binding associated with the first binding phase occurs in 1-2s, while the diffusion of cadherins is on the order of 0.5 $\mu m^2/s$, it is

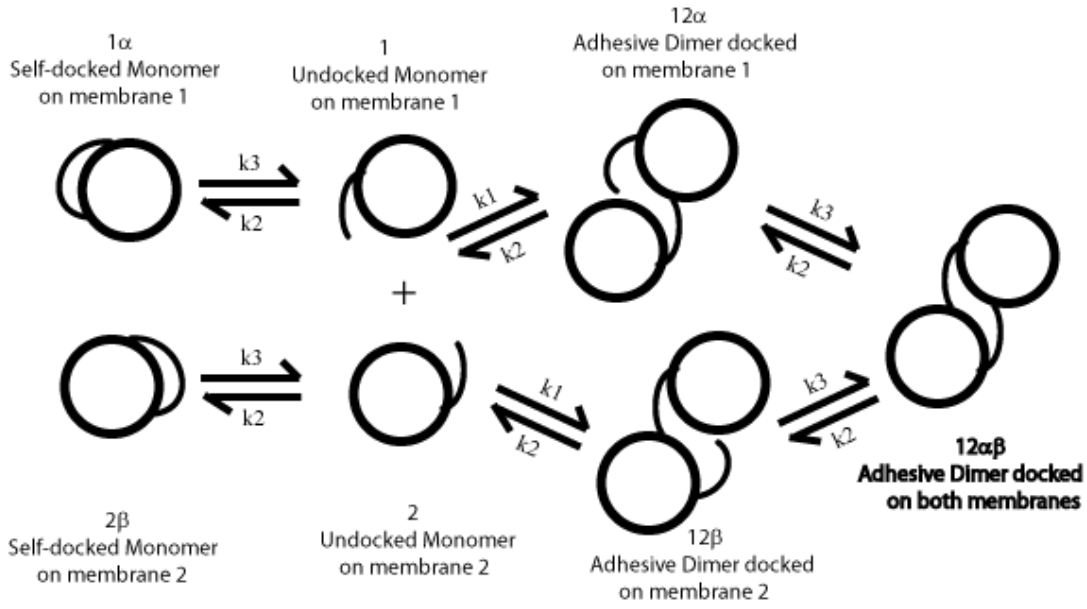

Figure 2.3 Schematic of strand exchange mechanism. Cadherins on each membrane surface can have W2-containing strands that are self-docked, open, or docked with a cadherin on an adjacent cell. The W2 exchanges are considered separate events, and each given its own rate constant.

reasonable to assume that lateral cadherin diffusion is negligible. The system of differential equations (Eqs 5-11) was solved numerically with Matlab, with the initial conditions of states 1 and 1α and 2 and 2β summing to the surface concentrations seen in experiments. The initial concentration of all *trans*-dimers set to 0.

In order to fully test this model, and observe if it was able to predict biphasic binding kinetics, the model parameters k_1, k_2, and k_3 were all varied over several orders of magnitude. For k_1 and k_3, values between 10^{-6} $\mu m^2/s$ and 10^{-2} $\mu m^2/s$ were tested. For k_2, values between 0.1 s^{-1} and 10 s^{-1} were tested.

Subsequently, the strand exchange model was also evaluated as an alternative model to Equation 4 for the initial rise in the binding probability. In this case, an algorithm was programmed to evaluate the values of k_1, k_2, and k_3 that gave the best fits to the micropipette data.

Estimation of Variation in the Data

To estimate the standard deviation of the data for error analysis, the binding probability was first assumed to follow a binomial function, since each contact cycle generated a one or a zero. The variance of a binomial distribution depends on the number of trials and the mean probability (Equation 12). This standard deviation was used to determine the weighting factor for the least squares regression.

$$\sigma^2 = Np(1-p) \tag{2.12}$$

Weighted Non-Linear Least Squares Regression

To determine the best-fit parameters for the first binding phase, a weighted non-linear least squares regression technique was used. The non-linear regression was performed in OriginPro

8.5 (OriginLab, Northampton, MA) using their non-linear analysis tool. Equation 2.4, the simple binding mechanism, was programmed as a user equation in the non-linear least squares analysis tool. The binding probability time course was entered as the base data. Because of the spread of variations, a weighted non-linear least squares regression was performed, using the calculated variance as described above. Each data point is weighted by the inverse of its variance, so the greatest weight is given to the data points with the least variability. Using the non-linear analysis tool, the weighting factors, and the programmed version of Equation 2.4, the best fit kinetic parameters were calculated. After the calculation of the parameters, a lack of fit test was used for validation of the model fit to the given data.

Parsing the Two Phases of Cadherin Kinetics

To properly split the first phase of the two-phase kinetics for modeling, a non-linear lack of fit test for a system with repeated observations was used (Neill, 1988, The Annals of Statistics, Vol 16, No 2, 733-740). The test utilizes the multiple measurements at each time point, and compares the intrinsic variability in the data to the residuals between the data and the proposed model. The test statistic follows an F-distribution (Equation 2.13).

$$F = \frac{\sum_{i=1}^{n} n_i (\bar{y}_i - \hat{y}_i)^2 / (n-2)}{\sum_{i=1}^{n}\sum_{j=1}^{n_i} (y_{ij} - \bar{y}_i)^2 / (N-n)} \qquad (2.13)$$

For this test statistic, n is the number of distinct time points observed, n_i is the number of observations at each time point, $\bar{y}_i$ means the average value of observations at time point i, $\hat{y}_i$ refers to the model prediction at time point i, y_{ij} refers to each individual measurement, and N is the total number of observations.

The null hypothesis for this test is that the model describes the data, so the calculated statistic exceeds the critical F-value when the model is no longer valid. For each experiment, the kinetic parameters for the first phase were estimated using non-linear least squares regression, followed by testing for lack of fit using the statistic in equation 2.13 to determine if those time points were part of the first phase. The parameters reported for the first phase are those for the maximum number of measurements where the simple ligand-receptor model was valid.

2.3 Results

Strand Exchange Model Does not Predict Biphasic Kinetics

The strand exchange model was tested for its ability to predict biphasic kinetics. In order to see two-phase kinetics, each strand swap was treated as a unique process. If the two exchanges are given the same forward reaction parameter, the system is identical to a simultaneous strand swap. As the parameters were varied over the variable space ($10^{-6}<k1$, $k3<10^{-2}$ μm^2; $0.1<k2<10$ 1/s), a pattern emerged that there was no lag phase. If $k1>>k3$, it was possible to see the rises start to separate, but they were both continuous rises towards a plateau. The strand exchange mechanism, a favored explanation of cadherin behavior, does not account for the observed cadherin binding kinetics. After the full evaluation using Matlab, it was decided to determine whether the Strand Exchange Model provided a quality fit for the first phase of the data. This was due to the similarities in qualitative shape of the binding probability curve predicted by the strange exchange model and the observed data.

Sequential binding model does not provide superior model of first phase

The same sequential strand exchange model examined for a lag phase was further studied to

determine if it improved fits to the first binding step. The same protocol previously described for determining binding probability from concentration calculations was used. This time, only the first step of the model, including data up to 5s, was considered. The optimum values for k1, k2, and k3 were determined using weighted, non-linear least squares regression (Table 2.1). Four sets of data were tested, and the fitted parameters k1, k2, and k3 were compared to the parameters determined using the model in Equation 2.4 (Table 2.2).

Table 2.1: Fitted Parameters Using Strand Exchange Model

Cell	Density ($1/\mu m^2$)	Protein	Density ($1/\mu m2$)	k1 ($\mu m^2/s$)	k3 ($\mu m/s$)	k2 (1/s)	Lsqr
*NCHO	15	N-cadherin-Fc-RBC	69	1.78	32.7	4.63	1.04
*NCHO	17	N-cadherin-Fc-RBC	178	0.0756	0.758	0.822	9.68
*NCHO	15	N-cadherin-Fc-RBC	33	0.126	1.12	1.37	0.518
*CCHO	18	C-cadherin-Fc-RBC	10	5.67	39.4	3.47	6.07

Table 2.2: Fitted Parameters Using Simple Binding Mechanism Model

Cell	Density ($1/\mu m^2$)	Protein	Density ($1/\mu m2$)	kon ($1/\mu m^2*s$)	koff (1/s)	Lsqr
*NCHO	15	N-cadherin-Fc-RBC	69	0.000185	1.13	1.04
*NCHO	17	N-cadherin-Fc-RBC	178	0.000127	1.02	13.2
*NCHO	15	N-cadherin-Fc-RBC	33	0.000277	1.08	0.564
*CCHO	18	C-cadherin-Fc-RBC	10	0.00106	0.589	6.13

An F-distributed statistic determined if the model with more parameters provided a statistically significant improvement in the data fit. If the three parameter model including strand exchange is given the number 1, and the simple model is given the number 2, and there are N total observations, the formula for the F-statistic depends on the sum of squared residuals (SSR). The statistic was calculated for each experimental system (Table 2.3).

$$F = \frac{\frac{SSR_2 - SSR_1}{3-2}}{\frac{SSR_1}{N-3}} \qquad (3)$$

Table 2.3: F-statistic Calculation

Experiment	F values
1	-0.017464017
2	3.224536509
3	0.795939307
4	0.084144094

Since N = 12 for these experimental data, the F-distribution has (1, 9) degrees of freedom. For this case, the critical F-value for 90% confidence is 3.360. Even in Experiment 2, where the second model provides the most substantial improvement in fit, you cannot say that the improvement is statistically significant. When the F-value is less than F-critical, the model with additional parameters provides a statistically similar quality of fit as the model with fewer parameters. The conclusion is that there is no gain in accuracy by using the more complex model and additional parameter. Thus, the first order model is sufficient to describe the first step.

Establishment of First Phase Affinities

After establishing that the simple binding mechanism was the proper model to use for the first phase of the kinetic parameters, non-linear least squares fitting of the data to the model were conducted. Following those tests, the model was evaluated using a lack-of-fit test. Generally, data up until 5 seconds could be accounted for using the simple binding mechanism, and that data was included when calculating the kinetic parameters. The affinities and dissociation rate

constants were calculated for the micropipette data (Table 2.4). The margins of error shown are the 95% confidence intervals for the statistic, and very appropriately describe the data (Figure 2.4, Appendix A)

Table 2.4: Affinities for N-cadherin, E-cadherin, and C-cadherin interactions

CHO Cell Protein	Protein on CHO Cell Density (μm^{-2})	RBC Protein	Protein on RBC Density (μm^{-2})	Ka (x 10^{-4} μm^2)	koff (1/s)
*N-cadherin	15	N-cadherin-Fc	69	1.9±0.3	1.1±0.4
*N-cadherin	17	N-cadherin-Fc	178	1.3±0.2	1.0±0.3
*N-cadherin	15	N-cadherin-Fc	33	2.8±0.5	1.1±0.4
*C-cadherin	18	C-cadherin-Fc	10	11±2	0.6±0.2
*C-cadherin	18	C-cadherin-Fc	20	8.0±0.9	0.5±0.1
*E-cadherin	16	E-cadherin-Fc	14	4±1	0.7±0.3
*E-cadherin	16	E-cadherin-Fc	57	3.0±0.4	1.0±0.3
*E-cadherin	16	E-cadherin-Fc	44	3.3±0.5	1.0±0.3
*N-cadherin,1	15	C-cadherin-Fc	103	1.9±0.2	0.4±0.1
*N-cadherin,1	15	C-cadherin-Fc	49	1.9±0.2	0.7±0.2
*N-cadherin,1	15	C-cadherin-Fc	221	1.0±0.2	0.6±0.2
*N-cadherin,1	15	C-cadherin-Fc	19	3.2±0.7	0.8±0.4
C-cadherin,1	14	N-cadherin-Fc	38	3.5±0.2	1.3±0.3
*N-cadherin	16	E-cadherin-Fc	49	2.8±0.3	1.9±0.7
*N-cadherin	16	E-cadherin-Fc	33	2.6±0.4	1.2±0.5
*C-cadherin	18	E-cadherin-Fc	20	3.5±0.6	0.9±0.4
*C-cadherin	18	E-cadherin-Fc	33	3.3±0.5	1.3±0.4
*C-cadherin S78A	46	C-cadherin-Fc	16	1.7±0.3	1.4±0.6
*C-cadherin S78A	46	C-cadherin-Fc	33	1.3±0.2	1.0±0.3
*C-cadherin S78A	46	N-cadherin-Fc	9	2.3±0.4	1.7±0.8
*C-cadherin K8NS10P	41	C-cadherin-Fc	6	10.3±0.8	1.2±0.3
*C-cadherin K8NS10P	41	N-cadherin-Fc	9	2.5±0.4	1.6±0.8
*C-cadherin M92I	16	C-cadherin-Fc	16	4.2±0.5	2.3±0.7
*C-cadherin M92I	16	N-cadherin-Fc	44	1.9±0.2	1.9±0.6
*C-cadherin K8NS10P	25	C-cadherin-Fc	5.7	10.4±0.2	1.2±0.5

1 Heterophilic experiments of C-cadherin and N-cadherin where significant affinity differences were observed between experiments.

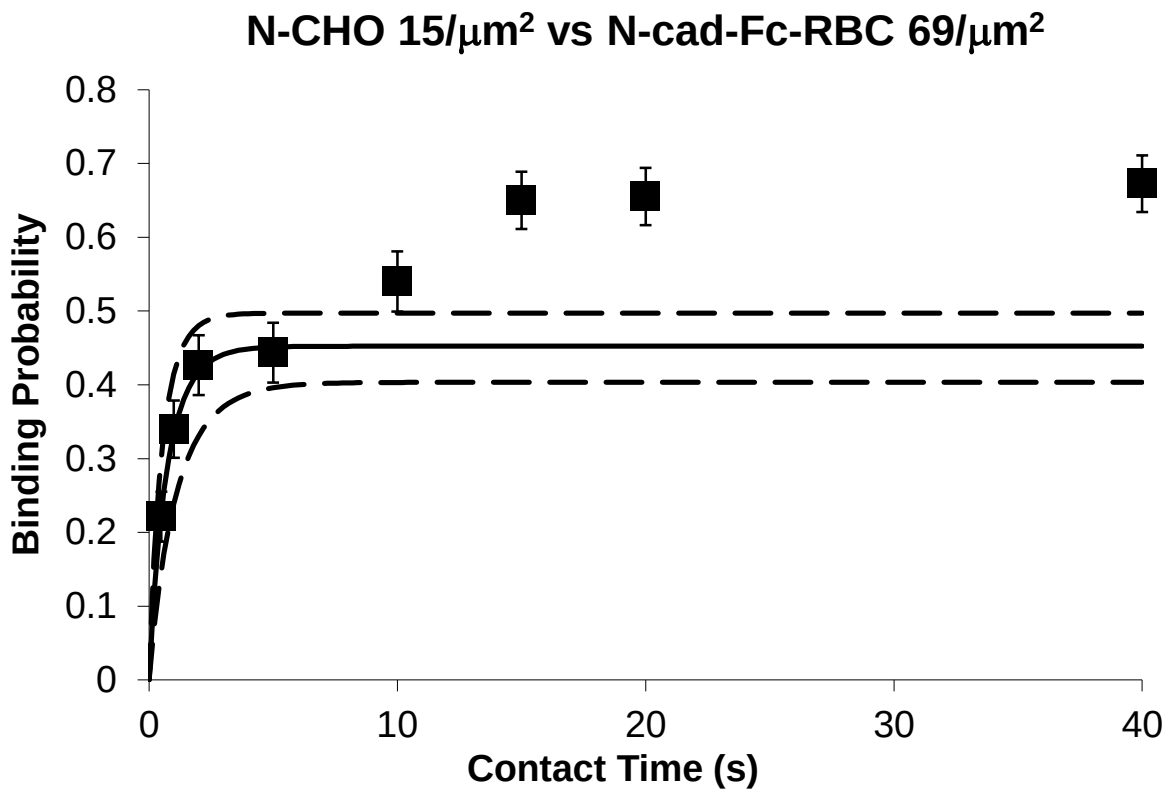

Figure 2.4: Homophilic Binding Probability Data for N-cadherin. The density on the CHO cell is 15/μm2. The density of N-cad-Fc on the RBC is 69/μm2. The fit to the first phase is the solid line, with the dashes lines representing the 95% confidence intervals.

Resolution of N-cadherin/C-cadherin Heterophilic Affinity

The only instance of significant variation of affinity within a protein pairing was the N-cadherin/C-cadherin heterophilic pairing. In the four experiments tested, two gave an affinity around 2 x 10^{-4} μm^2 and the other experiments split, with one test showing increased affinity, and the other test showing reduced affinity. To resolve this discrepancy, a micropipette experiment was run reversing the protein on the CHO cell and the protein on the RBC, using an C-CHO cell and N-cadherin-Fc on an RBC. From the data collected, the affinity was determined to be 3.5±0.2 x 10^{-4} μm^2 and the reverse reaction rate constant was 1.3±0.3 1/s (Figure 2.5).

2.4 Discussion

These results show the determination of the affinity and reverse reaction rate constant for the initial, EC1 dependent portion of cadherin adhesion from binding probability. These data have strong implications for how cadherin adhesion is explained. As discussed in section 1.6, one of the prevailing theories of cadherin adhesion had been the Differential Adhesion Hypothesis (DAH), which stated that the intersurface free energy, determined by cadherin affinities, would be minimized as cells went to thermodynamic equilibrium. With the affinities calculated in this chapter, coupled with experiments of overall cell behavior, it was possible to test the predictions of the DAH directly.

The differential adhesion hypothesis predicts four regimes of cell sorting behavior for two cell types A and B, based on the respective free energy changes, W_{AA}, W_{AB}, W_{BB} when two cells of type A, a cell of each type, or two cells of type B are brought into contact, assuming that W_{AA} is larger than W_{BB}. If the free energy of cross-type contact $W_{AB} \geq (W_{AA}+W_{BB})/2$, the hypothesis

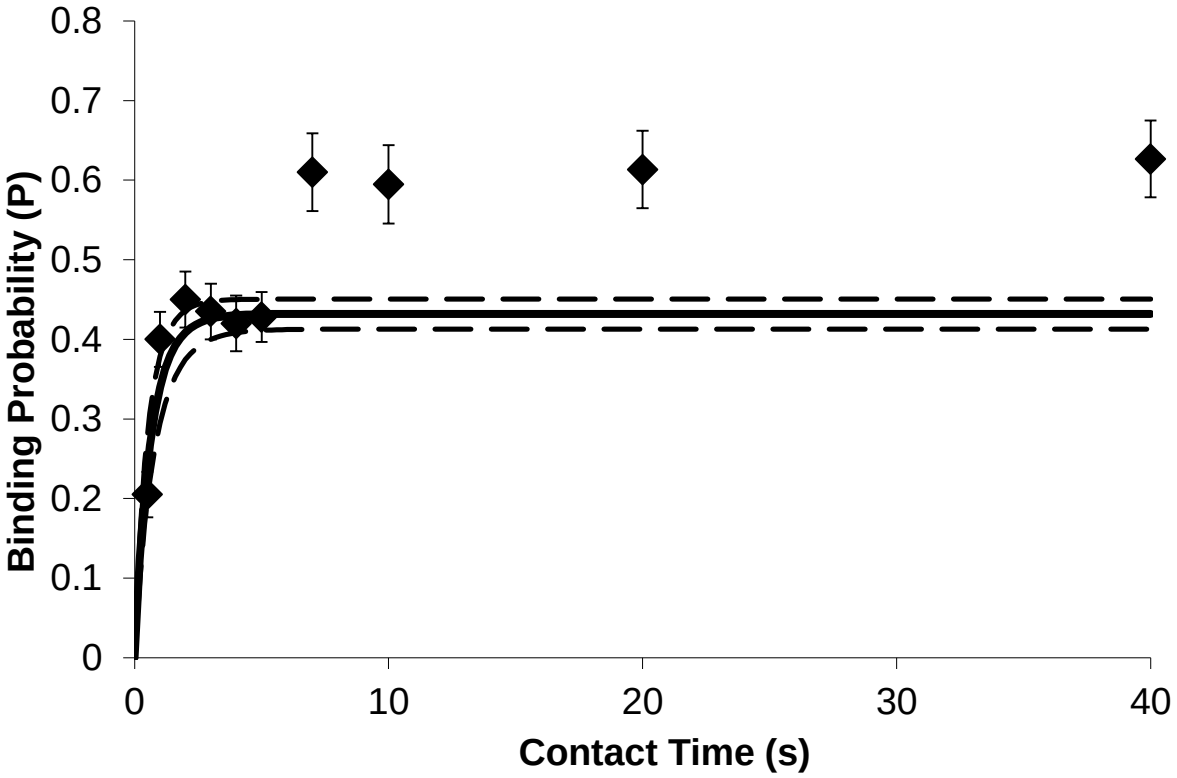

Figure 2.5: Heterophilic Binding Probability Data between CHO cells expressing C-cadherin and RBCs coated with N-cad-Fc. The density of C-cadherin on the CHO cells is 14/μm2. The density of N-cad-Fc on the RBCs is 38/μm2. The solid line represents the fit of the first phase with the best fit parameters given in Table 2.4. The dashed lines represent the 95% confidence interval.

predicts intermixing. If, instead, the heterophilic adhesion energy is in the range $W_{BB} \leq W_{AB} < (W_{AA}+W_{BB})/2$, the hypothesis predicts cell type B forming an envelope around cell type A. If the cross type adhesion energy falls in the range $0<W_{AB}<W_{BB}$, then there would be partial envelopment of cells of type A with cells of type B. Finally, if $W_{AB}=0$, the cells would separate completely. From the affinities, alongside published studies of cell sorting behavior, it is possible to test the differential adhesion hypothesis rigorously (Table 2.5).

Table 2.5: Evaluation of Differential Adhesion Hypothesis

Cell Type 1	Cell Type 2	K_{11}	K_{22}	K_{12}	DAH Prediction	Cell Sorting Result
C-CHO	E-CHO	0.00106	0.00033	0.00036	Partial Envelopment	Intermixing
C-CHO	N-CHO	0.00106	0.00018	0.00035	Complete Envelopment	"Partial Envelopment"
E-CHO	N-CHO	0.00033	0.00018	0.00027	Complete Envelopment	Intermixing

In all three cases, the behavior that is predicted by the DAH based upon the affinity measurements is not observed in cell sorting assays [67]. This would demonstrate that the DAH is not sufficient to explain all cadherin-mediated cell sorting behavior.

If the adhesion energies of cadherin extracellular regions are insufficient to explain the sorting behavior of cells, there is the question of what other factors may be involved. Studies have demonstrated that cortical tension can impact cell sorting behavior [6, 7]. Cortical tension is regulated through a variety of proteins, including integrins and cadherins, interacting with the actin cytoskeleton. The energetic impacts of these changes may outweigh the differences in adhesion energy among the classical cadherins.

Chapter 3

Structural Origins of Cell Sorting in Cadherins

Note: The C-cadherin mutant cell lines were constructed, and micropipette data characterizing them was obtained by Yuan-Hung Chien.

3.1 Introduction

From the cell sorting studies discussed in the previous chapter, the most notable result was that cells expressing N-cadherin and C-cadherin at similar densities would separate from each other. Following up on this study, it was decided to investigate the differences in the outermost extracellular domain, to determine if there were any motifs responsible for the specificity in adhesion observed in the cell sorting assays.

When the sequences are aligned, and examined in the context of the structure, there are several potentially significant differences that stand out (Figure 3.1). First of all, in the vicinity of the binding pocket for the W2 of the adjacent protein, amino acids 78 and 92 are different. By altering the charge state or the electron density of the binding site, affinities are potentially altered, which may result in different sorting behavior. There have also been studies which have mutated these amino acids, and have observed a change in cadherin-mediate adhesion [34, 79]. In addition, amino acids 8 and 10 are different for C-cadherin and N-cadherin. Those two amino

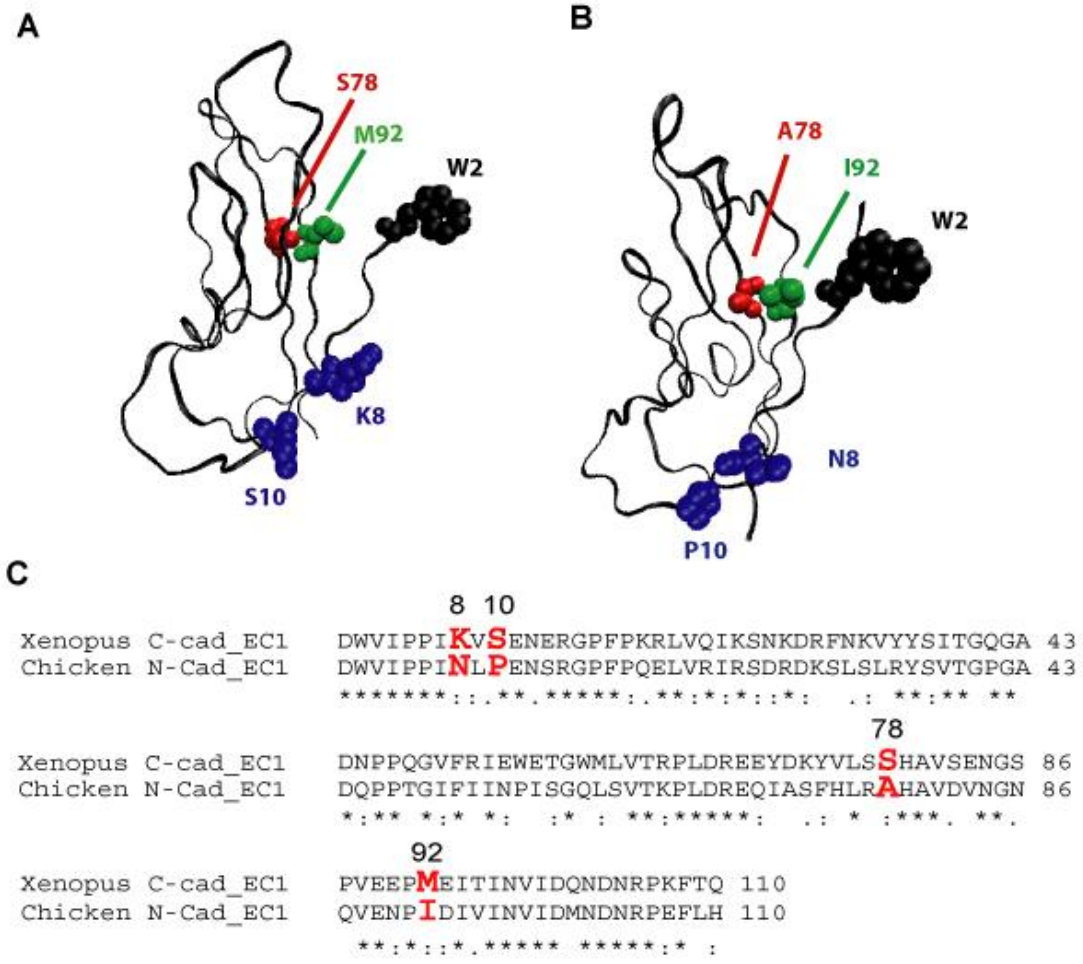

Figure 3.1: (A) The structure of domain 1 of C-cadherin demonstrating the positions of the key amino acids (pdb ID: 1L3W). (B) The structure of domain 1 of N-cadherin (pdb ID: 1NCI) (C) A sequence comparison of C-cadherin and N-cadherin, highlighting in red the differences that gave rise to the tested mutations.

acids form the hinge which connects the W2 containing beta strand to the rest of the domain, and varying them potentially alters the orientation of the docked W2 [80]. Through the creation of C-cadherin mutants that replace the native C-cadherin sequence with one or two amino acids from the N-cadherin sequence, it is possible to analyze the structural motifs that give rise to cadherin specificity.

In this chapter, work is presented demonstrating how a single amino acid change was able to alter specificity in sorting from C-cadherin to N-cadherin. Micropipette data is given which shows the changes in intrinsic cadherin binding properties which match the observed sorting patterns. Finally, other work will be discussed which demonstrates that cadherins may act as mediators for outside-in signaling.

3.2 Materials and Methods

Plasmids and Cell Lines

The cDNAs for the full length *Xenopus* C-cadherin in pEE14 plasmid was a gift from B. Gumbiner (Univ of Virginia, Charlottesville, VA). The cDNA encoding the full-length chicken N-cadherin in the pEGFP-N1 plasmid was generously given by Dr. Andre Sobel (Institut du Fer a Moulin; Gif-sur-Yvette, France). Stable CHO-K1 cells expressing the full length C-cadherin were grown in Glasgow MEM medium containing 10% dialyzed fetal bovine serum (FBS) and 25 μM methionine sulfoximine (Sigma-Aldrich, St Louis, MO) [23]. CHO-K1 cells expressing the full-length chicken N-cadherin were grown in Dulbecco's Modified Eagle Medium (DMEM) containing 10% FBS and 800 μg/ml G418 (Sigma-Aldrich, St Louis, MO). The G418 selection agent was used for at least four weeks. The cadherin expression levels were determined by

quantitative flow cytometry. The S78A, M92I, and K8NS10P mutants were generated previously from the cDNA for *Xenopus* C-cadherin using a Quickchange Site Directed Mutagenesis Kit (Stratagene, Cedar Creek, TX).

Quantification of cadherin surface expression levels of CHO cells

Cadherin surface expression levels were measured using quantitative flow cytometry [53, 58]. Stably transfected CHO-K1 cells expressing cadherins on their surface were labeled with protein-specific antibodies for the ectodomains. CHO cells expressing C-cadherin were labeled with anti-C-cadherin antibody (C/EP/B-Cadherin (clone xC-12), Santa Cruz Biotechnology, Santa Cruz, CA) followed by the secondary fluorescein isothiocyanate (FITC)-conjugated anti-goat IgG (whole molecule; Sigma-Aldrich, St Louis, MO). Chicken N-cadherin expressing CHO-K1 cells were labeled with monoclonal mouse anti-N-cadherin (Clone GC-4, Sigma-Aldrich, St Louis, MO) and then with fluorescein-isothiocyanate (FITC)-conjugated anti-mouse IgG (whole molecule; Sigma-Aldrich, St Louis, MO). The antibody labeling was done in phosphate buffered saline (PBS) containing 1w/v% bovine serum albumin (BSA) and 0.5 mM EDTA at pH 7.4. The fluorescence intensities of labeled cells were measured with an LSR II flow cytometer (BD Biosciences) [71]. The fluorescence intensity calibration curve was obtained with calibrated FITC-labeled standard beads (Bangs Laboratories, Inc., Fishers, IN) [71].

Selection of CHO Cells with a Desired Expression Level

Cadherin-expressing CHO cells which demonstrated a broad range of expressions upon initial testing, Fluorescence Activated Cell Sorting (FACS) was used. Cells were prepared for FACS in the same manner as they were prepared for quantitative flow cytometry. The cell sorting was conducted on a BD Biosciences FACS Aria cell sorter. Cells labeled with the

secondary antibody, but not the primary antibody, were run through the cytometer portion of the sorter to establish baseline fluorescence for non-specific adhesion. Subsequently, calibrated FITC-labeled standard beads (Bangs Laboratories, Inc., Fishers, IN) were run through the cytometer to establish a calibration curve between fluorescence and surface density. Based on this calibration, the expected fluorescence for cells with expression levels near $25/\mu m^2$ was calculated. The sorting gates were set to separate cells with expression levels between $20/\mu m^2$ and $30/\mu m^2$. A total of 500,000 cells were sorted, and the resultant sorted cell count was always in excess of 25,000.

Hanging drop cell sorting assay

Cell sorting measurements used the hanging drop method [37]. CHO cells with cadherin expression levels within 15% of each other were labeled with fluorescent dye (DiI or DiO; Molecular Probes) according to the manufacturer's instructions for the labeling of adherent cells. Flasks of cells with 80% confluent monolayers were incubated with growth medium supplemented with 5 μL/mL of the appropriate dye for 60 minutes. After washing with growth medium to remove excess dye, cells were detached from the culture plates with 0.01% in trypsin in Hank's Balanced Salt Solution (HBSS) (Invitrogen, Carlsbad, CA) supplemented with 2 mM $CaCl_2$ [81]. Cells were resuspended in HBSS with 2 mM $CaCl_2$ and 5% fetal bovine serum at a concentration of 1×10^6 cell/ml. For the Rac1 inhibitor control, this buffer contained 50 mM NSC 23766 (Tocris Bioscience, Ellisville, MO). A 10-μl aliquot of each of the two cell populations was mixed on the lid of a 10-cm Petri dish, and suspended above a dish containing 10 ml of PBS (Invitrogen, Carlsbad, CA). The hanging drops were stored in an incubator at 37°C and maintained under 5% CO_2. Cell aggregates were imaged at 24h and at 36h under a 10x objective with a Zeiss Axiovert 200 inverted fluorescence microscope equipped with a Zeiss

Axiocam MR camera. To quantify the sorting, the aggregates present in the images were counted and classified. Aggregates of three or more cells were scored as containing red cells, green cells, or both red and green cells [82]. In all cases, at least 50 aggregates were scored.

3.3 Results

CHO Cell Lines had Similar Surface Densities

The cadherin expressing CHO cell lines that had been generated previously were tested for their cadherin expression level. Following quantitative flow cytometry, it was determined that the C-CHO, N-CHO, and M92I cell lines required further sorting to achieve a narrower range of expression levels. Cell sorting was performed on those cell lines to reduce the spread in expression levels observed, and to ensure similar expression levels across cell lines. After flow cytometry, the cadherin surface expression levels of the cell lines were determined, and validated for subsequent sorting experiments (Table 3.1).

Table 3.1: Surface density of Engineered Cadherin Cell Lines

Cell Line	Cadherin Surface Density (μm^{-2})
C-CHO	18
N-CHO	16
K8NS10P	20
M92I	19
S78A	22

CHO Cells Expressing N-cadherin and C-cadherin Sort in Aggregation Assays

CHO cells expressing N-cadherin and C-cadherin were tested to confirm cell sorting for that heterophilic interaction. In addition to controlling for the density of cadherins on the surface, the sample drops included ~10,000 cells (10^6 cells/mL). Two experiments were run to test that

homophilic cadherin interactions promoted intermixing, and in those cases, cell populations labeled red and green intermixed fully over the 24-36 hours of the experiment. In the case of the heterophilic interaction, the N-cadherin and C-cadherin expressing CHO cells separated into clusters that were entirely one cell type or the other (Figure 3.2, A). When all imaged aggregates were counted and scored as containing red cells, green cells, or both colors, the majority of aggregates formed with cells expressing identical cadherins were found to have both colors, but the majority of aggregates formed with C-CHO and N-CHO mixtures contained a single cell type (Figure 3.2, D).

Point Mutations Modulate Sorting Patterns

Following these aggregation studies, the C-cadherin to N-cadherin mutants that had been constructed were tested for their sorting behaviors under identical conditions. Each mutant was tested for its sorting behavior when mixed with wild type N-CHO or with C-CHO. The K8NS10P mutant displayed nearly identical sorting behavior as the wild type protein, intermixing with C-CHO and separating from N-CHO (Figure 3.2, B and C left). In the case of the M92I mutant, the sorting behavior was changed so that the cells intermixed with both C-CHO and N-CHO (Figure 3.2, B and C middle). The S78A mutant demonstrated the greatest change from the behavior of wild type C-cadherin. Its sorting specificity was completely switched, so that it intermixed with N-CHO and separated from C-CHO in the aggregation assay (Figure 3.2, B and C right). When all of the aggregates were scored, the general pattern in the data was similar to what was qualitatively observed in the figures (Figure 3.2, D). In all, single amino acid changes resulted in a variety of altered cell sorting behaviors, ranging from almost no change to complete specificity reversal.

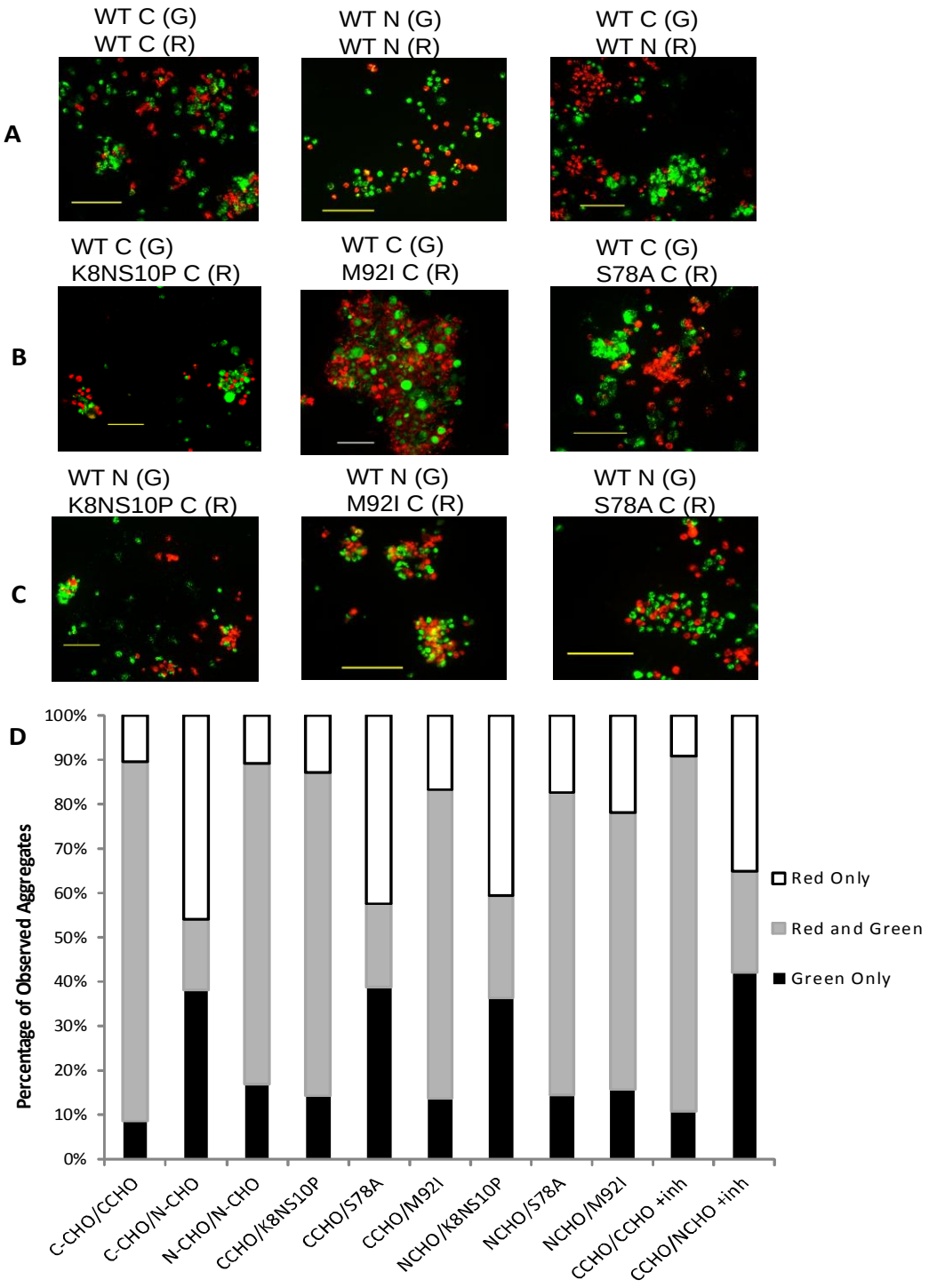

Figure 3.2: Hanging drop in vitro sorting assay. Cells expressing the different C-cadherin variants were intermixed with an equal number of CHO cells expressing either wt C-Cadherin or wt N-cadherin. Scale bars represent 100 μm. (A) CHO cells expressing WT C-cadherin and WT N-cadherin (B) CHO cells expressing wt C-cadherin mixed with the different C-cadherin variants. (C) CHO cells expressing WT N-cadherin mixed with the C-cadherin variants. The cells expressing the different cadherin variants were labeled with DiI (red) and the partner cells expressing WT C-cadherin or WT N-cadherin were labeled with DiO (green). (D) Quantification of the cell sorting data. Aggregates were scored as red, green, or red and green. An aggregate was defined as a cluster of 3 or more cells, and more than 50 aggregates were counted in all cases.

Change in sorting behavior correlates with affinity

Micropipette studies of cadherin binding kinetics were conducted with the mutants, to examine whether the observed cell sorting behaviors correlated with changes in the affinity of the first phase of the cadherin kinetics. The analyses focused on the first phase of the binding kinetics, because it is attributed to binding between the specificity-determining EC1 domains.

Utilizing the protocol developed in Chapter 2, micropipette data was analyzed, and the affinities and reverse reaction rate constants were determined (Table 3.2, Figure 3.3, Appendix A). The affinities correlated with the sorting data. The K8NS10P mutant had an affinity for both C-cadherin and N-cadherin that was statistically similar to the wild type C-CHO. The S78A mutant, which had sorting behavior perfectly reversed from wild type C-CHO, possessed a greater than six-fold reduced affinity for C-cadherin, and an affinity for N-cadherin that was very similar to wild type NCHO.

Table 3.2: Affinities and reverse reaction rate constants

CHO Cell Protein	Protein on CHO Cell Density (μm^{-2})	RBC Protein	Protein on RBC Density (μm^{-2})	Ka (x 10^{-4} μm^2)	koff (1/s)
N-cadherin	15	N-cadherin-Fc	69	1.9±0.3	1.1±0.4
C-cadherin	18	C-cadherin-Fc	10	11±2	0.6±0.2
N-cadherin	15	C-cadherin-Fc	19	3.2±0.7	0.8±0.4
C-cadherin	14	N-cadherin-Fc	38	3.5±0.2	1.3±0.3
C-cadherin S78A	46	C-cadherin-Fc	16	1.7±0.3	1.4±0.6
C-cadherin S78A	46	C-cadherin-Fc	33	1.3±0.2	1.0±0.3
C-cadherin S78A	46	N-cadherin-Fc	9	2.3±0.4	1.7±0.8
C-cadherin K8NS10P	41	C-cadherin-Fc	6	10.3±0.8	1.2±0.3
C-cadherin K8NS10P	41	N-cadherin-Fc	9	2.5±0.4	1.6±0.8
C-cadherin M92I	16	C-cadherin-Fc	16	4.2±0.5	2.3±0.7
C-cadherin M92I	16	N-cadherin-Fc	44	1.9±0.2	1.9±0.6
C-cadherin K8NS10P	25	C-cadherin-Fc	5.7	10.4±0.2	1.2±0.5

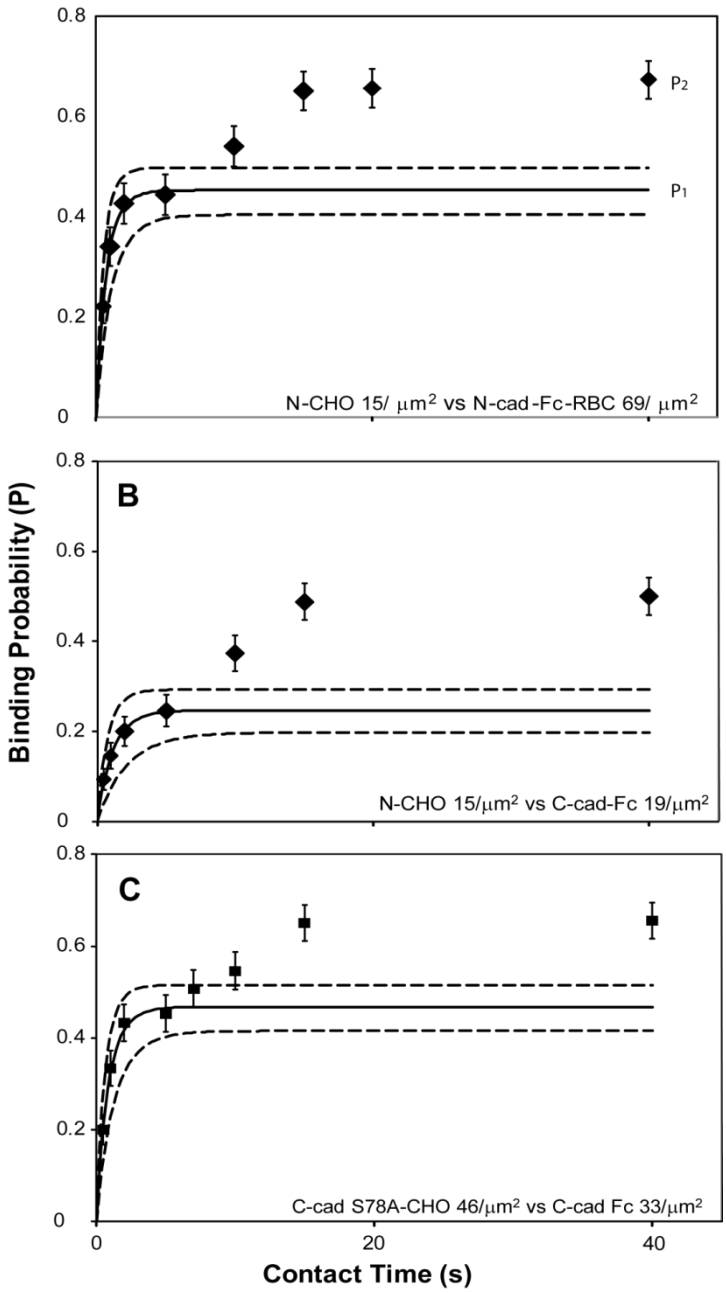

Figure 3.3. (A) Binding probability P versus the intercellular contact time measured between CHO cells expressing WT N-cadherin (15/μm^2) and NEC1-5-Fc (69/μm^2) on the opposing RBC. The binding occurs in two stages. P_1 indicates the first binding plateau, and P_2 indicates the second binding plateau. The solid line is the best fit of the first binding stage (<10s) to Equation 2.4, with the best-fit parameters given in the text and in Table 3.2. The dashed lines are the 95% confidence intervals for the fits. Each time point indicates the average and standard deviation of ~ 50 measurements with at least three different cell pairs. (B) Binding probability P versus the intercellular contact time measured between a CHO cell expression WT N-cadherin (15/μm^2) and CEC1-5-Fc (19/μm^2) on the opposing RBC. The solid line is the best fit of the first binding stage (<10s) to Equation 2 with the best-fit parameters given in the text and in Table 3.2. The dashed lines are the 95% confidence intervals for the fit. Each time point indicates the average and standard deviation of ~ 50 measurements with at least three different cell pairs. (C) Binding probability versus contact time between CHO cells expressing S78A (46/μm^2) and CEC1-5-Fc (33/μm^2) coated RBCs. The solid line is the best fit of the first binding stage (<10s) to Equation 2.4 with the best-fit parameters given in the text and in Table 3.2. The dashed lines are the 95% confidence intervals. Each time point indicates the average and standard deviation of ~ 50 measurements with at least three different cell pairs.

The M92I, which mixed with both C-CHO and N-CHO, demonstrated a reduced affinity for C-CHO, but only by a factor of 2, rather than the factor of 6 for the S78A mutant. Its affinity for N-cadherin was similar to that of the other C-cadherin mutants.

3.4 Discussion

This study identified a mutation in the tryptophan binding pocket on C-cadherin that substantially attenuated the affinity and correspondingly switched cell aggregation specificity. Further, in agreement with the results in Chapter 2, it was demonstrated that above an apparent threshold difference in cadherin affinities, in vitro cell sorting correlates with quantitative differences between two-dimensional affinities of cell surface cadherins. The switch in cell sorting specificity by the S78A C-cadherin mutant correlates with a six-fold decrease in the two-dimensional affinity for WT C-cadherin. By contrast, the 2.5-fold decrease in the affinity of the M92I mutant resulted in M92I cells intermixing with both WT C-CHO and N-CHO. These results support a model in which relatively large differences in two-dimensional binding affinities for the same overall protein scaffold, *e.g. C-cadherin* correlate with in vitro cell sorting.

The highly conserved W2 binding site is clearly critical to proper cadherin function. These kinetic measurements demonstrate that a change of even one amino acid in that region can generate substantial differences in affinity, allowing for significant affinity differences between cadherin subtypes. Positions 78 and 83 appear to be particularly crucial for cadherin function; S78A significantly reduced the C-cadherin affinity, A78M ablated N-cadherin adhesive function [83], and mutations at positions 78 and 83 in human E-cadherin altered in vitro sorting patterns of L1 cells expressing the proteins [84]. The A78M mutation also allosterically altered epitope accessibility on EC1 [85]. Distinct from earlier reports, this study quantified the biophysical differences of the membrane-bound proteins underlying altered cell adhesion and sorting.

The logarithm of two-dimensional affinities of both homophilic and heterophilic WT N-cadherin and WT C-cadherin bonds is directly proportional to previously measured adhesion energies [52, 86], but important differences between micropipette and adhesion measurements are i) the affinities and kinetic rates are not determined by mechanically breaking cadherin bonds and are force-independent and ii) micropipette measurements probe full-length cadherins on the cell membrane. The micropipette data demonstrate that cadherins with similar affinities (< ~3 fold differences), and correspondingly similar adhesion energies will not support cell sorting, when expressed at similar levels. This agrees with prior studies [87, 88], and may explain the absence of correlated adhesion and sorting by others [43, 82].

Chapter 4

Comparison of Affinities of Cadherins Expressed on Different Cell Types

4.1 Introduction

For cadherin-mediated cell adhesions *in vivo*, cadherin interaction with the actin cytoskeleton is a critical requirement for proper adhesive function [33]. Additionally, cadherin ligation activates several signaling pathways, including the ERK pathway, the Wnt signaling pathway, and signaling through the Rho family of GTPases [24, 89].

A possible limitation of the measurements of cadherin affinity in the prior chapters of this thesis is that the cadherins were expressed on cells that do not express endogenous cadherins. If the signaling is also important for proper cadherin function, altering the cell context could affect the cadherin binding function. In particular, if signals from inside the cell modulate cadherin behavior, the affinities measured for cadherin interactions on CHO cells may not correlate with those seen in cells with endogenous cadherin expression. Integrins, the adhesion molecules that bind to extracellular matrix, are known to be modulated by inside-out signaling [90], so the suggestion that cadherin activity may also depend on intracellular factors was plausible.

This chapter describes work undertaken to address this possibility, by determining the impact of the cell context on measured affinities. Multiple cell lines are examined, and it is determined that the same protein pairings have similar affinities independent of the cell type.

4.2 Materials and Methods

Plasmids and cell lines

The HEK293 cell lines expressing soluble, recombinant E-cadherin-Fc and N-cadherin-Fc constructs were cultured in DMEM supplemented with 10% FBS and 400 μg/mL G418. The conditioned media was purified with a Protein A affinity column, and subsequent purification done with anion exchange chromatography, as described previously [48]. The MDCK, MCF7, MDA-MB-435, and MDA-MB-231Tet On cell lines were all cultured in DMEM supplemented with 10v/v% FBS. The MDA-MB-231 Tet On cell line is a modification of the normal MDA-MB-231 cell line that can be induced to express E-cadherin [91]. The C2C12 cells were grown in low glucose DMEM supplemented with 20v/v% FBS.

Quantification of cadherin surface expression levels

Cadherin surface expression levels were quantified by flow cytometry [53, 58]. Cells expressing cadherins were labeled with protein-specific antibodies against the ectodomains. E-cadherin expressing cells were labeled with DECMA-1 (Sigma, St. Louis, MO), which is an antibody to the extracellular region of E-cadherin that is produced by rat cells. The secondary antibody was fluorescein-isothiocyanate (FITC)-conjugated anti-rat IgG (whole molecule, Sigma-Aldrich, St. Louis, MO). Chicken N-cadherin expressing CHO-K1 cells were labeled with monoclonal mouse anti-N-cadherin (Clone GC-4, Sigma-Aldrich, St Louis, MO) and then with fluorescein-isothiocyanate (FITC)-conjugated anti-mouse IgG (whole molecule; Sigma-Aldrich, St Louis, MO). The antibody labeling was done in phosphate buffered saline (PBS) containing 1w/v% bovine serum albumin (BSA) at pH 7.4. The fluorescence intensities of labeled cells were measured with an LSR II flow cytometer (BD Biosciences) [71]. The fluorescence intensity

calibration curve was generated with calibrated FITC-labeled standard beads (Bangs Laboratories, Inc., Fishers, IN) [71].

Surface modification of erythrocytes with oriented cadherin extracellular domains.

Erythrocytes were isolated from human whole blood collected from healthy donors. The whole blood was stored in Vacutainers™, and proper protocols were followed for handling human-derived materials. The erythrocytes were isolated with Histopaque 1119 (Sigma-Aldrich, St Louis, MO), following the manufacturer's protocol. A 12 ml aliquot of Histopaque 1119 was prepared in a 50 ml centrifuge tube. Then 7 ml whole blood and 7 ml of 0.9 w/v% NaCl were mixed, and then slowly transferred to the tube containing Histopaque. The mixture was centrifuged at 800 x g for 20 minutes at room temperature in an Eppendorf 5810R benchtop centrifuge. The supernatant was discarded as biological waste, and the remaining cells were resuspended in 7 ml of 0.9 w/v% NaCl prior to the addition of 1.5 ml of 6 w/v% Dextran. The cells were incubated at room temperature for 45 minutes, during which they settled to the bottom of the tube. After discarding the supernatant, the red blood cells (RBC) were washed twice at room temperature with 0.9 w/v% NaCl, and resuspended in 12 ml EAS45 (2.0 mM Adenine, 110.0 mM dextrose, 55.0 mM Mannitol, 50.0 mM NaCl, 10.0 mM glutamine and 20.0 mM Na_2HPO_4, at pH 8.0) [74]. The purified RBC suspension in EAS45 is stored at 4°C, and can be used for up to 3 weeks, after which the RBCs are treated with bleach and discarded.

Covalently bound antibodies on the RBCs were used to capture the Fc-tagged cadherin ectodomains. Antibodies were covalently coupled to the RBCs using the $CrCl_3$ coupling method [75, 76]. We used either goat polyclonal anti-human immunoglobin G (IgG) Fc or goat polyclonal anti-mouse IgG Fc antibodies (Sigma-Aldrich, St Louis, MO). Approximately 10^6 RBCs were washed five times with 0.85 w/v% NaCl, and then resuspended in 250 μL of 0.85 %

NaCl with 1 μg of the desired antibody. The $CrCl_3$ solution was diluted to concentrations below 0.01 w/v% with 0.02 mM sodium acetate containing 0.85 w/v% NaCl. To chemically activate glycoproteins on RBCs, 250 μL of diluted $CrCl_3$ solution was mixed with 250 μL of the red blood cell/antibody mixture and incubated at room temperature for 5 minutes. The reaction was stopped with 500 μL of "stop solution" (PBS with 0.5 mM EDTA and 1% BSA). The cells were then washed twice with the "stop solution". The concentration of $CrCl_3$ determined the density of antibodies immobilized to the surface of the RBCs, but the antibody density varies. Treating the RBCs with different $CrCl_3$ concentrations was necessary to achieve the desired antibody surface density.

After the antibody immobilization, approximately 20,000 modified RBCs were incubated with 3 μl of 1mg/mL Cadherin-Fc fragments. The resulting cadherin surface densities were then quantified by flow cytometry [53, 58].

Micropipette measurements of cell binding kinetics

The binding probability was determined as a function of contact time with the micropipette manipulation technique, described in section 2.2 [53, 57, 58, 71, 77]. The binding probability P(t) is the ratio of the number of binding events n_b to the total N_T cell-cell touches, n_b/N_T. In these measurements, a cadherin-expressing CHO cell and a RBC modified with Fc-tagged cadherin ectodomains were partially aspirated into opposing micropipettes (Figure 2.1). The cells were maintained in the chamber with L15 medium (Invitrogen, Carlsbad, CA) supplemented with 1 w/v% BSA, which is a hypo-osmotic condition for the RBCs, and keeps them rounded. Cells were visualized with a 100x oil immersion objective on a Zeiss Axiovert 200 microscope, and images were recorded with a DAGE-MTI CCD100 CCD camera (DAGE-

MTI Inc, Michigan City, In) interfaced to a high resolution, flat screen TV monitor. Cells were positioned with automated piezo-electric controllers programmed to cyclically bring the two cells into contact for a defined period. The contact area was controlled at ~7 μm^2 (~1.5 μm diameter). Adhesion events are identified from the surface deformation of the RBC during separation and recoil at adhesive failure. Contact times are controlled with the programmed piezo-electric actuator. Each cell pair was tested for 50 repetitive cell-cell touches ($N_T = 50$), and each contact time represents measurements with at least three different cell pairs ($N > 150$). The reported probabilities P are the mean $\pm$ standard deviation from the mean.

Data analysis

The micropipette data was analyzed as outlined in Chapter 2.2. Briefly, the data were weighted based upon the determined variance of data at each time point, and then a non-linear least squares regression method was used to fit Equation 2.4 to data in the first phase of the kinetic profile, which comprises time points up to 5s.

4.3 Results

Cadherin expressing cells were viable in the micropipette assay

The first phase of this project was to identify the cell types that were viable in the micropipette manipulation assay. Cells had to be approximately the same size as CHO cells. The cell size needs to be compatible with the micropipette diameters used. Otherwise it becomes difficult to manipulate the cell into the micropipette without either rupturing the membrane or drawing the entire cell into the pipette. Additionally some cells extend processes, such that the cell morphology changes significantly over the course of a series of adhesion tests. This prevents the

same contact area from being measured in successive cycles, such that the determined binding probability becomes less meaningful. Finally, some cells begin differentiating under the serum-free, hypo-osmotic conditions used in the assays.

Based on these criteria, of the cell lines that natively expressed cadherin, the MCF7, MDCK, and MDA-MB-435 cell lines proved suitable for micropipette measurements. C2C12 cells and MDA-MB-231 Tet On cells were incompatible with these measurements (Table 4.1). C2C12 cells extended processes, and began to differentiate during the experiment. MDA-MB-231 Tet On cells were more fragile and tended to rupture when partially aspirated into a micropipette.

Table 4.1: Assessment of Feasibility for Micropipette

			Micropipette Viability	
Cell Line	Species	Cadherin	Usable	Notes
MDCK	Canine	E-cadherin	Yes	
MCF7	Human	E-cadherin	Yes	
MDA-MB-231 Tet On	Human	E-cadherin	No	Membrane would rupture during aspiration
MDA-MB-435	Human	N-cadherin	Yes	
C2C12	Mouse	N-cadherin	No	Extended Cell Processes, differentiates without serum

Affinities determined with cells expressing endogenous cadherin

Following these viability tests, the MDCK, MCF7, and MDA-MB-435 cell lines were used in micropipette experiments, in order to determine the affinities between the expressed cadherins and canine E-cadherin-Fc or chicken N-cadherin-Fc immobilized on red blood cells. The binding probability curves were determined as described in section 2.2.

In all cases studied, cell-cell binding kinetics exhibit a biphasic increase in the binding probability with contact time, as reported in section 2.3. That signature was preserved with both E-cadherin and N-cadherin expressing cells, and across cadherins from different species. Therefore, the biphasic kinetics are an intrinsic property of cadherin-dependent cell-cell binding, and independent of the cell context in which they are expressed.

Using the analysis protocol developed in Chapter 2, the data associated with the first binding phase were identified, and the corresponding two-dimensional affinity and reverse reaction rate constant were determined for each pairwise cadherin interaction studied. The best fit kinetic parameters are summarized in Table 4.2, Figure 4.1, and Appendix A. The kinetic parameters determined for canine E-CHO or chicken N-CHO binding to RBCs modified with canine E-cadherin-Fc are included for comparison. With the heterophilic pair of canine E-cadherin and chicken N-cadherin, tested with CHO cells and with canine E-cadherin expressed on the MDCK cells, the kinetic parameters were similar.

To further test the role of cell context and signaling in cadherin function, the role of Rac1 signaling was investigated. Since E-cadherin ligation triggers Rac1 activation [92], the MCF7-canine Ecadherin-Fc pair was chosen to test that concept. Following treatment with the Rac inhibitor NSC23766 (Tocris Bioscience, Ellisville, MO), cadherin binding kinetics were still biphasic. From the binding probability curve and the best-fit kinetic parameters, the data show that Rac1 inhibition did not have a statistically significant effect on the kinetic parameters associated with the first binding step.

Table 4.2: Affinity and Reverse Reaction Rate Parameters for Cadherin Expressing Cell Lines. MDA-MB-435 and MCF7 are human cell lines. MDCK is a canine cell line. E-CHO and N-CHO are Chinese Hamster Ovary Cells Engineered to express canine E-cadherin and chicken N-cadherin, respectively. The cadherin-Fc constructs are canine E-cadherin-Fc and chicken N-cadherin-Fc.

Surface 1	Surface 1 Density (μm^{-2})	Surface 2 Protein	Surface 2 Density (μm^{-2})	K_a (10^{-4} μm^2)	K_{off} (s^{-1})
E-CHO	16	E-cadherin-Fc-RBC	14	3.86±0.97	0.69±0.34
N-CHO	16	E-cadherin-Fc-RBC	33	2.64±0.41	1.21±0.47
MDA-MB-435	93	N-cadherin-Fc-RBC	32	0.7±0.06	1.93±0.29
MDA-MB-435	93	E-cadherin-Fc-RBC	7	1.2±0.2	1.46±0.28
MDCK	17	E-cadherin-Fc-RBC	7	3.6±0.2	1.65±0.30
MDCK	17	N-cadherin-Fc-RBC	20	2.5±0.2	1.49±0.42
MCF7	7	E-cadherin-Fc-RBC	18	4.2 ± 0.2	2.4±0.4
MCF7	7	N-cadherin-Fc-RBC	37	2.7±0.1	2.2±0.4
MCF7(-Rac)	7	E-cadherin-Fc-RBC	18	4.3 ± 0.2	2.6±0.6

4.4 Discussion

The most significant finding of this study is that the kinetics of binding between cadherin extracellular domains are unaffected by the cells on which the proteins are expressed, at least with the cell types examined here. Importantly, the two-dimensional affinities are the same quantitatively regardless of the cell context, and this confirms that these micropipette manipulation measurements are measuring the intrinsic binding properties of the extracellular domains of the classical cadherins. This means that, in the context of these short time studies, cellular context and associated factors such as signaling proteins do not alter cadherin ligation kinetics. This strongly argues against the potential for cadherin adhesive function to be regulated

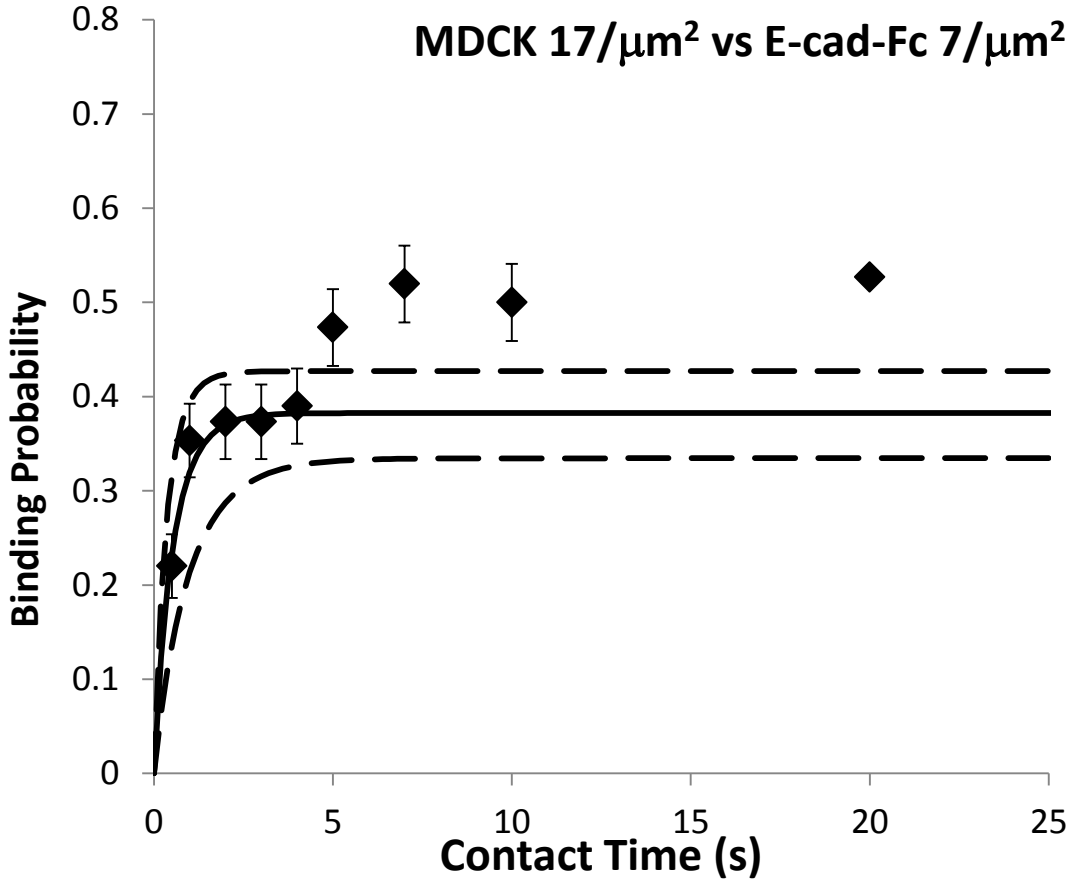

Figure 4.1: Binding probability versus contact time between MDCK cells and RBCs modified with E-cad-Fc. The surface density of canine E-cadherin on the MDCK cells was 17/μm^2. The density of E-cadherin-Fc on the RBC was 7/μm^2. The solid line represents the best-fit parameters, which are given in Table 4.2.

from inside the cell under the conditions investigated in these studies. This marks a significant difference between cell-cell junctions and integrins at cell-ECM adhesions.

This work also has additional, important implications. It means that when studying cadherin interactions, it is possible to vary the cell type without altering the intrinsic cadherin binding affinity. This is beneficial because different cellular properties lead to different responses in studies of cell mechanics. From the similarities in cadherin adhesion in the initial stages, it may be possible to generalize the results of binding studies, as it occurs in a manner that is independent of the overall cell type and cell environment.

Chapter 5

N-Glycosylation Directly Modulates Cadherin Adhesion

Note: The enzymatic treatment of N-cad-Fc in this chapter was performed by Nitesh Shashikanth. The immunoblots were performed by Huabei Guo

5.1 Introduction

As discussed in section 1.3, although the first phase of cadherin kinetics were attributed to the EC1 strand swapping interaction of W2, the second phase of the cadherin kinetics is not yet fully characterized. It is known that domain 3 is necessary to maintain the full kinetic signature [58]. To better understand the factors involved in the second phase, mutations that alter cadherin functionality on the cell level were examined. In addition to mutations in the primary structure, aberrant N-glycosylation of cadherin extracellular domains is linked to the metastatic phenotype of several cancers [93-100]. Epithelial cadherin (E-cad) has several N-glyocosylation sites along the extracellular region. E-cadherin in breast tumors exhibit highly branched N-glycans on extracellular domains EC4 and EC5, and hyper-glycosylation at these sites destabilized epithelial junctions and increased tumor progression [97, 99, 101, 102]. Conversely, hypo-glycosylation, achieved by ablating an N-glycosylation site in EC4 enhanced intercellular junction assembly, cytoskeletal remodeling at junctions, and barrier integrity [95-97, 103]. Neural cadherin (N-cad) contains eight N-glycosylation sequences in the extracellular segment that are post-translationally modified [94]. Mutating all eight sites increased intercellular junction stability,

enhanced ERK signaling, and reduced cell migration in a scratch wound-healing assay [94]. Cross-linking studies also evidenced an increase in lateral dimers on cell surfaces, suggesting that *N*-glycosylation modulates *cis* dimerization. Eliminating three *N*-glycosylation sites located on extracellular domains EC2 and EC3 by mutating Asn273, Asn325, and Asn402, which are distal to the adhesive EC1 domain (Figures 5.1A,B), had the same functional impact as mutating all eight sites [94].

Collectively, these results suggest that *N*-glycosylation alters cadherin-dependent functions, but evidence that *N*-glycosylation affects the intrinsic adhesive function of cadherins has been circumstantial. This is because glycosylation could also perturb lateral interactions with other cell surface proteins such as growth factor receptors [104-108]. Moreover, the mechanism by which *N*-glycosylation of EC2-5 could disrupt intercellular adhesion is not obvious because these sites are distal from the adhesive EC1 interface.

In this chapter, work is described that used micropipette manipulation measurements to quantify the impact of *N*-glycosylation mutants on the intrinsic dynamics of N-cadherin-mediated intercellular binding. Micropipette measurements have been used to determine the two-dimensional affinities and dissociation rates of several adhesion protein receptors, in the context of the cell membrane [54-56, 58, 62, 68-71]. Such measurements showed that C-cadherin kinetics exhibits a two-stage process in which an initial, fast EC1-dependent binding step is followed by a short lag period and a further, slower increase in binding probability [58]. Domain deletion studies showed that EC1 is required for the first, fast binding step, but the full extracellular domain is needed for the lag and second binding step [58]. Here we describe the effect of ablating *N*-glycosylation sites in EC2 and EC3 of neural cadherin (N-cad) on this kinetic signature. The findings suggest a binding mechanism in which initial, *trans* cadherin ligation is followed by additional cadherin interactions, which augment binding but are modulated by *N*-glycosylation.

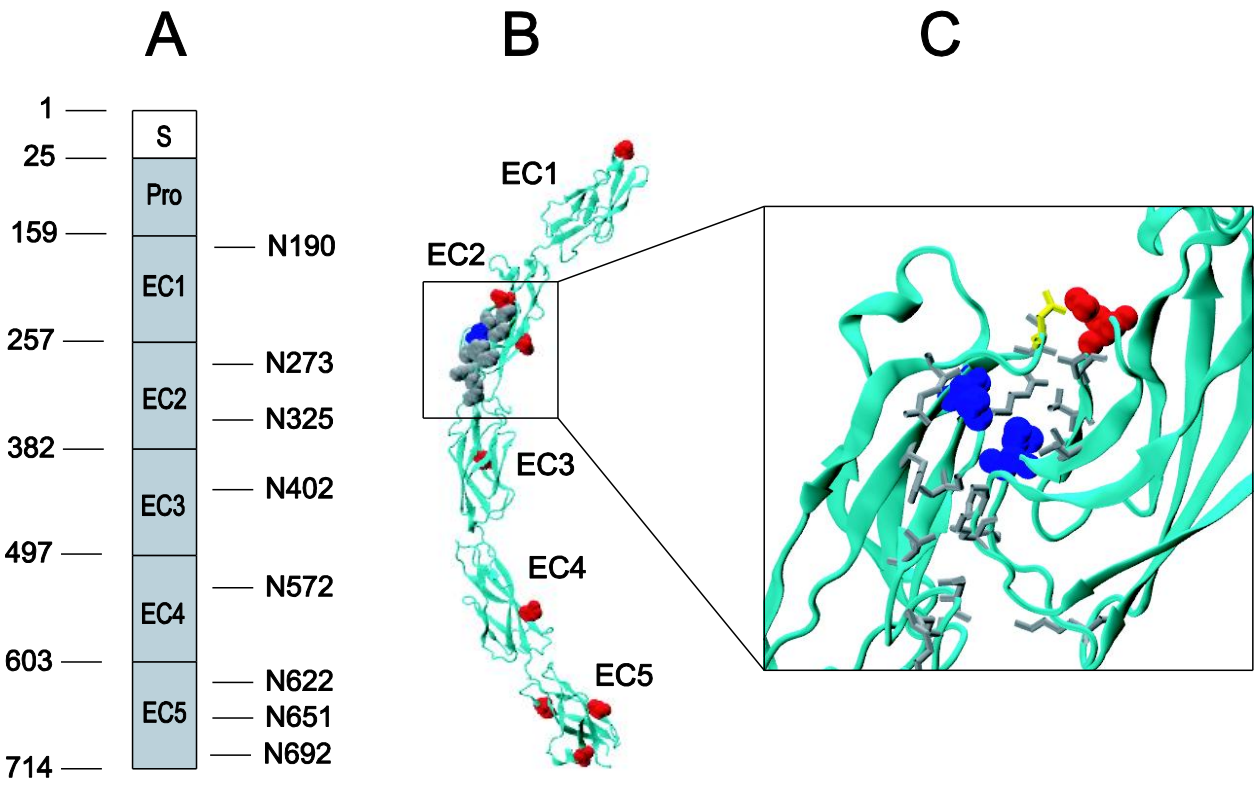

Figure 5.1. (A) Schematic of putative *N*-glycosylation sites in five extracellular domains (EC1–EC5). S, signal peptide; Pro, pro-domain; EC, extracellular domain. (B) Structure of the extracellular domain of mouse N-cadherin (3Q2W). The Asn residues of the *N*-glycosylation sites are shown in red. Amino acids from the extracellular domain 2 (EC2) portion that contribute to the putative *cis*-binding interface are in gray. (C) An expanded view of the putative *cis*-binding interface between adjacent cadherins. The *N*-glycosylation site N273 is red, and is in close proximity to N243 (yellow) from the adjacent cadherin.

5.2 Materials and Methods

Plasmids and Cell Lines

The extracellular region of chicken N-cadherin fused to a mouse-Fc tag (N-cad-Fc) was previously stably expressed in HEK293 cells [109]. Cells were cultured in Dulbecco's Modified Eagle Medium (DMEM) containing 10% FBS (Invitrogen) and 0.4 mg/mL G418 (Sigma-Aldrich, St Louis, MO) as a selection marker. The N-cad-Fc construct was purified from cell supernatant using a Protein A affinity column (Biorad) followed by gel filtration chromatography, as described previously [35, 109]. CHO-K1 cells expressing the full-length human N-cadherin and glycosylation mutants of N-cadherin [94] were cultured in DMEM containing 10% FBS and 0.4 mg/ml G418. Quantitative flow cytometry and immuno-blotting determined the cadherin expression levels.

Quantification of the cadherin surface expression levels in CHO cells

Quantitative flow cytometry determined the density of cadherins expressed on the cell surface [53, 58]. Human N-cadherin expressing CHO-K1 cells were labeled with mouse, anti-N-cadherin antibody and then with fluorescein-isothiocyanate (FITC)-conjugated anti-mouse IgG antibody (Sigma-Aldrich, St Louis, MO). The antibody labeling was in phosphate buffered saline (PBS) (137 mM NaCl, 2.7 mM KCl, 10 mM sodium phosphate dibasic, 2 mM potassium phosphate monobasic, 0.5 mM EDTA, and 1w/v% bovine serum albumin (BSA) at pH 7.4). An LSR II flow cytometer (BD Biosciences) measured the fluorescence intensities of labeled cells and of fluorescent bead standards [71]. The fluorescence calibration curve was obtained with calibrated FITC-labeled standard beads (Bangs Laboratories, Inc., Fisher, IN).

Immobilization of oriented cadherin extracellular domains on erythrocytes

Human whole blood was collected from healthy donors. The whole blood was stored in Vacutainers™. The erythrocytes were isolated with Histopaque 1119 solution (Sigma-Aldrich, St Louis,

MO), following the manufacturer's protocol. A mixture of 7 ml whole blood and 7 ml of 0.9 w/v% NaCl was added to a 12 ml aliquot of Histopaque 1119 in a 50 mL centrifuge tube. The RBCs were separated by centrifuging the tube at 800 x g for 20 minutes at room temperature in an Eppendorf 5810R benchtop centrifuge. The supernatant was discarded as biological waste. The concentrated RBCs at the bottom of the tube were resuspended in 7 ml of 0.9 w/v% NaCl, followed by the addition of 1.5 mL of 6 w/v% Dextran. The cells were incubated at room temperature for 45 minutes, during which they settled to the bottom of the tube. After discarding the supernatant, the RBCs were washed twice at room temperature with 0.9 w/v% NaCl, and resuspended in 12 mL EAS45 solution (2.0 mM adenine, 110.0 mM dextrose, 55.0 mM mannitol, 50.0 mM NaCl, 10.0 mM glutamine and 20.0 mM Na_2HPO_4, at pH 8.0) [74]. The purified RBC suspension in EAS45 can be maintained at 4°C for up to 3 weeks, after which the RBCs are treated with bleach and discarded.

Goat polyclonal anti-mouse IgG Fc-specific antibodies (Sigma-Aldrich, St Louis, MO) were covalently coupled to the RBCs using $CrCl_3$ activation [75, 76]. Approximately 10^6 RBCs were washed five times with 0.85 w/v% NaCl, and then resuspended in 250 μL of 0.85 % NaCl with 1 μg of the antibody. A $CrCl_3$ solution was diluted to concentrations below 0.01 w/v% in 0.02 mM sodium acetate containing 0.85 w/v% NaCl. Next, 250 μL of diluted $CrCl_3$ solution was mixed with an equal volume of the red blood cell/antibody mixture. After 5 minutes, 500 μL of "stop solution" (PBS with 5 mM EDTA and 1% BSA) was added, and cells were washed twice with the "stop solution". The labeled RBCs were stored in EAS45. The resulting density of antibodies immobilized to the RBC surface is variable, so that the $CrCl_3$ concentration is titrated, in order to achieve the desired coverage. The density of cadherin-Fc bound to the antibody-modified RBCs was determined by quantitative flow cytometry [53, 58].

Immuno-blot Analysis of Cell Surface Expression Levels

Subconfluent cells were washed and detached using 2 mM EDTA. Cells were washed with ice-cold PBS and incubated with 1 mg/mL NHS-LC-biotin in PBS for 20 min at 4 °C on a rocking platform.

After washing, cells were lysed. Cell surface proteins were precipitated with streptavidin-agarose at 4 °C overnight and detected by Western blot as described [110].

Micropipette measurements of cell binding kinetics

The micropipette manipulation technique [53, 58, 71, 111, 112] experimentally determines the binding probability as a function of intercellular contact time. The binding probability P(t) is the ratio of the number of binding events n_b to the total N_T cell-cell touches, n_b/N_T. The binding kinetics of full-length human N-cadherin expressed on CHO cells was probed with the Fc-tagged extracellular region EC1-5 of chicken N-cadherin (N-cad-Fc) immobilized and oriented on the adjacent red blood cell (RBC) (Figure 2.1). The CHO cell expressing membrane-bound wild type human N-cadherin (N-CHO WT) has been previously described [113]. The wild type hN-cadherin was expressed on CHO cells (hN-CHO WT) at 18 cadherins/μm^2. The sequences of the N-terminal extracellular domain 1 (EC1) of chicken N-cadherin and of human N-cadherin are 95% identical (BLAST, P10288|165-729 and P19022|160-723).

Throughout the experiment, the cells were maintained in L15 medium (Invitrogen, Carlsbad, CA) supplemented with 1 w/v% BSA. Cell-cell contact was observed with at 100x (Zeiss Axiovert 200 microscope), interfaced with a DAGE-MTI CCD100 CCD camera (DAGE-MTI Inc, Michigan City, In) to record images. The cells were positioned with a programmable piezo-electric controller, which was used to cyclically bring two cells into contact for a defined period. The contact area was controlled at ~7 μm^2 (~1.5 μm diameter). Adhesion events are identified from the RBC deformation during cell-cell separation and the recoil at bond rupture. Each cell pair was tested for 50 cell-cell touches ($N_T \sim 50$), and each contact time represents measurements with at least three cell pairs ($N > 150$). The probabilities P are the mean $\pm$ standard deviation from the mean.

Enzymatic De-Glycosylation of Cadherin-Fc Constructs

The N-cad-Fc constructs were enzymatically treated to remove glycans, by incubating the protein with exoglycosidases (PNGase F, β-1,4-Galactosidase, Neuraminidase) and Enodglycosidase (EndoH).

The exoglycosidase reactions used 1x G6 buffer (50 mM sodium acetate, 5 mM $CaCl_2$, pH 5.5), while the EndoH reaction was carried out in 1x G5 buffer (50 mM sodium citrate, pH 5.5). Reactions containing both EndoH and the exoglycosidases were done in 1 x G6 buffer. To determine optimum conditions, 5 μg protein was used for each reaction, which was carried out for 24 hr at 37 °C in a water bath. Then 4 μL of 6x SDS-Commasie Blue solution was added to stop the reaction. The contents were heat-denatured and separated on a 7.5% SDS-Polyacrylamide gel. The combination of all enzymes gave the greatest decrease in molecular weight, so this condition was used to treat 250μg of N-cad-Fc, which was then purified from the reaction mixture on a Protein-A affinity column.

5.3 Results

Wild Type Human N-cadherin (hN-Cad) Displays Biphasic Kinetics

Studies of cell-cell binding kinetics showed that C-cadherin, which is also a Type I classical cadherin, displayed biphasic kinetics when studied with the micropipette manipulation technique [58]. Figure 5.2 shows the binding kinetics measured between hN-CHO WT (18 cadherins/μm^2) and RBCs modified with ckN-cad-Fc at a density of 10 cadherins/μm^2. The kinetic time course is biphasic, and occurs in two stages. The first stage is a fast, initial rise to a plateau P_1 at ~0.41 within the first two seconds. This is followed by a 2-5 second lag or induction phase, and then a slower, second rise to a higher binding probability at P_2 ~0.55.

A prior study demonstrated that the first step requires EC1-2 [58]. The solid line is the nonlinear least squares fit of the kinetic data for the first binding step to a simple model for *trans* EC1-EC1 binding, using Equation 2.4 from Chapter 2. The solid line in Figure 5.2 is the nonlinear least squares fit of the data to Equation 2.4. The best-fit affinity and dissociation rate are, respectively, $4.2 \pm 0.4 \times 10^{-4}$ μm^2 and 2.0 ± 0.5 s^{-1} (Table 5.1). Importantly, equation 2.4 does not describe the entire kinetic profile.

Furthermore, the inclusion of a transient encounter complex [114, 115] predicts an exponential rise to a single plateau, but it does not predict the two-stage kinetics shown here.

As described in section 2.2, a lack-of-fit test was used to parse the data into the two, distinct kinetic stages: namely the rise to P_1 and to P_2. This test compares the least squares residuals of the model to the intrinsic variability of the data (Equation 2.13). When the test statistic exceeds the critical value for a given time point, then the model does not describe the data in question. To determine the dissociation rate and two-dimensional affinity for the initial step, Equation 2.4 was fit to the maximum number of time points in each data set that did not fail the lack-of-fit test. This approach demonstrated that Equation 2.4 does not describe the second increase at longer times.

N-glycosylation alters N-cadherin binding kinetics

To determine the effect of *N*-glycosylation on N-cadherin kinetics, the binding probability data were obtained with hN-cadherin mutants in which all eight of the *N*-glycosylation sites were mutated to Ala (hN-CHO MuALL) or sites 2,3 and 4 were mutated to alanine (hN-CHO Mu234) (Figures 5.1A,B). In subsequent kinetic measurements, N-cadherin mutants were expressed on CHO cells at similar levels, as verified by Western blot (Figure 5.3A). According to quantitative FACs measurements, the expression levels are ~18 cadherins/μm^2. The impact of hypo-glycosylation on the kinetics would depend on whether the lesser (limiting) protein ligand is the mutant expressed on CHO cells or the glycosylated ckN-cad-Fc bound to the RBCs. This is because the limiting reagent will dominate the kinetics. We therefore carried out measurements in which we varied the density of ckN-cad-Fc on the RBCs, so that the glycosylated protein was either less than (limiting) or in excess of the hN-cadherin (or mutant) on the CHO cells. The ckN-cad-Fc, which is expressed in mammalian cells, is glycosylated (Figure 5.3B).

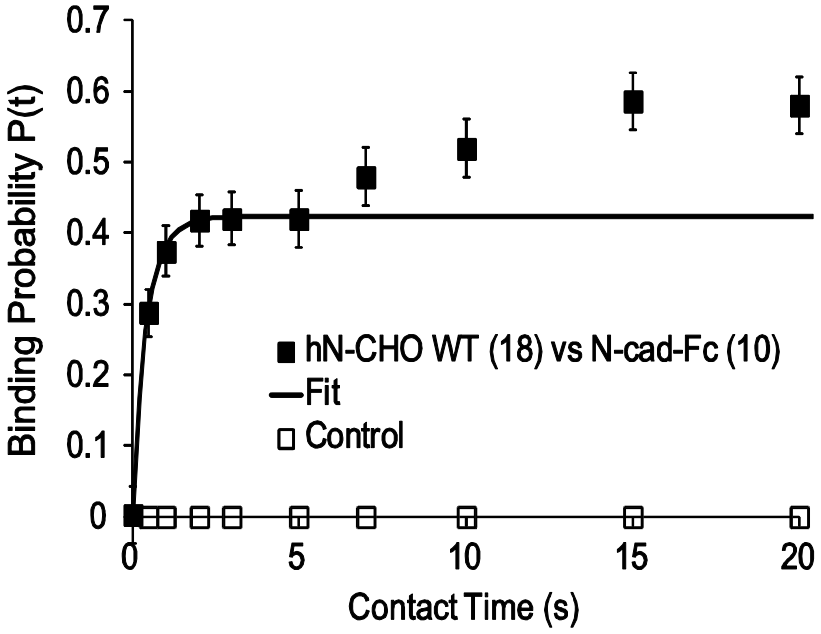

Figure 5.2 Binding probability P(t) as a function of intercellular contact time for interactions between hN-CHO WT and RBCs modified with untreated N-cad-Fc. The solid line is the nonlinear least squares fit of data for the fast, first phase to the model in Equation 2.4, and the best-fit kinetic parameters are summarized in Table 5.1.

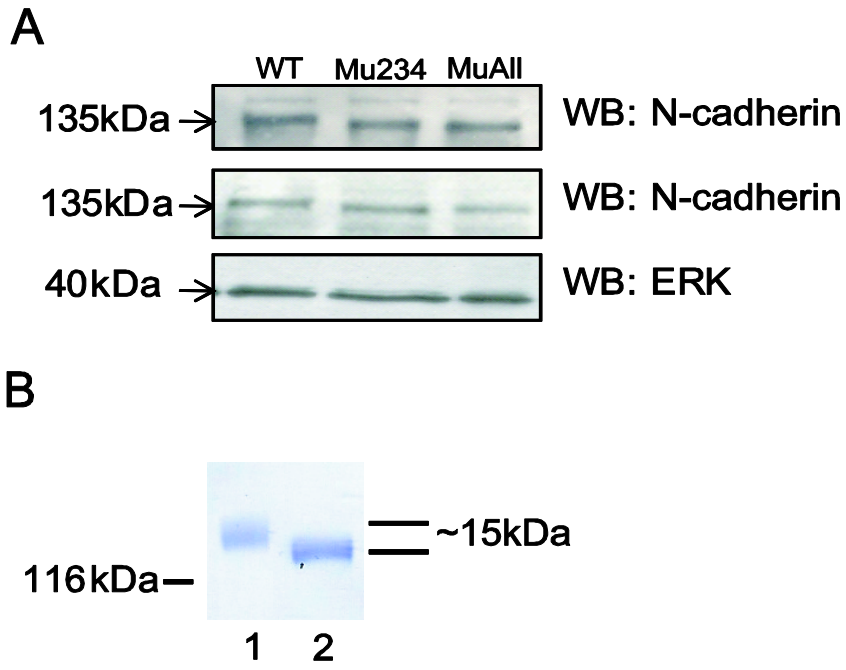

Figure 5.3. (A) Loss of *N*-glycosylation sites has no effect on N-cadherin trafficking to the cell surface. Cells were labeled with NHS-LC-biotin, followed by precipitation with streptavidin-agarose, SDS-PAGE, and blotting with anti-N-cadherin (*Top*). As control, total cell lysates were used for Western-blot analysis with anti-N-cadherin (*Middle*) and anti-ERK as the loading control (*Bottom*). WT: wild-type N-cad; Mu234: N-cad with N273, N325, N402 mutations; MuAll: N-cad with all 8 putative sites mutated. WB: Western-blotting. (B) SDS-PAGE (7.5%) of chicken N-cad-Fc before (lane 1) and after (lane 2) enzymatic digestion under non-denaturing conditions with a mixture of PNGase, Neuraminidase, β-galactosidase, and EndoH. *Western Blots were performed by Dr. Huabei Guo (University of Georgia) and the SDS-PAGE was performed by Nitesh Shashikanth (UIUC).

Table 5.1 Best-fit two-dimensional affinity and dissociation rate measured between RBCs modified with ckN-cad-Fc and cells expressing the indicated ligand.

Ligand	Ligand density (#/μm^2)	ckN-cad-Fc (#/μm^2)	Affinity (μm^2)	Dissociation rate (s^{-1})
hN-cad WT	18	10	$4.2 \pm 0.4 \times 10^{-4}$	2.0 ± 0.5
hN-cad Mu2,3,4	18	7	$4.0 \pm 0.5 \times 10^{-4}$	1.4 ± 0.6
hN-cad MuALL	18	7	$4.3 \pm 0.4 \times 10^{-4}$	2.2 ± 0.5

Figure 5.4A shows the impact of the hypo-glycosylation mutations on binding kinetics, when the densities of hN-cadherin mutants expressed on the CHO cells are limiting. The time course measured between hN-CHO WT (18 cadherin/μm^2) and ckN-cad-Fc (37 cadherins/μm^2) exhibits the biphasic kinetic signature (Figure 5.4A). By contrast, ablating eight *N*-glycosylation sites (hNCHO MuALL, ~18 cadherin/μm^2) nearly eliminates the induction phase, and the binding probability rises smoothly to the higher probability plateau at P_2 ~0.63. The data do not exhibit a single exponential rise, indicating that at least two processes contribute to the overall kinetics.

Prior findings indicated that *N*-glycosylation sites in hN-cadherin domains EC2-3 (Figure 5.1B) have the greatest effect on cadherin dimerization, cell migration, and ERK signaling [94]. The binding kinetics of the hN-CHO Mu234 variant is similar to that of hN-CHO MuALL, and the time course also exhibits a rapid rise to P_2 ~0.73 (Figure 5.4A). The difference in amplitudes (P_2) measured with hN-CHO MuALL and hN-CHO Mu234 is attributed to the different ckN-cad-Fc densities used in the different measurements. Importantly, there is no significant induction phase observed with either of the hypoglycosylated N-cadherin mutants, when their densities are limiting. The altered kinetics relative to hN-CHO WT clearly shows that *N*-glycosylation on N-cadherin EC2-3 domains directly affects the intrinsic cadherin binding dynamics.

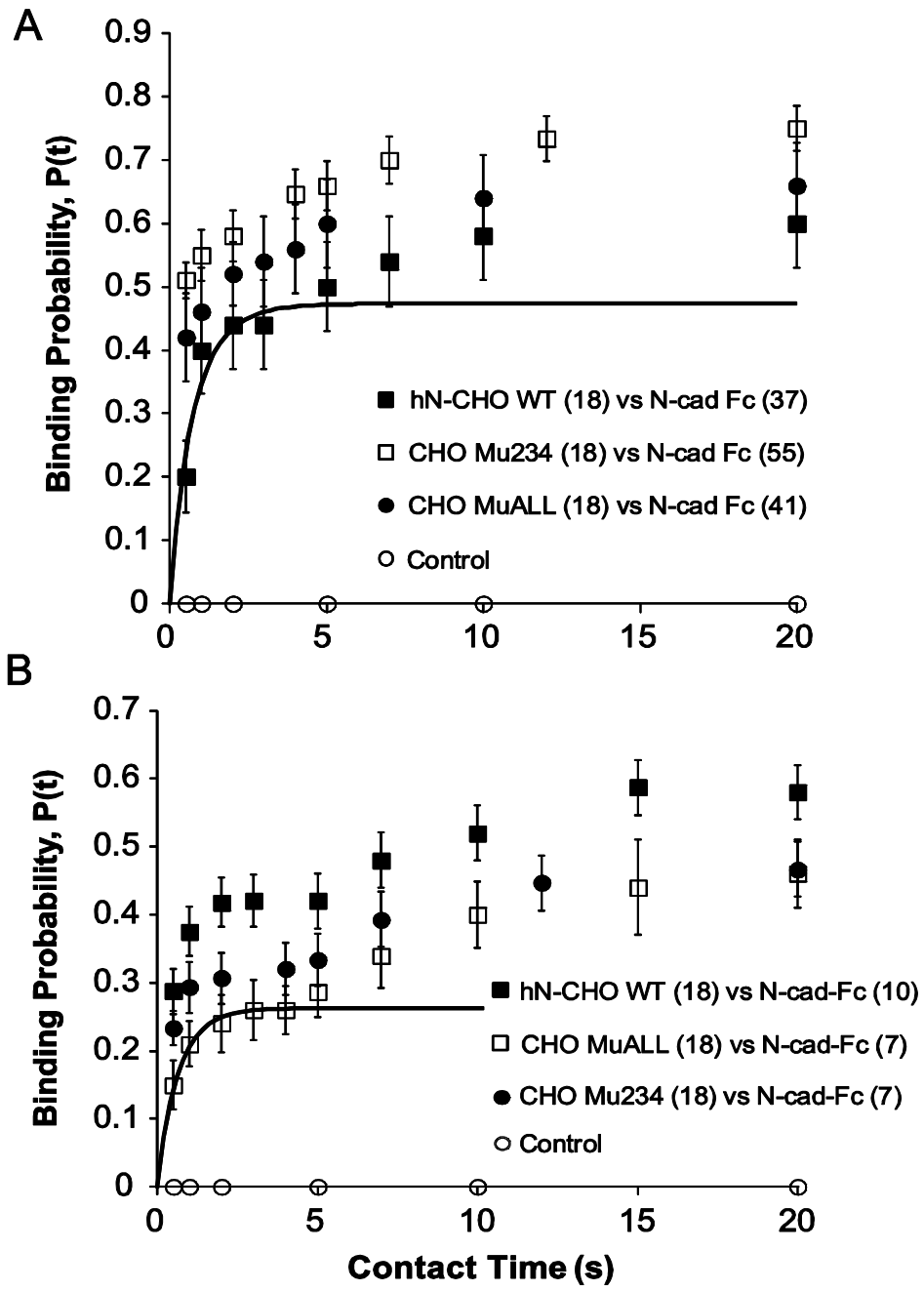

Figure 5.4 (A) Binding probability P(t) versus intercellular contact time when glycosylated N-cad-Fc is in excess over expressed N-cadherin. Kinetics were measured between ckN-cad-Fc on RBCs and hN-CHO WT (black squares), hN-CHO Mu234 (white squares), or hN-CHO MuALL (black circles) at densities of ~18 cadherins/μm^2. The ckN-cad-Fc surface densities (#/μm^2) are in parentheses. Control data (white circles) were obtained with N-CHO and RBCs without ckN-cad-Fc. (B) Binding probability P(t) versus intercellular contact time when glycosylated N-cad-Fc is limiting. The kinetics was measured between glycosylated ckN-cad-Fc on the RBCs (7 or 10 cadherins/μm^2) and hN-CHO WT (black squares), hN-CHO ALL (white squares), or hN-CHO Mu234 (black circles) (~18 cadherin/μm^2).

By contrast, when hypo-glycosylated N-cadherin is in excess and the glycosylated ckN-cad-Fc is the limiting ligand, the binding kinetics displays the induction phase. Figure 5.5B shows the kinetic profiles measured with ckN-cad-Fc on the RBCs at 10/μm^2 and 7/μm^2. Measurements with hN-CHO WT and with the two, hypo-glycosylation mutants all exhibit the two-stage kinetic profile, as expected if the glycosylated ckN-cad-Fc densities were rate limiting and the glycans affect the kinetics. Interestingly, the best-fit, two-dimensional affinities for the first binding step, as measured with wild type hN-cadherin and with the two glycosylation mutants (Table 5.1), are statistically similar, indicating that *N*-glycan removal does not affect EC1-EC1 binding.

Enzymatic deglycosylation of N-cad-Fc eliminates the induction phase

To test whether the lag phase observed in Figures 5.2, 5.5B is due to carbohydrates on ckN-cad-Fc, the glycans were trimmed enzymatically with exoglycosidases and EndoH under nondenaturing conditions. Treatment with a mixture of EndoH, neuraminidase, PNGase, and 1,4 β-galactosidase reduced the apparent N-cad-Fc molecular weight by ~15 kDa relative to the untreated protein (Figure 5.3B). Under nondenaturing conditions, this procedure removes branched carbohydrates, but it does not remove core glycan from the Asn side chain.

Consistent with expectations, the kinetics measured with ckN-cad-Fc did not exhibit the induction phase (Figure 5.5A), at densities where ckN-cad-Fc is limiting (compare with Figure 5.4B). In particular, the time course measured with enzymatically treated ckN-cad-Fc versus hN-CHO MuALL exhibits a smooth rise to a plateau at P ~ 0.6. The kinetic features measured with hN-cadherin mutants are similar qualitatively to the kinetics measured when the hypo-glycosylated mutant was limiting (compare with Figure 5.4A).

The kinetics measured with hN-CHO WT and RBCs modified with treated (Figure 5.5A, black circles) or untreated N-cad-Fc (Figure 5.5B, black squares) show that N-cad-Fc hypo-glycosylation eliminates the lag phase, and accelerates the rise to the higher binding probability P_2. For the hN-CHO

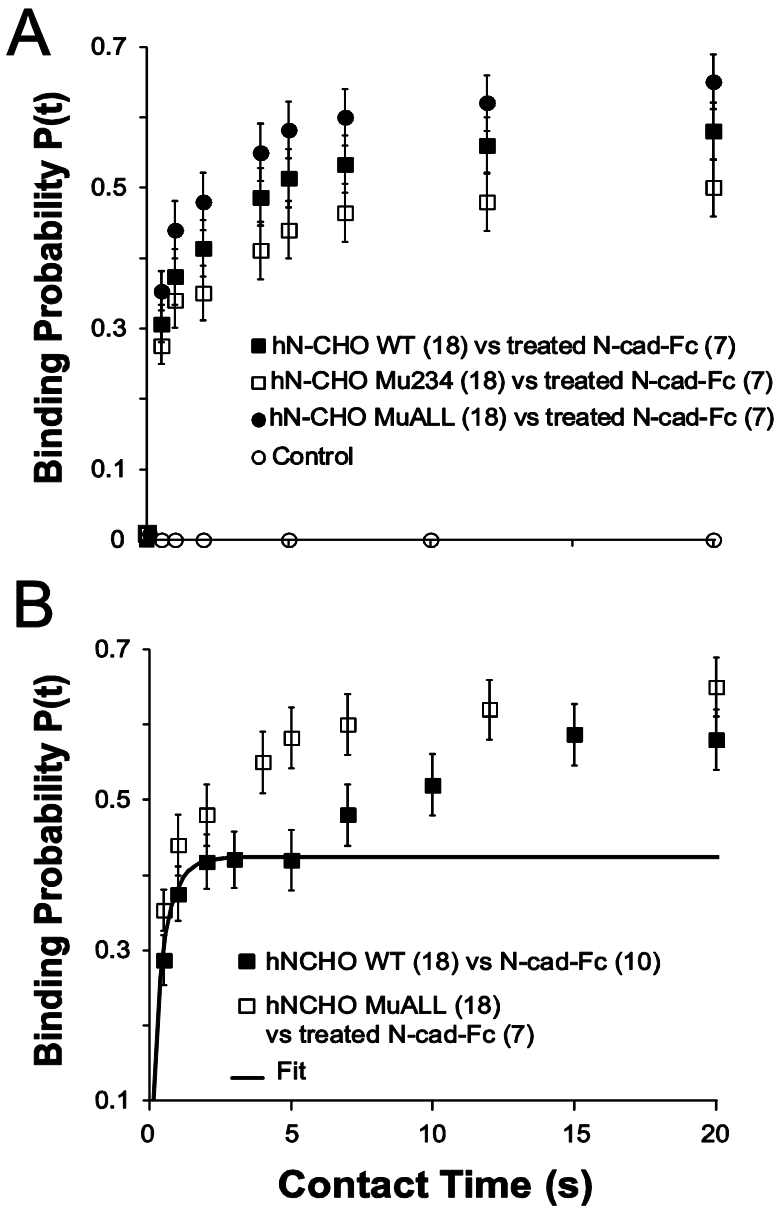

Figure 5.5 (A) Binding probability P(t) versus contact time between RBCs modified with immobilized, enzymatically treated ckN-cad-Fc (7cadherins/μm^2) and hN-CHO WT (filled squares), hN-CHO Mu234 (open squares), or hN-CHO MuALL cells at ~18cadherins/μm^2. Open circles indicate controls with RBCs lacking ckN-cad-Fc and hN-CHO. (B) Comparison of the binding probability P(t) versus contact time between the hN-CHO WT and RBCs modified with untreated ckN-cad-Fc (black squares) with the kinetics measured between hN-CHO MuAll and RBCs modified with enzymatically treated ckN-cad-Fc (open squares). The cadherin surface densities (#/μm^2) on the CHO cells and on the RBCs are in parentheses. The solid line through the data is the nonlinear least squares fit of the strand-swapping model to the data for the first binding step, and the best-fit parameters are summarized in Table 5.1.

Mu234 cells, the 2 s data point gives the appearance of a lag. However the R^2 of a fit of Equation 2.4 to the first two seconds of data is only ~0.7, and when the five second time point is included, the data fails the lack of fit test (Equation 2.13). Figure 5.5B contrasts the kinetics measured with glycosylated proteins on both cells with those in which proteins on both cells are hypo-glycosylated. Similarly, the binding kinetics between identical RBCs modified with untreated ckN-cad-Fc (7cadherins/μm^2) exhibited no induction phase, even at low cadherin densities (not shown). A comparison of the kinetics measured with treated N-cad-Fc and either N-CHO MuALL or N-CHO WT (Figure 5.5A) reveals a slightly higher limiting binding probability with the N-CHO-MuALL cells, despite similar cadherin densities on the cells in both cases. Although this could be due to slight differences in the intrinsic cadherin binding properties, the final binding probabilities measured with RBCs modified with either treated and untreated N-cad-Fc (7 cadherins/μm^2) were the same.

5.4 Discussion

The extent of neural cadherin glycosylation directly alters the intrinsic intercellular binding kinetics. An increasing number of studies link aberrant glycosylation to altered cadherin-dependent cell functions, in the context of different cancers. Phenotypic changes include altered cell motility in scratch wound-healing assays, cytoskeleton reorganization, metastasis, ERK signaling, and barrier function [94, 95, 97, 99, 101, 103, 116, 117]. In the case of N-cadherin, the N-glycosylation sites at N273, N325, and N402 are highly conserved. Mutating these sites alters cell functions, but not cadherin trafficking to the membrane [94]. These findings collectively suggested that glycosylation perturbs cadherin-dependent cell adhesion. Here, we present direct evidence that *N*-glycosylation alters the intrinsic binding function of N-cadherin and the dynamic assembly of cell-cell junctions.

In the two-stage cadherin binding kinetics, *N*-glycosylation modulates the dynamics of the induction (lag) phase and subsequent increase in binding probability, but not the intrinsic affinity of the EC1-EC1 bond of N-cadherin. This glycosylation-independence of the affinity agrees with the similar

dimerization affinities of N-cadherin EC1-2 fragments expressed in bacteria and in mammalian cells [39]. The underlying mechanism of action therefore differs from the effect of neural cell adhesion molecule glycosylation, where the large excluded volume of polysialic acid blocks protein-protein binding [118]. Instead, *N*-glycosylation mutations at N273, N325, and N402 increased the prevalence of *cis* N-cadherin dimers on cell membranes [94]. The latter result, together with two-stage kinetic data presented here, suggests a model in which initial adhesion enables lateral dimerization and enhanced binding (Figure 5.6). We attribute the second, slower rise in binding probability to lateral association, which is impeded by the *N*-glycosylation state of the protein. Glycosylated N-cadherin does not dimerize significantly outside of cell-cell contacts, suggesting that cell-cell adhesion is needed to overcome the energy barrier to lateral association. Entropy contributes to this barrier, but glycosylation also appears to play a role. Hypo-glycosylation through enzymatic treatment, point mutations, or glycosyltransferase down-regulation would reduce lateral repulsion, facilitate *cis* dimerization, and reduce or eliminate the induction period, as we report here.

This postulated mechanism is similar to that suggested by recent simulations of the adhesion-dependent coalescence of cadherin lattices between opposed surfaces [119]. The simulations constrained lateral cadherin bonds to mimic contacts in a recent crystal structure, where a frequently observed contact between EC1 and EC2 (Figure 5.1B) is postulated to be the *cis*-binding interface [120]. It is noteworthy that N166, which is one of the sites investigated in this study, lies at this postulated interface. The crystal structures were of deglycosylated proteins [120], so it is not possible to visualize how that interface might accommodate a large carbohydrate. The latter would likely generate a substantial steric barrier that could impede or disrupt the protein-protein interface.

Glycans on N-cadherin in melanoma lines were characterized, but the glycan structure and molecular weight at each site is unknown and would vary with cell type and culture conditions [121]. The 15kDa shift in N-cadherin molecular weight following enzymatic treatment (Figure 5.3B) gives an upper bound. Prior characterization of the *N*-glycosylation mutants of human N-cadherin showed that each of

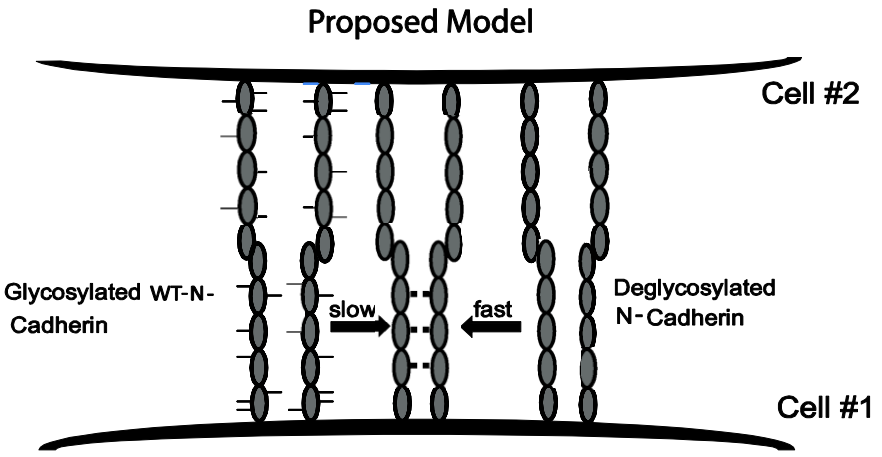

Figure 5.6. Proposed model for the effect of N-glycosylation on the dynamics of N-cadherin-mediated intercellular junction assembly. In this model, opposing cadherin monomers initially form *trans* adhesive bonds. This initial binding in turn facilitates lateral cadherin association, which is slowed by *N*-glycans on the cadherin ectodomain.

the N273, N325, or N402 mutants alone did not generate the Mu234 or MuALL phenotype. Instead, eliminating the induction phase required ablating all three *N*-glycosylation sites on both EC2 and EC3 domains. This result suggests that the *cis* interface involves more extensive contacts between ectodomains—a possibility that is supported by a prior finding that the extracellular domain EC3 of C-cadherin is required for the induction phase and second kinetic step [58].

Despite qualitative similarities between our findings and the simulation results [119], there are important differences. First, the putative lateral dimerization step in measured cadherin kinetics requires EC3 [58], which was not implicated in the structure-based model. Second, the effect of N325 glycosylation on the putative *cis*-interface and junction organization is unknown. Third, it is unclear whether the sparse cadherin densities used in our studies could nucleate clusters, as depicted in the simulations. The use of Fc-tagged C-cadherin dimers decreased the induction period relative to hexahistidine-tagged monomers at similar overall protein densities, suggesting that only a few proteins are needed for this kinetic signature [58]. Previous single-bond rupture studies and cell adhesion data reported that dimers enhance adhesion relative to monomers [23, 122]. Although there may be different interpretations of the structural basis of these experimental observations, these results are consistent with a process in which adhesion triggers subsequent changes in cadherin organization at cell-cell junctions that further enhances binding and is modulated by *N*-glycans.

In summary, we present direct evidence that the *N*-glycosylation of neural cadherin directly impacts the intrinsic dynamics of cadherin-dependent intercellular junction assembly. Glycosylation does not affect EC1-dependent affinities, but the two-stage kinetic fingerprint and prior cross-linking results support a binding mechanism in which initial, EC1-dependent *trans* binding is followed by additional cadherin interactions that enhance binding. *N*-glycans localized at three sites in the EC2-EC3 domains of N-cadherin alter the second step in the kinetic profile to modulate the junction assembly dynamics.

Chapter 6

Conclusions and Future Work

6.1 Conclusions

Methodology Developed for Analysis of Biphasic Kinetic Data

From the measurements of cadherin binding kinetics made using the micropipette manipulation technique, a methodology was developed for analysis of the first phase of biphasic data. The first phase corresponds with domain EC1 of the cadherin protein, which is responsible for specificity, so analysis of the first phase was necessary to directly evaluate prior theories of cadherin sorting, which specified that affinity differences should drive cell sorting behavior. To examine the cell sorting behavior directly, hanging drop cell sorting experiments of C-cadherin, N-cadherin, and three mutants of C-cadherin were conducted. From these evaluations, it was determined that the Differential Adhesion Hypothesis is incomplete, and cell sorting is not completely described by a comparison of cadherin affinities.

Initial Cadherin Ligation is Cell Context Independent

Cadherin affinities were tested in multiple cell contexts, to determine if changing the cell environment modulated intrinsic cadherin bond affinities. These data demonstrate that cadherin bonds have similar properties in multiple cell contacts, giving strong evidence against the existence of signaling from inside the cell playing a role in cadherin adhesion.

N-Glycosylation Regulates N-Cadherin Binding Kinetics

In light of studies that had demonstrated the effect of N-glycosylation on N-cadherin mediated adhesion in cells, the kinetics of N-glycosylation mutants were tested and compared with normal N-cadherin. It was determined that the induction phase, the 2-5s time where the binding probability does not change, required N-glycosylation of domains EC2 and EC3. Additionally, the first phase affinity was quantified to be very similar for the glycosylation mutants. From the data collected in this study, combined with measurements of cadherins from the field, a model was proposed where a lateral interaction is made more favorable when the N-glycans are removed.

6.2 Future Work

There are potential avenues for future research which can further illuminate the mechanism of cadherin interactions. First of all, recent work by a collaborator has identified activating antibodies, which can alter cell morphology and increase E-cadherin mediated adhesion. By studying how these antibodies modulate cadherin binding kinetics, and by looking at their epitopes, further insight may be gained into the mechanism for adhesion.

Additionally, other studies of cadherins have looked at adding glycosylation sites to cadherins, as appear in metastatic cancers. By examining the kinetics exhibited by cadherins modified in this manner, further insight may be gained into other loci on cadherin that are mechanistically relevant in the interaction.

Finally, to complement the experimental research, and test any model of cadherin interactions, simulation methods should be developed and employed in parallel with the experiments. These studies will involve using Monte Carlo methods to model a surface and capture the diffusion of

protein, and be informed by the probabilistic binding data from micropipette. Through careful experimentation and research, the mechanism of cadherin interactions will be fully deduced.

References

1. Gumbiner, B.M., *Cell Adhesion: The Molecular Basis of Tissue Architecture and Morphogenesis.* Cell, 1996. **84**: p. 345-357.
2. Gumbiner, B.M., *Regulation of cadherin-mediated adhesion in morphogenesis.* Nat Rev Mol Cell Biol, 2005. **6**(8): p. 622-34.
3. Juliano, R.L., *SIGNAL TRANSDUCTION BY CELL ADHESION RECEPTORS AND THE CYTOSKELETON: Functions of Integrins, Cadherins, Selectins, and Immunoglobulin-Superfamily Members.* Annual Review of Pharmacology and Toxicology, 2002. **42**(1): p. 283-323.
4. Sperry., R.W., *Chemoaffnity in the orderly growth of nerve fiber patterns and connec-*

tions. . Proceedings of the National Academy of Sciences USA, 1963. **50**: p. 703-10.
5. Steinberg, M.S., *Reconstruction of tissues by dissociated cells. Some morphogenetic tissue movements and the sorting out of embryonic cells may have a common explanation.* Science, 1963. **141**: p. 401-8.
6. Lecuit, T. and P.F. Lenne, *Cell surface mechanics and the control of cell shape, tissue patterns and morphogenesis.* Nat Rev Mol Cell Biol, 2007. **8**(8): p. 633-44.
7. Manning, M.L., et al., *Coaction of intercellular adhesion and cortical tension specifies tissue surface tension.* Proceedings of the National Academy of Sciences, 2010. **107**(28): p. 12517-12522.
8. Krieg, M., et al., *Tensile forces govern germ-layer organization in zebrafish.* Nat Cell Biol, 2008. **10**: p. 429-36.
9. Takeichi, M., *Morphogenetic roles of classic cadherins.* Current Opinion in Cell Biology, 1995. **7**: p. 619-627.
10. Vincent, P.A., et al., *VE-cadherin: adhesion at arm's length.* American Journal of Physiology - Cell Physiology, 2004. **286**(5): p. C987-C997.
11. Zbar, A.P., C. Simopoulos, and A.J. Karayiannakis, *Cadherins: an integral role in inflammatory bowel disease and mucosal restitution.* Journal of Gastroenterology, 2004. **39**(5): p. 413-421.
12. Takeichi, M., *Cadherin cell adhesion receptors as a morphogenetic regulator.* Science, 1991. **251**: p. 1451-1455.
13. Detrick, R., Dickey, D., Kintner, C.R., *The effects of N-cadherin misexpression on morphogenesis in Xenopus embryos.* Neuron, 1990. **4**: p. 493-506.
14. Tepass, U., D. Godt, and R. Winklbauer, *Cell sorting in animal development: signalling and adhesive mechanisms in the formation of tissue boundaries.* Curr Opin Genet Dev, 2002. **12**(5): p. 572-82.
15. Fujimori, T., Miyatani, S., Takeichi, M., *Ectopic expression of N-cadherin perturbs histogenesis in Xenopus embryos.* Development, 1990. **110**: p. 97-104.
16. Radice, G.L., et al., *Developmental Defects in Mouse Embryos Lacking N-Cadherin.* Developmental Biology, 1997. **181**(1): p. 64-78.
17. Bronner-Fraser, M., J.J. Wolf, and B.A. Murray, *Effects of antibodies against N-cadherin and N-CAM on the cranial neural crest and neural tube.* Developmental Biology, 1992. **153**(2): p. 291-301.
18. Onder, T.T., et al., *Loss of E-Cadherin Promotes Metastasis via Multiple Downstream Transcriptional Pathways.* Cancer Research, 2008. **68**(10): p. 3645-3654.

19. Becker, K.-F., et al., *E-Cadherin Gene Mutations Provide Clues to Diffuse Type Gastric Carcinomas.* Cancer Research, 1994. **54**(14): p. 3845-3852.
20. Pertz, O., et al., *A new crystal structure, Ca2+ dependence and mutational analysis reveal molecular details of E-cadherin homoassociation.* EMBO J, 1999. **18**(7): p. 1738-47.
21. Häussinger, D., et al., *Calcium-dependent Homoassociation of E-cadherin by NMR Spectroscopy: Changes in Mobility, Conformation and Mapping of Contact Regions.* Journal of Molecular Biology, 2002. **324**(4): p. 823-839.
22. Boggon, T.J., et al., *C-cadherin ectodomain structure and implications for cell adhesion mechanisms.* Science, 2002. **296**(5571): p. 1308-13.
23. Brieher, W.M., A.S. Yap, and B.M. Gumbiner, *Lateral dimerization is required for the homophilic binding activity of C-cadherin.* J Cell Biol, 1996. **135**(2): p. 487-96.
24. Guo, H.-B., et al., *Regulation of Homotypic Cell-Cell Adhesion by Branched N-Glycosylation of N-cadherin Extracellular EC2 and EC3 Domains.* J Biol Chem, 2009. **284**(50): p. 34986-34997.
25. Liwosz, A., T. Lei, and M.A. Kukuruzinska, *N-Glycosylation Affects the Molecular Organization and Stability of E-cadherin Junctions.* Journal of Biological Chemistry, 2006. **281**(32): p. 23138-23149.
26. Harrison, O.J., et al., *The Extracellular Architecture of Adherens Junctions Revealed by Crystal Structures of Type I Cadherins.* Structure, 2011. **19**(2): p. 244-256.
27. Ciatto, C., et al., *T-cadherin structures reveal a novel adhesive binding mechanism.* Nat Struct Mol Biol, 2010. **17**(3): p. 339-347.
28. Harrison, O.J., et al., *Two-step adhesive binding by classical cadherins.* Nat Struct Mol Biol, 2010. **17**(3): p. 348-357.
29. Geng, F., et al., *The expression of core fucosylated E-cadherin in cancer cells and lung cancer patients: prognostic implications.* Cell Res, 2004. **14**(5): p. 423-433.
30. Nita-Lazar, M., et al., *Overexpression of DPAGT1 Leads to Aberrant N-Glycosylation of E-Cadherin and Cellular Discohesion in Oral Cancer.* Cancer Research, 2009. **69**(14): p. 5673-5680.
31. Pinho, S.S., et al., *Role of E-cadherin N-glycosylation profile in a mammary tumor model.* Biochemical and Biophysical Research Communications, 2009. **379**(4): p. 1091-1096.
32. Jamal, B.T., et al., *Glycosylation Status of E-cadherin Controls Cytoskeletal Dynamics through the Organization of Distinct β-catenin- and γ-catenin-containing AJs.* Cell Health and Cytoskeleton, 2009. **1**(1): p. 67-80.
33. Nose, A., A. Nagafuchi, and M. Takeichi, *Expressed recombinant cadherins mediate cell sorting in model systems.* Cell, 1988. **54**(7): p. 993-1001.
34. Nose, A., K. Tsuji, and M. Takeichi, *Localization of specificity determining sites in cadherin cell adhesion molecules.* Cell, 1990. **61**(1): p. 147-55.
35. Chappuis-Flament, S., et al., *Multiple cadherin extracellular repeats mediate homophilic binding and adhesion.* J Cell Biol, 2001. **154**(1): p. 231-43.
36. Shan, W., et al., *The Minimal Essential Unit for Cadherin-mediated Intercellular Adhesion Comprises Extracellular Domains 1 and 2.* Journal of Biological Chemistry, 2004. **279**(53): p. 55914-55923.
37. Foty, R.A. and M.S. Steinberg, *The differential adhesion hypothesis: a direct evaluation.* Dev Biol, 2005. **278**(1): p. 255-63.
38. Steinberg, M.S., *Differential adhesion in morphogenesis: a modern view.* Current Opinion in Genetics & Development, 2007. **17**(4): p. 281-286.
39. Katsamba, P., et al., *Linking molecular affinity and cellular specificity in cadherin-mediated adhesion.* Proc Natl Acad Sci U S A, 2009. **106**(28): p. 11594-9.
40. Langer, M.D., *Surface Plasmon Resonance Studies of E-cadherin Binding*, in *Chemical Engineering*. 2006, University of Illinois-Urbana Champaign: Urbana.

41. Zhang, Y., et al., *Resolving cadherin interactions and binding cooperativity at the single-molecule level.* Proceedings of the National Academy of Sciences, 2009. **106**(1): p. 109-114.
42. Sivasankar, S., et al., *Characterizing the Initial Encounter Complex in Cadherin Adhesion.* Structure (London, England : 1993), 2009. **17**(8): p. 1075-1081.
43. Duguay, D., R.A. Foty, and M.S. Steinberg, *Cadherin-mediated cell adhesion and tissue segregation: qualitative and quantitative determinants.* Dev. Biol., 2003. **253**: p. 309-23.
44. Niessen, C.M. and B.M. Gumbiner, *Cadherin-mediated cell sorting not determined by binding or adhesion specificity.* J Cell Biol, 2002. **156**(2): p. 389-399.
45. Leckband, D. and J. Israelachvili, *Intermolecular forces in biology.* Q Rev Biophys, 2001. **34**(2): p. 105-267.
46. Sivasankar, S., B. Gumbiner, and D. Leckband, *Direct measurements of multiple adhesive alignments and unbinding trajectories between cadherin extracellular domains.* Biophys J, 2001. **80**(4): p. 1758-68.
47. Zhu, B., et al., *Functional Analysis of the Structural Basis of Homophilic Cadherin Adhesion.* Biophys J, 2003. **84**(4033-42).
48. Prakasam, A.K., V. Maruthamuthu, and D.E. Leckband, *Similarities between heterophilic and homophilic cadherin adhesion.* Proc Natl Acad Sci U S A, 2006. **103**(42): p. 15434-9.
49. Evans, E., Ritchie, K., *Dynamic Strength of Molecular Adhesion Bonds.* Biophys J, 1997. **72**: p. 1541-55.
50. Bayas, M.V., et al., *Lifetime measurements reveal kinetic differences between homophilic cadherin bonds.* Biophys J, 2006. **90**(4): p. 1385-95.
51. Perret, E., et al., *Trans-bonded pairs of E-cadherin exhibit a remarkable hierarchy of mechanical strengths.* Proc Natl Acad Sci U S A, 2004. **101**(47): p. 16472-7.
52. Shi, Q., et al., *Allosteric Cross Talk between Cadherin Extracellular Domains.* Biophysical Journal, 2010. **99**(1): p. 95-104.
53. Chesla, S.E., P. Selvaraj, and C. Zhu, *Measuring two-dimensional receptor-ligand binding kinetics by micropipette.* Biophys J, 1998. **75**(3): p. 1553-72.
54. Chesla, S.E., et al., *The membrane anchor influences ligand binding two-dimensional kinetic rates and three-dimensional affinity of FcgammaRIII (CD16).* J Biol Chem, 2000. **275**(14): p. 10235-46.
55. Huang, J., et al., *Quantifying the effects of molecular orientation and length on two-dimensional receptor-ligand binding kinetics.* J Biol Chem, 2004. **279**(43): p. 44915-23.
56. Huang, J., et al., *Kinetics of MHC-CD8 interaction at the T cell membrane.* J Immunol, 2007. **179**(11): p. 7653-62.
57. Huang, J., et al., *The kinetics of two-dimensional TCR and pMHC interactions determine T-cell responsiveness.* Nature, 2010. **464**(7290): p. 932-936.
58. Chien, Y.H., et al., *Two stage cadherin kinetics require multiple extracellular domains but not the cytoplasmic region.* J Biol Chem, 2008. **283**(4): p. 1848-56.
59. Yap, A.S., et al., *Lateral clustering of the adhesive ectodomain: a fundamental determinant of cadherin function.* Curr Biol, 1997. **7**(5): p. 308-15.
60. Troyanovsky, R.B., E. Sokolov, and S.M. Troyanovsky, *Adhesive and lateral E-cadherin dimers are mediated by the same interface.* Mol Cell Biol, 2003. **23**(22): p. 7965-72.
61. Wu, Y., et al., *Transforming binding affinities from three dimensions to two with application to cadherin clustering.* Nature, 2011. **475**(7357): p. 510-513.
62. Williams, T.E., et al., *Quantifying the impact of membrane microtopology on effective two-dimensional affinity.* J Biol Chem, 2001. **276**(16): p. 13283-8.
63. Chen, C.P., et al., *Specificity of cell-cell adhesion by classical cadherins: Critical role for low-affinity dimerization through beta-strand swapping.* Proc Natl Acad Sci U S A, 2005. **102**(24): p. 8531-6.

64. Renaud-Young, M. and W.J. Gallin, *In the First Extracellular Domain of E-cadherin, Heterophilic Interactions, but Not the Conserved His-Ala-Val Motif, Are Required for Adhesion.* Journal of Biological Chemistry, 2002. **277**(42): p. 39609-39616.
65. Chappuis-Flament, S., et al., *Multiple cadherin extracellular repeats mediate homophilic binding and adhesion.* The Journal of Cell Biology, 2001. **154**(1): p. 231-243.
66. Steinberg, M.S., *Differential adhesion in morphogenesis: a modern view.* Curr Opin Genet Dev, 2007. **17**: p. 281-6.
67. Shi, Q., Y.H. Chien, and D. Leckband, *Biophysical properties of cadherin bonds do not predict cell sorting.* J Biol Chem, 2008. **283**(42): p. 28454-63.
68. Jiang, N., et al., *Two-stage cooperative T cell receptor-peptide major histocompatibility complex-CD8 trimolecular interactions amplify antigen discrimination.* Immunity, 2011. **34**(1): p. 13-23.
69. Leckband, D., *Measuring the forces that control protein interactions.* Annu Rev Biophys Biomol Struct, 2000. **29**: p. 1-26.
70. Long, M., et al., *Kinetic measurements of cell surface E-selectin/carbohydrate ligand interactions.* Annals Biomed Eng, 2001. **29**(11): p. 935-46.
71. Zhang, F., et al., *Two-dimensional kinetics regulation of alphaLbeta2-ICAM-1 interaction by conformational changes of the alphaL-inserted domain.* J Biol Chem, 2005. **280**(51): p. 42207-18.
72. Ahrens, T., et al., *Analysis of heterophilic and homophilic interactions of cadherins using the c-Jun/c-Fos dimerization domains.* J Biol Chem, 2002. **277**(22): p. 19455-60.
73. Klingelhofer, J., et al., *Amino-terminal domain of classic cadherins determines the specificity of the adhesive interactions.* J Cell Sci, 2000. **113**(16): p. 2829-2836.
74. Dumaswala, U.J., et al., *Glutamine- and phosphate-containing hypotonic storage media better maintain erythrocyte membrane physical properties.* Blood, 1996. **88**(2): p. 697-704.
75. Gold, E.R. and H.H. Fudenberg, *Chromic chloride: a coupling reagent for passive hemagglutination reactions.* J Immunol, 1967. **99**(5): p. 859-66.
76. Kofler, R. and G. Wick, *Some methodologic aspects of the chromium chloride method for coupling antigen to erythrocytes.* J Immunol Methods, 1977. **16**(3): p. 201-9.
77. Evans, E., et al., *Mechanical switching and coupling between two dissociation pathways in a P-selectin adhesion bond.* Proceedings of the National Academy of Sciences of the United States of America, 2004. **101**(31): p. 11281-11286.
78. Shapiro, L., et al., *Structural basis of cell-cell adhesion by cadherins.* Nature, 1995. **374**(6520): p. 327-37.
79. Tamura, K., et al., *Structure-function analysis of cell adhesion by neural (N-) cadherin.* Neuron, 1998. **20**(6): p. 1153-63.
80. Pokutta, S. and W.I. Weis, *Structure and mechanism of cadherins and catenins in cell-cell contacts.* Annu Rev Cell Dev Biol, 2007. **23**: p. 237-61.
81. Nose, A., A. Nagafuchi, and M. Takeichi, *Expressed recombinant cadherins mediate cell sorting in model systems.* Cell, 1988. **54**: p. 993-1001.
82. Niessen, C.M. and B.M. Gumbiner, *Cadherin-mediated cell sorting not determined by binding or adhesion specificity.* J. Cell. Biol., 2002. **156**: p. 389-99.
83. Tamura, K., et al., *Structure-Function Analysis of Cell Adhesion by Neural (N-) Cadherin.* Neuron, 1998. **20**: p. 1153-63.
84. Nose, A., K. Tsuji, and M. Takeichi, *Localization of specificity determining sites in cadherin cell adhesion molecules.* Cell, 1990. **61**: p. 147-55.
85. Harrison, O.J., et al., *The mechanism of cell adhesion by classical cadherins: the role of domain 1.* J Cell Sci, 2005. **118**(Pt 4): p. 711-21.
86. Prakasam, A., et al., *Calcium site mutations in cadherin: impact on adhesion and evidence of cooperativity.* Biochemistry, 2006. **49**: p. 6930-39.

87. Prakasam, A., V. Maruthamuthu, and D.E. Leckband, *Similarities between Heterophilic and Homophilic Cadherin Adhesion.* Proc. Natl. Acad. Sci., 2006. **103**: p. 15434-39.
88. Shi, Q., Y.H. Chien, and D. Leckband, *Biophysical properties of cadherin bonds do not predict cell sorting.* J Biol Chem, 2008.
89. Weis, W.I. and W.J. Nelson, *Re-solving the cadherin-catenin-actin conundrum.* J Biol Chem, 2006. **281**(47): p. 35593-7.
90. Hynes, R.O., *Integrins: bidirectional, allosteric signaling machines.* Cell, 2002. **110**(6): p. 673-87.
91. Wong, A.S. and B.M. Gumbiner, *Adhesion-independent mechanism for suppression of tumor cell invasion by E-cadherin.* J Cell Biol, 2003. **161**(6): p. 1191-203.
92. Nakagawa, M., et al., *Recruitment and activation of Rac1 by the formation of E-cadherin-mediated cell-cell adhesion sites.* J Cell Sci, 2001. **114**(Pt 10): p. 1829-38.
93. Geng, F., et al., *The expression of core fucosylated E-cadherin in cancer cells and lung cancer patients: prognostic implications.* Cell Res, 2004. **14**(5): p. 423-33.
94. Guo, H.B., et al., *Regulation of homotypic cell-cell adhesion by branched N-glycosylation of N-cadherin extracellular EC2 and EC3 domains.* J Biol Chem, 2009. **284**(50): p. 34986-97.
95. Jamal, B.T., et al., *N-glycosylation status of E-cadherin controls cytoskeletal dynamics through the organization of distinct beta-catenin- and gamma-catenin-containing AJs.* Cell health and cytoskeleton, 2009. **2009**(1): p. 67-80.
96. Nita-Lazar, M., et al., *Hypoglycosylated E-cadherin promotes the assembly of tight junctions through the recruitment of PP2A to adherens junctions.* Exp Cell Res, 2010. **316**(11): p. 1871-84.
97. Pinho, S.S., et al., *Modulation of E-cadherin function and dysfunction by N-glycosylation.* Cell Mol Life Sci, 2011. **68**(6): p. 1011-20.
98. Kitada, T., et al., *The addition of bisecting N-acetylglucosamine residues to E-cadherin down-regulates the tyrosine phosphorylation of beta-catenin.* J Biol Chem, 2001. **276**(1): p. 475-80.
99. Vagin, O., et al., *Inverse Correlation between the Extent of N-Glycan Branching and Intercellular Adhesion in Epithelia.* J Biol Chem, 2008. **283**(4): p. 2192-2202.
100. Nita-Lazar, M., et al., *Overexpression of DPAGT1 Leads to Aberrant N-Glycosylation of E-Cadherin and Cellular Discohesion in Oral Cancer.* Cancer Res, 2009. **69**(14): p. 5673-5680.
101. Pinho, S.S., et al., *Role of E-cadherin N-glycosylation profile in a mammary tumor model.* Biochim Biophys Res Comm, 2009. **379**(4): p. 1091-6.
102. Pinho, S.S., et al., *The role of N-acetylglucosaminyltransferase III and V in the post-transcriptional modifications of E-cadherin.* Human molecular genetics, 2009. **18**(14): p. 2599-608.
103. Liwosz, A., T. Lei, and M.A. Kukuruzinska, *N-glycosylation affects the molecular organization and stability of E-cadherin junctions.* J Biol Chem, 2006. **281**(32): p. 23138-49.
104. Doherty, P. and F.S. Walsh, *CAM-FGF receptor interactions: a model for axonal growth.* Mol Cell Neurosci, 1996. **8**(2-3): p. 99-111.
105. Gumbiner, B.M., *Cell adhesion: the molecular basis of tissue architecture and morphogenesis.* Cell, 1996. **84**(3): p. 345-57.
106. Perrais, M., et al., *E-Cadherin Homophilic Ligation Inhibits Cell Growth and Epidermal Growth Factor Receptor Signaling Independent of Other Cell Interactions.* Mol Biol Cell, 2007. **18**(6): p. 2013-25.
107. Tzima, E., et al., *A mechanosensory complex that mediates the endothelial cell response to fluid shear stress.* Nature, 2005. **437**(7057): p. 426-31.
108. Williams, E.J., et al., *Identification of an N-cadherin motif that can interact with the fibroblast growth factor receptor and is required for axonal growth.* J Biol Chem, 2001. **276**(47): p. 43879-86.

109. Leckband, D. and A. Prakasam, *Mechanism and dynamics of cadherin adhesion.* Annu Rev Biomed Eng, 2006. **8**: p. 259-87.
110. Guo, H.-B., et al., *Aberrant N-Glycosylation of β1 Integrin Causes Reduced α5β1 Integrin Clustering and Stimulates Cell Migration.* Cancer Research, 2002. **62**(23): p. 6837-6845.
111. Huang, J., et al., *The kinetics of two-dimensional TCR and pMHC interactions determine T-cell responsiveness.* Nature, 2010. **464**(7290): p. 932-6.
112. Evans, E., et al., *Mechanical switching and coupling between two dissociation pathways in a P-selectin adhesion bond.* Proc Natl Acad Sci U S A, 2004. **101**(31): p. 11281-11286.
113. Gavard, J., et al., *Lamellipodium extension and cadherin adhesion: two cell responses to cadherin activation relying on distinct signalling pathways.* J Cell Sci, 2004. **117**(Pt 2): p. 257-70.
114. Sivasankar, S., et al., *Characterizing the initial encounter complex in cadherin adhesion.* Structure, 2009. **17**(8): p. 1075-81.
115. Harrison, O.J., et al., *Two-step adhesive binding by classical cadherins.* Nat Struct Mol Biol, 2010. **17**(3): p. 348-57.
116. Bajpai, S., et al., *{alpha}-Catenin mediates initial E-cadherin-dependent cell-cell recognition and subsequent bond strengthening.* Proc Natl Acad Sci U S A, 2008. **105**(47): p. 18331-6.
117. Zhao, H., et al., *N-glycosylation affects the adhesive function of E-Cadherin through modifying the composition of adherens junctions (AJs) in human breast carcinoma cell line MDA-MB-435.* J Cell Biochem, 2008. **104**(1): p. 162-75.
118. Johnson, C.P., et al., *Direct evidence that neural cell adhesion molecule (NCAM) polysialylation increases intermembrane repulsion and abrogates adhesion.* J Biol Chem, 2005. **280**(1): p. 137-45.
119. Harrison, O.J., et al., *The extracellular architecture of adherens junctions revealed by crystal structures of type I cadherins.* Structure, 2011. **19**(2): p. 244-56.
120. Brasch, J., et al., *Structure and binding mechanism of vascular endothelial cadherin: a divergent classical cadherin.* J Mol Biol, 2011. **408**(1): p. 57-73.
121. Ciołczyk-Wierzbicka, D., et al., *The structure of the oligosaccharides of N-cadherin from human melanoma cell lines.* Glycoconjugate J, 2003. **20**(7): p. 483-492.
122. Zhang, Y., et al., *Resolving cadherin interactions and binding cooperativity at the single-molecule level.* Proc Natl Acad Sci U S A, 2009. **106**(1): p. 109-14.

Appendix A

Kinetic Curves Obtained through Micropipette Experiments

This appendix contains the kinetic curves analyzed in this dissertation. The cell type and protein construct used are documented in the title of each graph. Each graph displays the average binding probability at each time point with the standard deviation. When applicable, the model fit for the first phase is shown with a solid line, and the 95% confidence interval of the fit is shown with dotted lines. All kinetic parameters from the fits are given at the end of the appendix. (Table A.1)

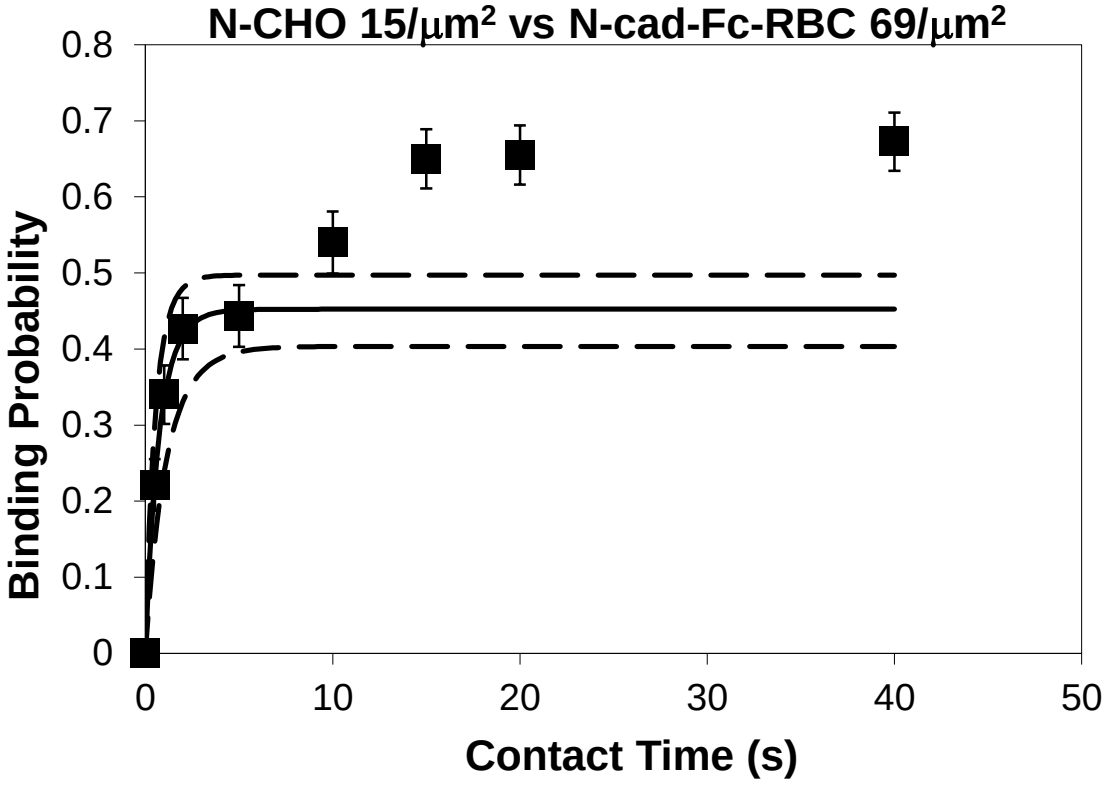
N-CHO 15/μm² vs N-cad-Fc-RBC 69/μm²
Binding Probability
0.8
0.7
0.6
0.5
0.4
0.3
0.2
0.1
0
0
10
20
30
40
50
Contact Time (s)

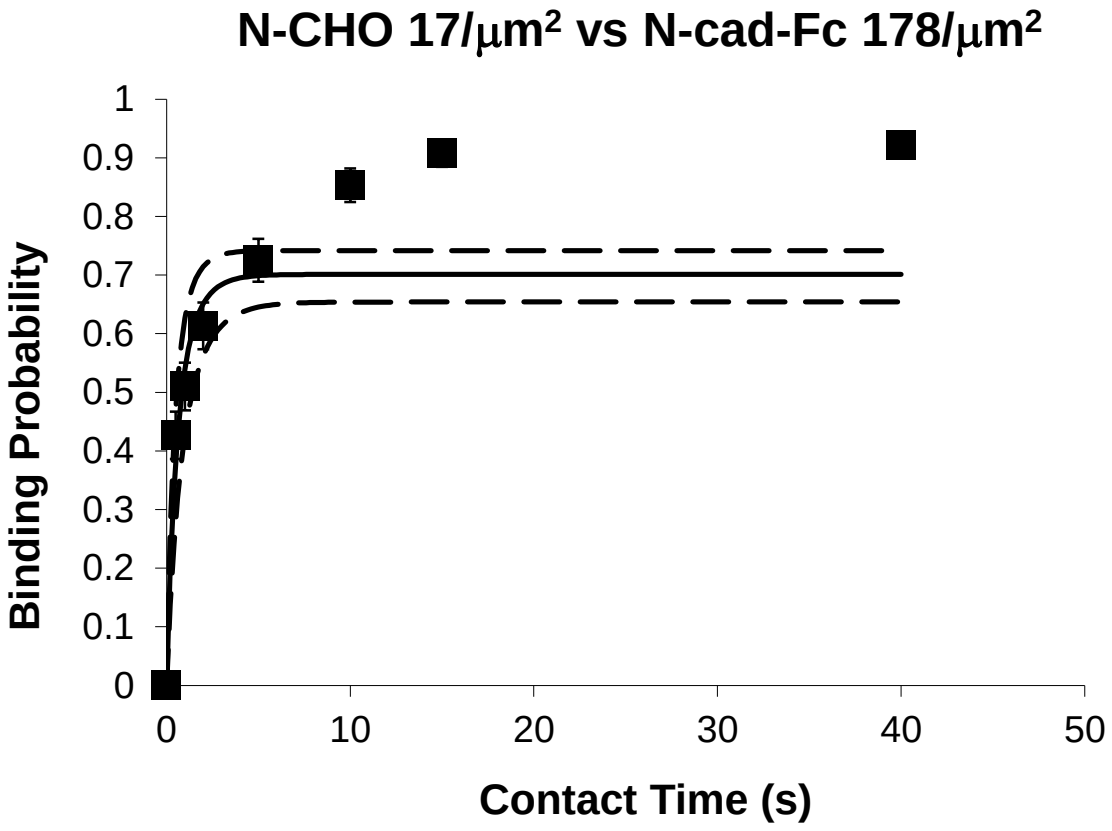
N-CHO 17/μm² vs N-cad-Fc 178/μm²
Binding Probability
1
0.9
0.8
0.7
0.6
0.5
0.4
0.3
0.2
0.1
0
0
10
20
30
40
50
Contact Time (s)

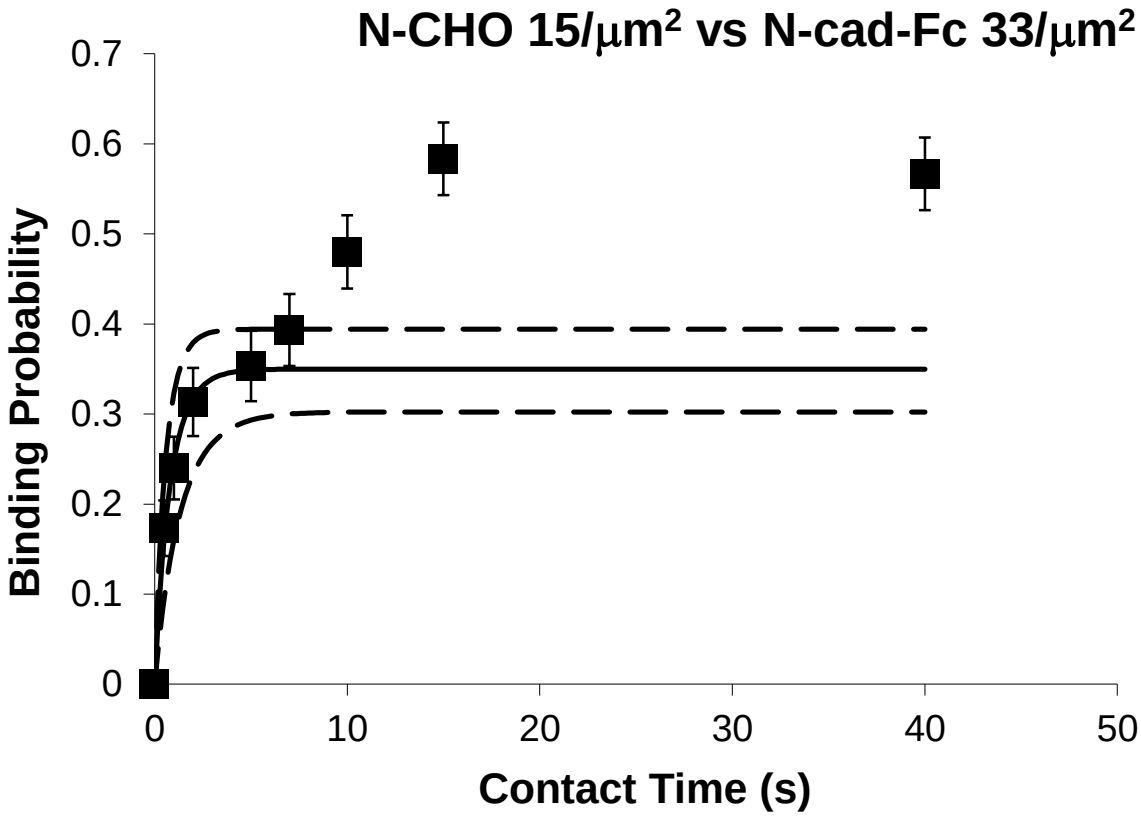
N-CHO 15/μm² vs N-cad-Fc 33/μm²
Binding Probability
0.7
0.6
0.5
0.4
0.3
0.2
0.1
0
0
10
20
30
40
50
Contact Time (s)

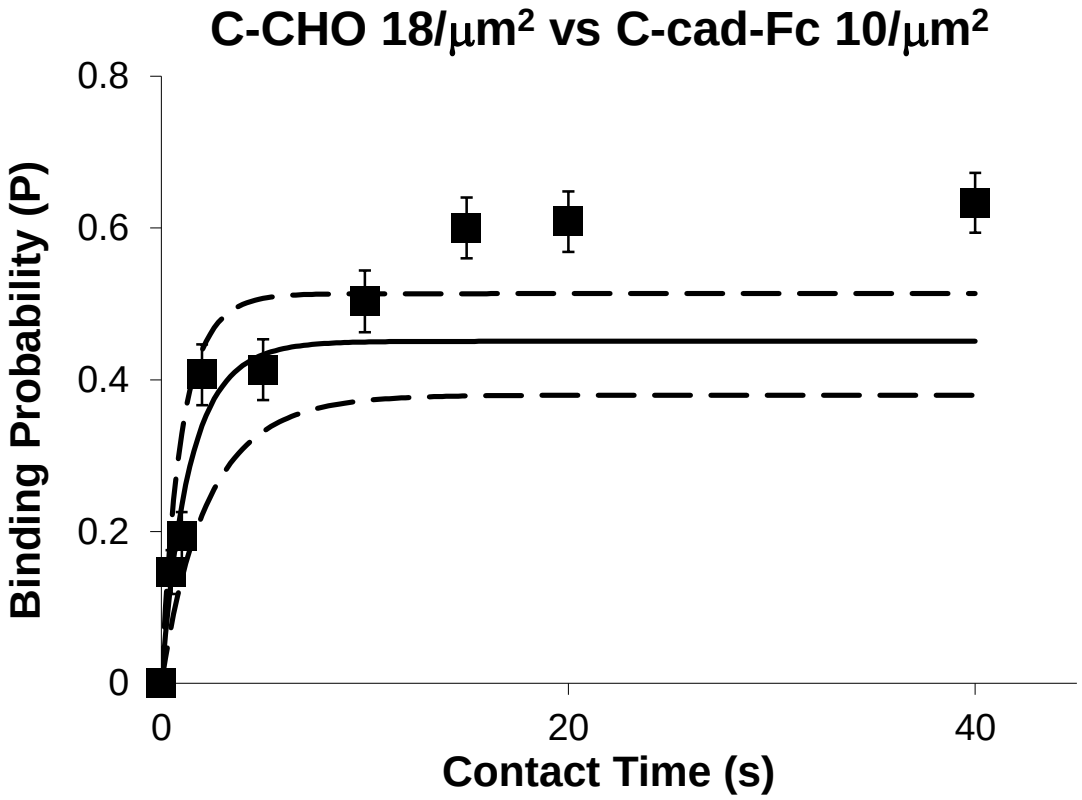
C-CHO 18/μm² vs C-cad-Fc 10/μm²
Binding Probability (P)
0.8
0.6
0.4
0.2
0
0
20
40
Contact Time (s)

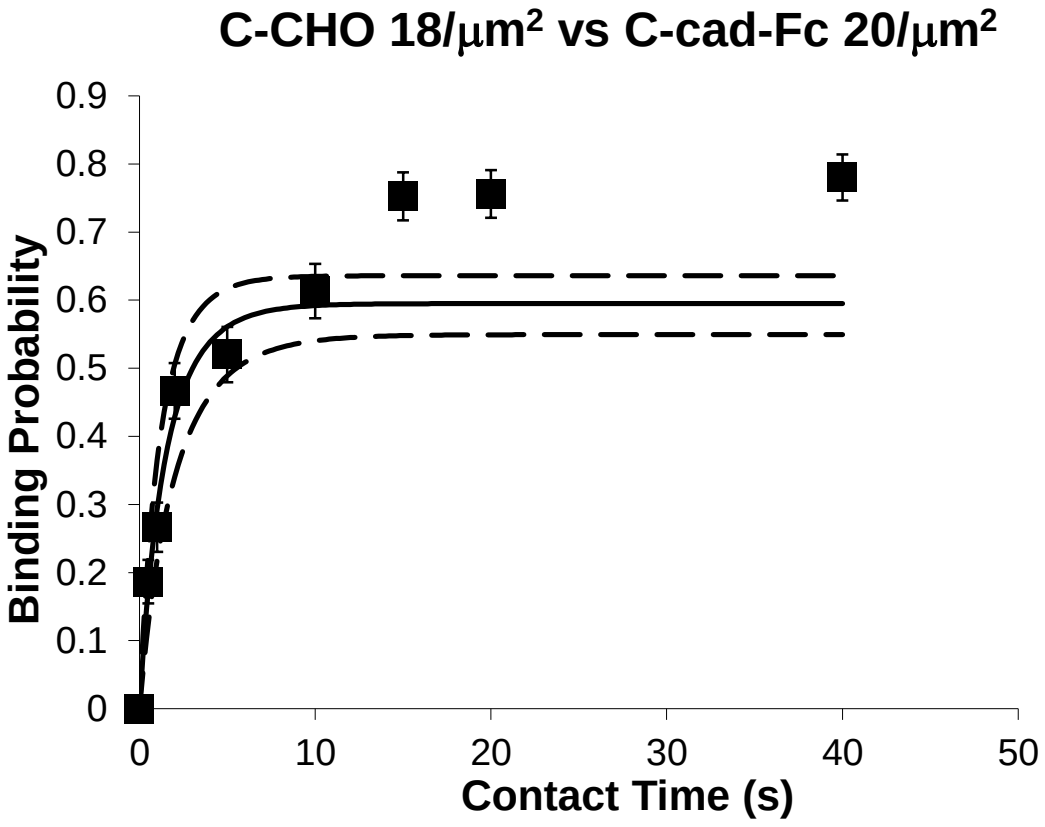
C-CHO 18/μm² vs C-cad-Fc 20/μm²
Binding Probability
0.9
0.8
0.7
0.6
0.5
0.4
0.3
0.2
0.1
0
0
10
20
30
40
50
Contact Time (s)

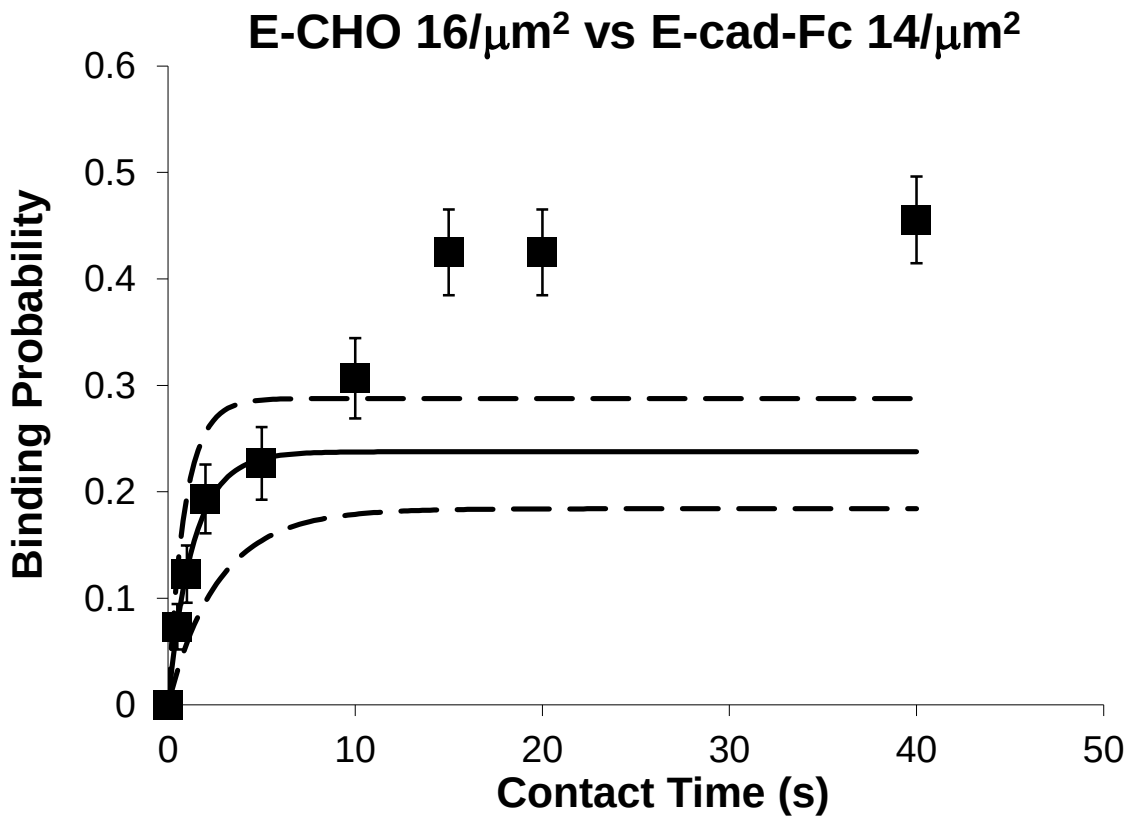
E-CHO 16/μm² vs E-cad-Fc 14/μm²
Binding Probability
0.6
0.5
0.4
0.3
0.2
0.1
0
0
10
20
30
40
50
Contact Time (s)

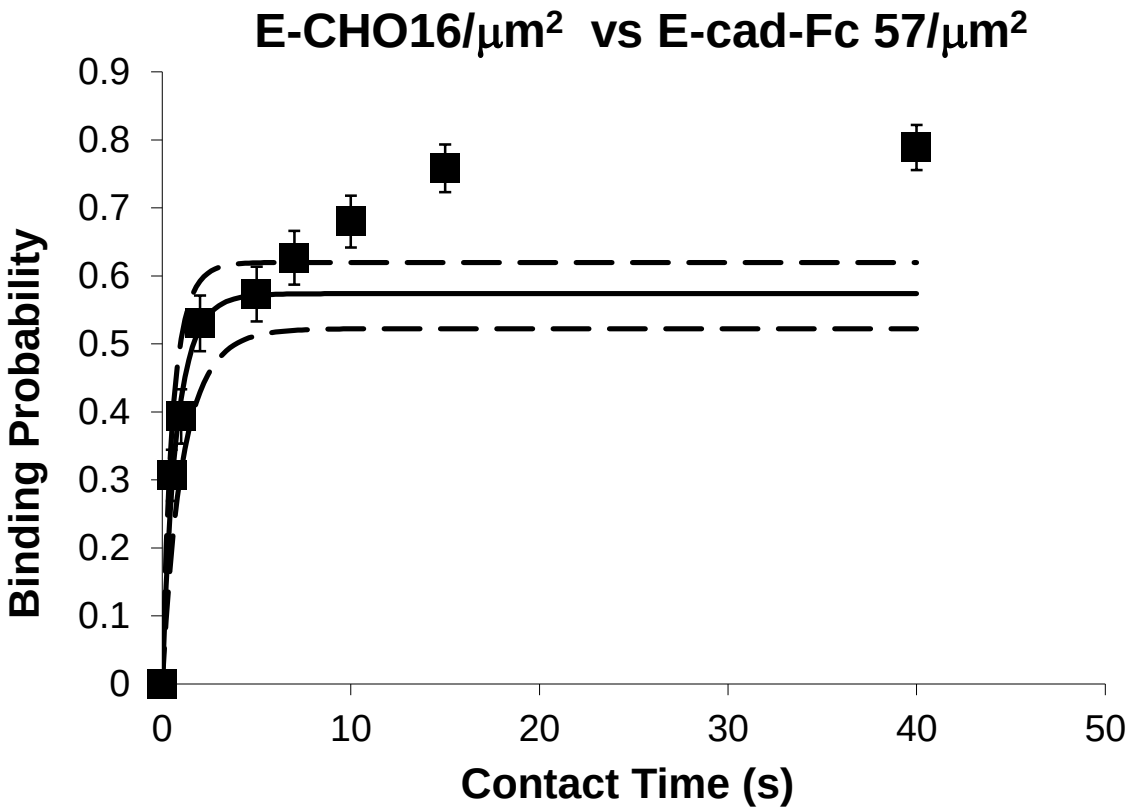
E-CHO16/μm² vs E-cad-Fc 57/μm²
Binding Probability
0.9
0.8
0.7
0.6
0.5
0.4
0.3
0.2
0.1
0
0
10
20
30
40
50
Contact Time (s)

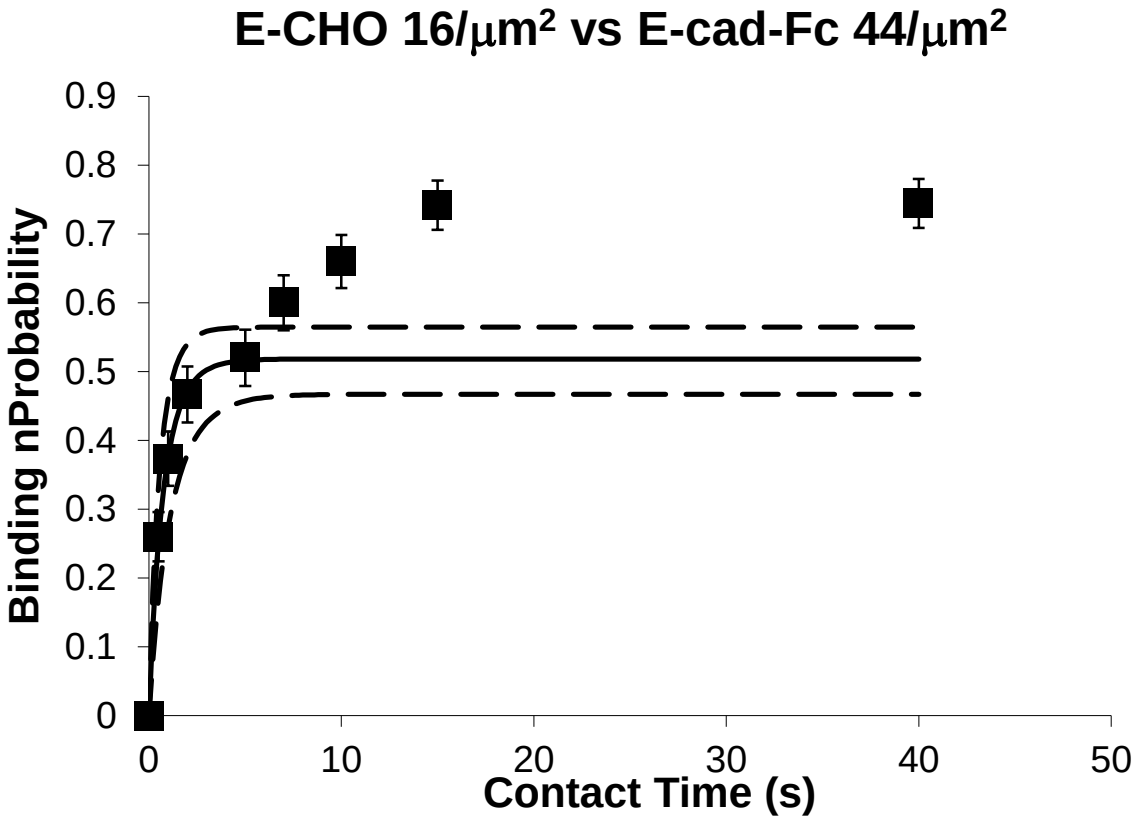
E-CHO 16/μm² vs E-cad-Fc 44/μm²
Binding nProbability
0.9
0.8
0.7
0.6
0.5
0.4
0.3
0.2
0.1
0
0
10
20
30
40
50
Contact Time (s)

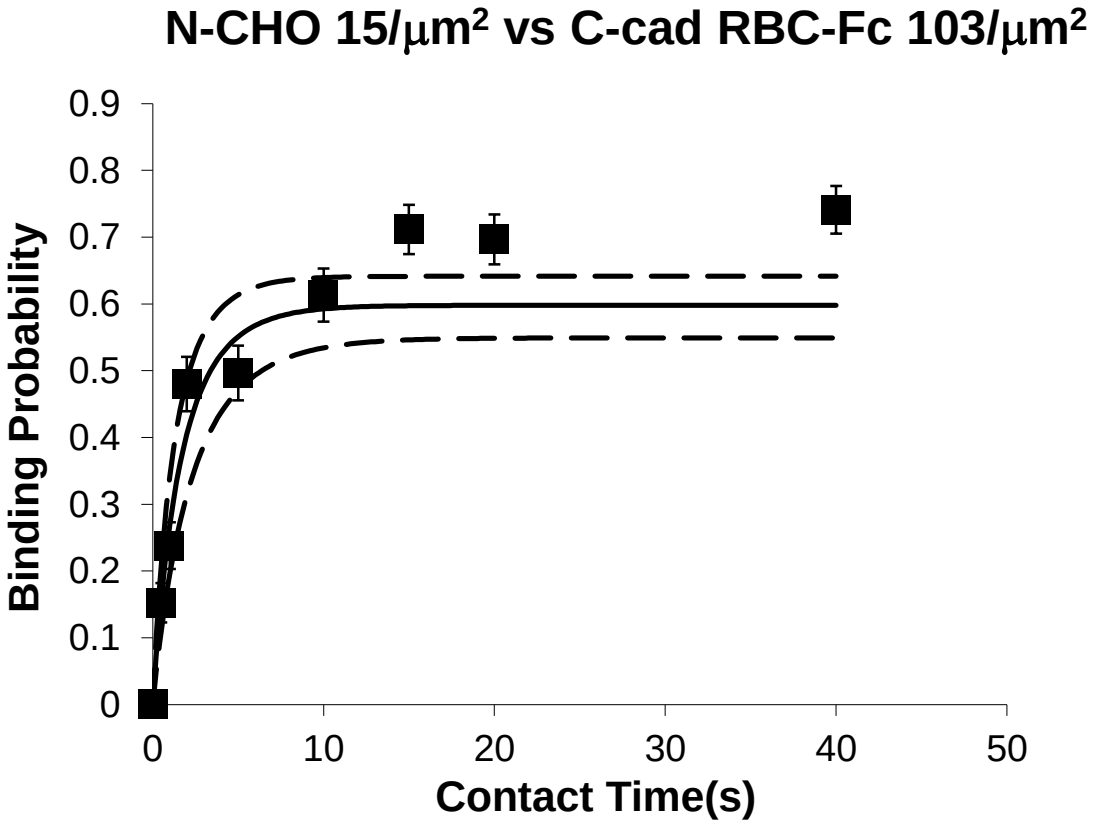
N-CHO 15/μm² vs C-cad RBC-Fc 103/μm²
Binding Probability
0.9
0.8
0.7
0.6
0.5
0.4
0.3
0.2
0.1
0
0
10
20
30
40
50
Contact Time(s)

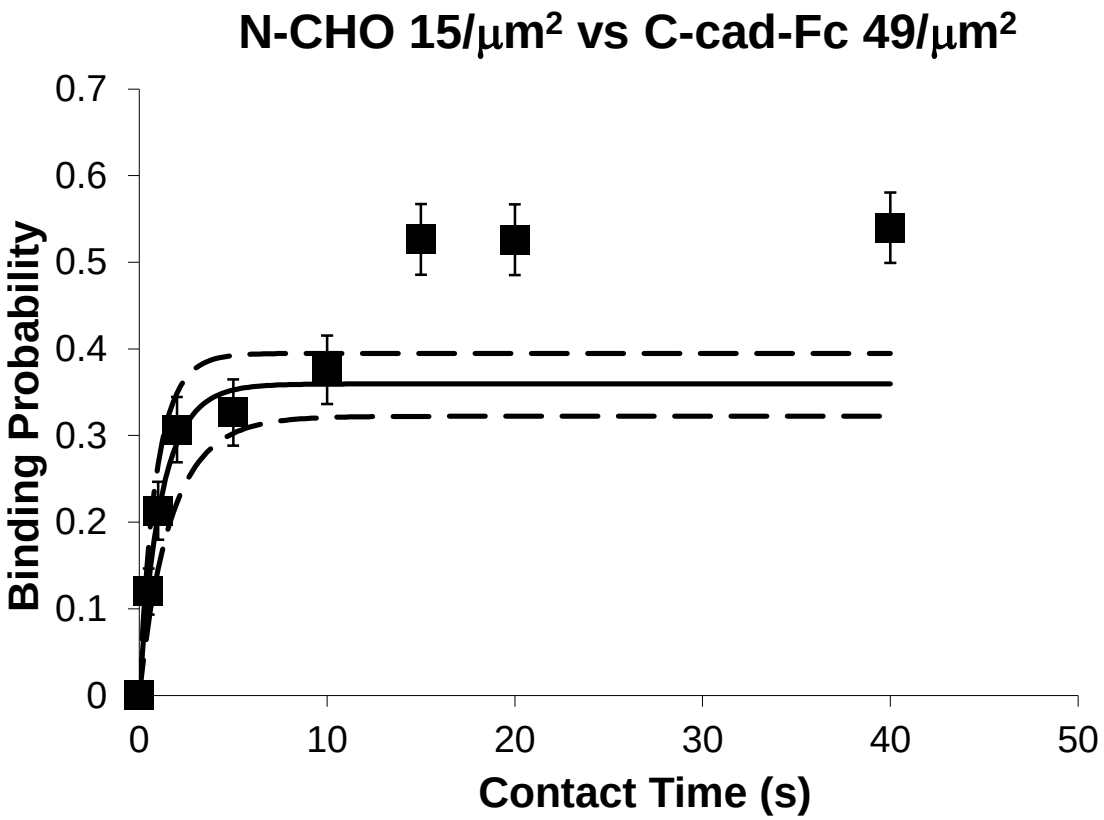
N-CHO 15/μm² vs C-cad-Fc 49/μm²
Binding Probability
0.7
0.6
0.5
0.4
0.3
0.2
0.1
0
0
10
20
30
40
50
Contact Time (s)

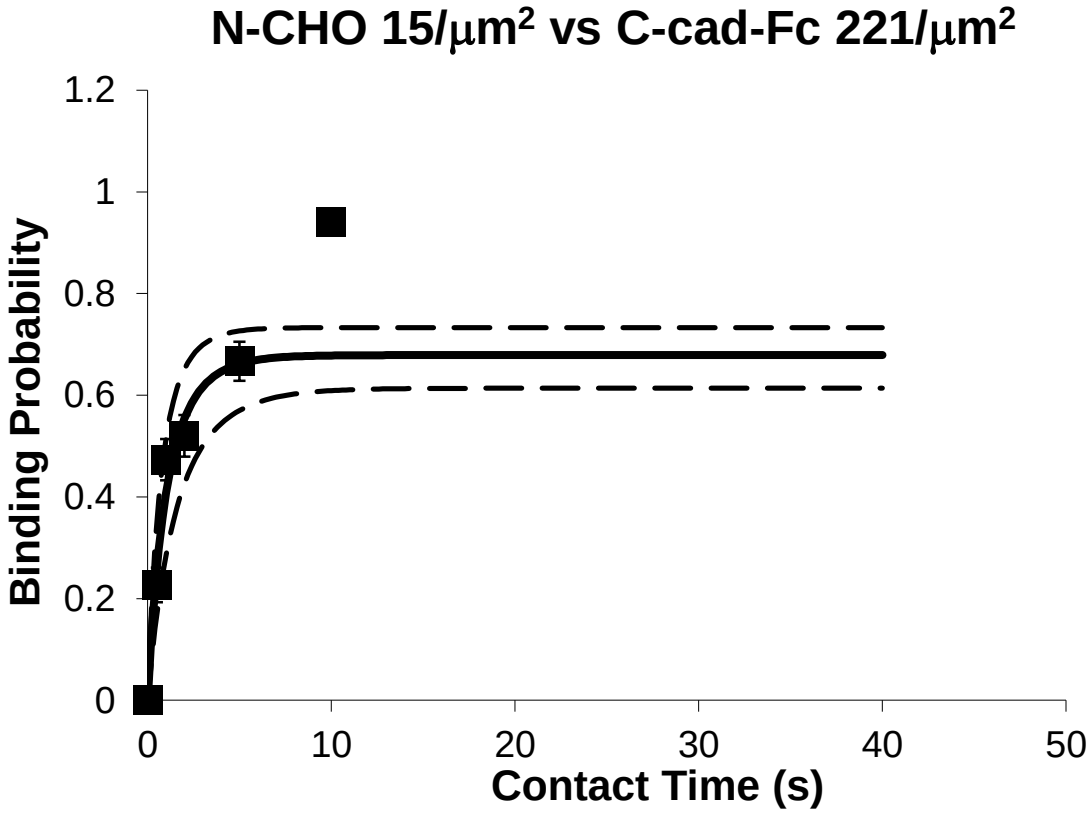
N-CHO 15/μm² vs C-cad-Fc 221/μm²
Binding Probability
1.2
1
0.8
0.6
0.4
0.2
0
0
10
20
30
40
50
Contact Time (s)

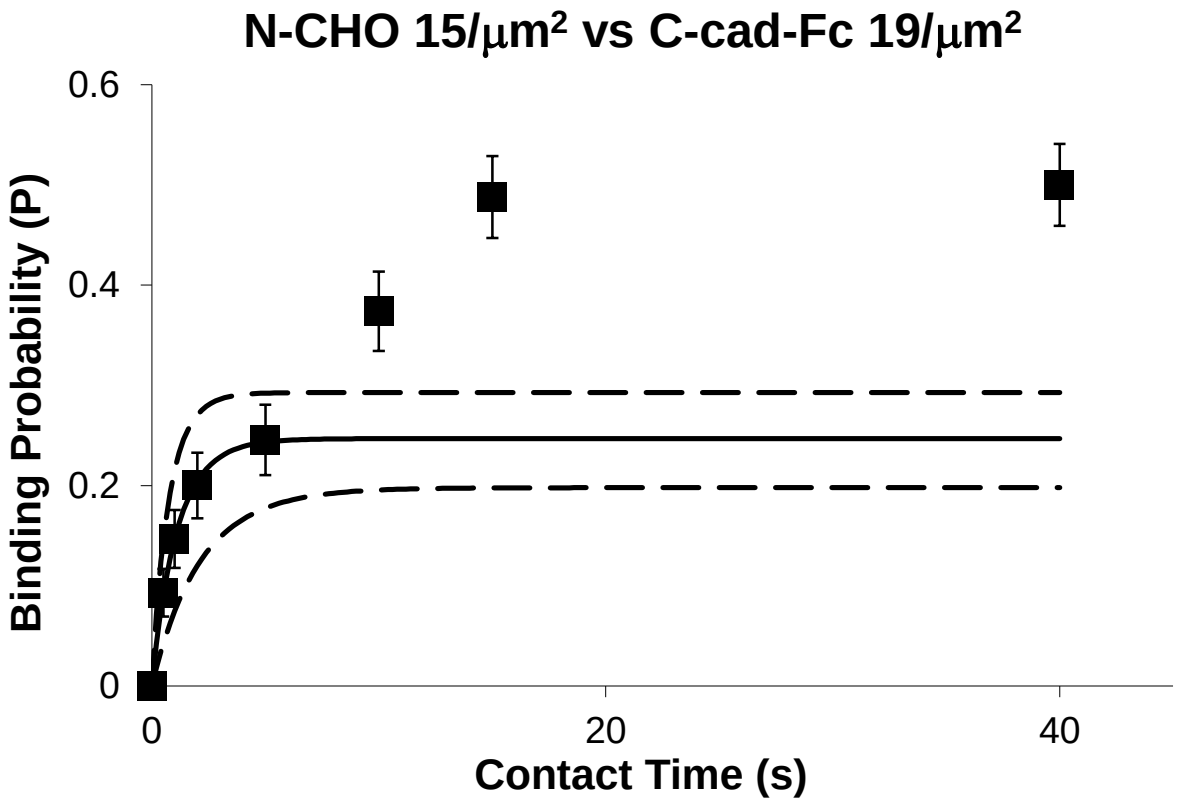
N-CHO 15/μm² vs C-cad-Fc 19/μm²
Binding Probability (P)
0.6
0.4
0.2
0
0
20
40
Contact Time (s)

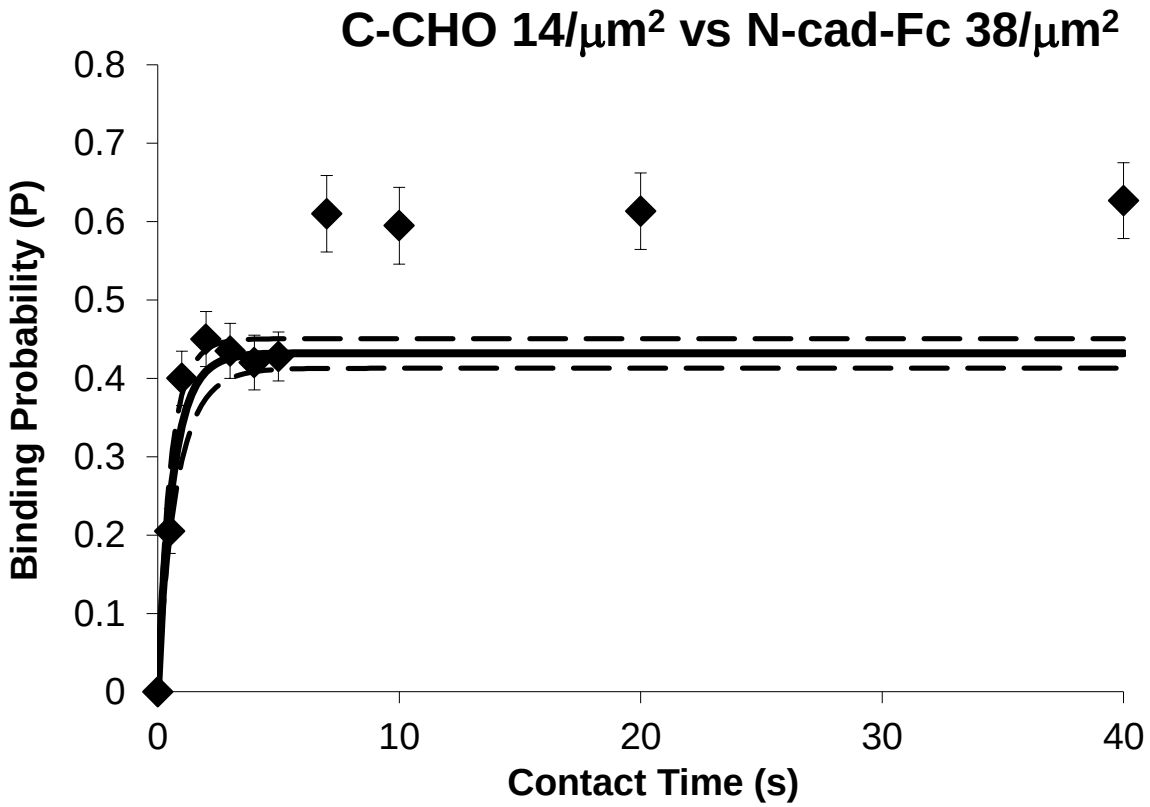
C-CHO 14/μm² vs N-cad-Fc 38/μm²
Binding Probability (P)
0.8
0.7
0.6
0.5
0.4
0.3
0.2
0.1
0
0
10
20
30
40
Contact Time (s)

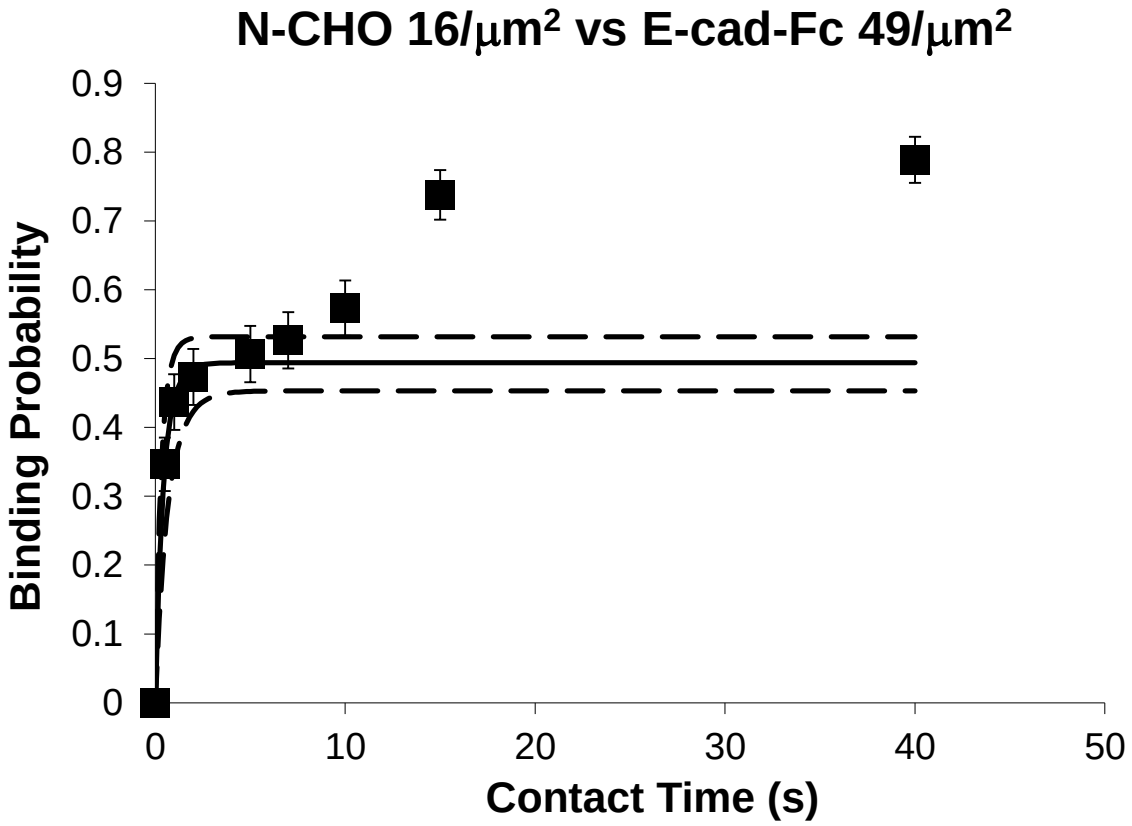
N-CHO 16/μm² vs E-cad-Fc 49/μm²
Binding Probability
0.9
0.8
0.7
0.6
0.5
0.4
0.3
0.2
0.1
0
0
10
20
30
40
50
Contact Time (s)

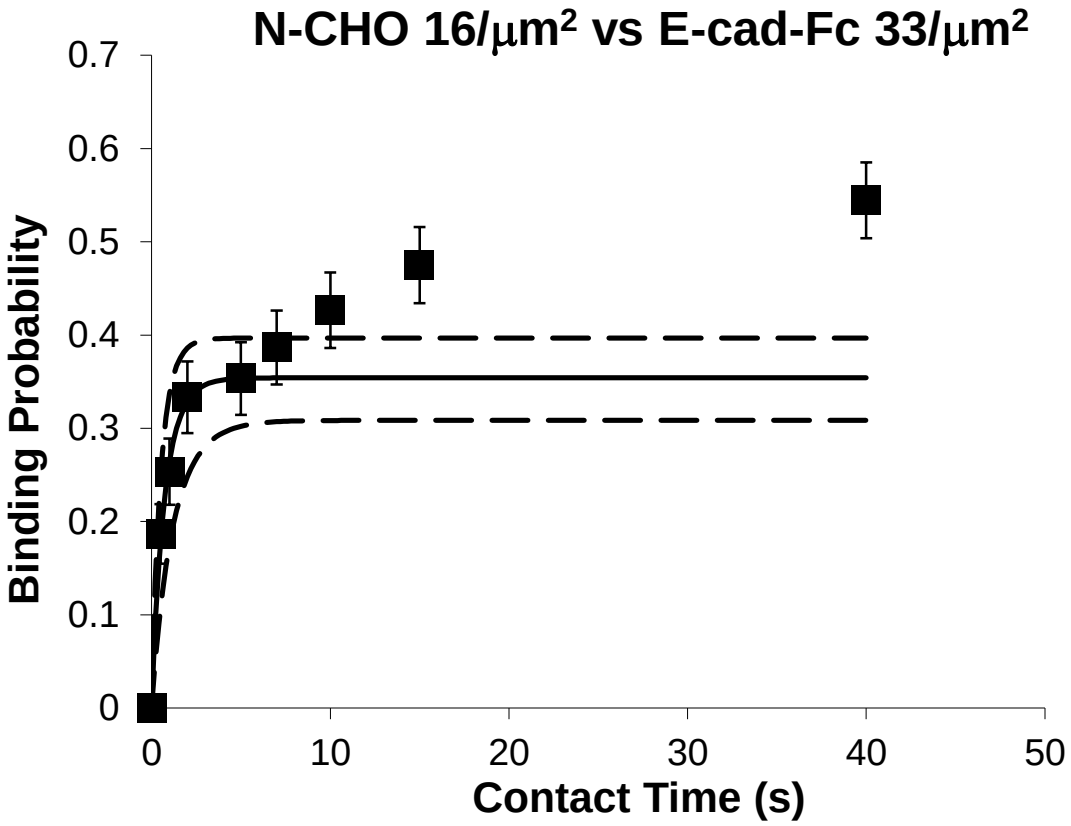
N-CHO 16/μm² vs E-cad-Fc 33/μm²
Binding Probability
0.7
0.6
0.5
0.4
0.3
0.2
0.1
0
0
10
20
30
40
50
Contact Time (s)

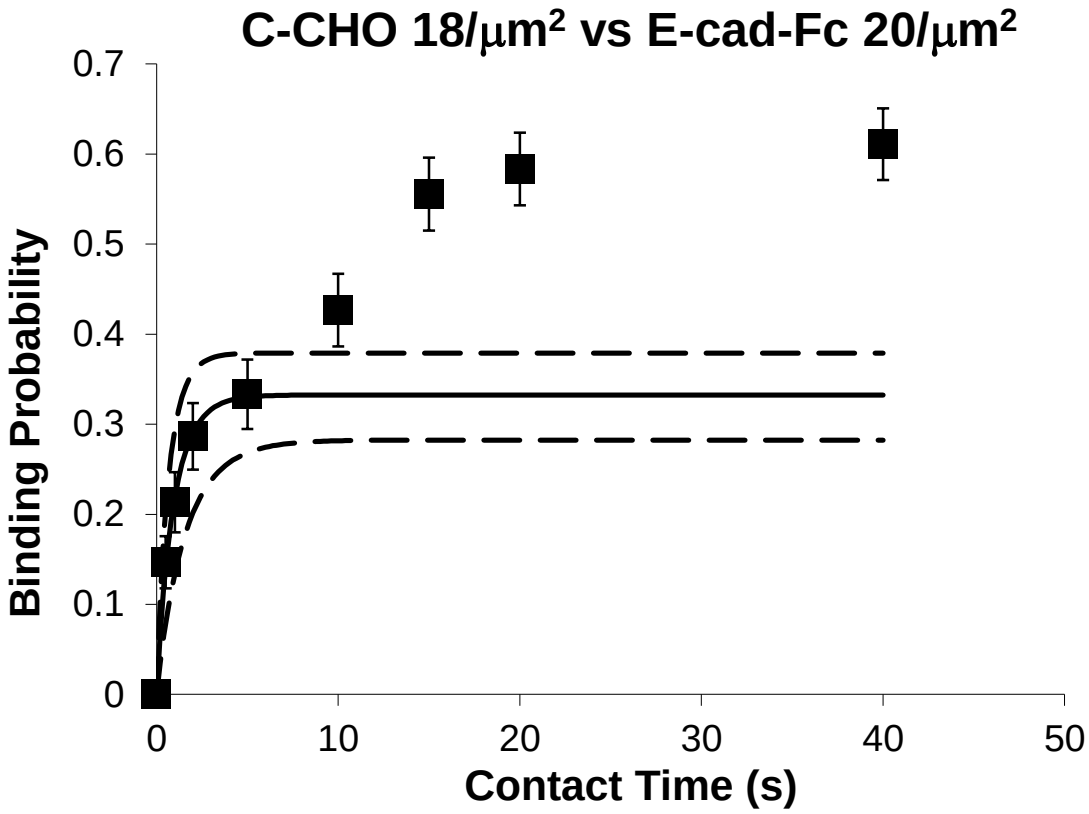
C-CHO 18/μm² vs E-cad-Fc 20/μm²
Binding Probability
0.7
0.6
0.5
0.4
0.3
0.2
0.1
0
0
10
20
30
40
50
Contact Time (s)

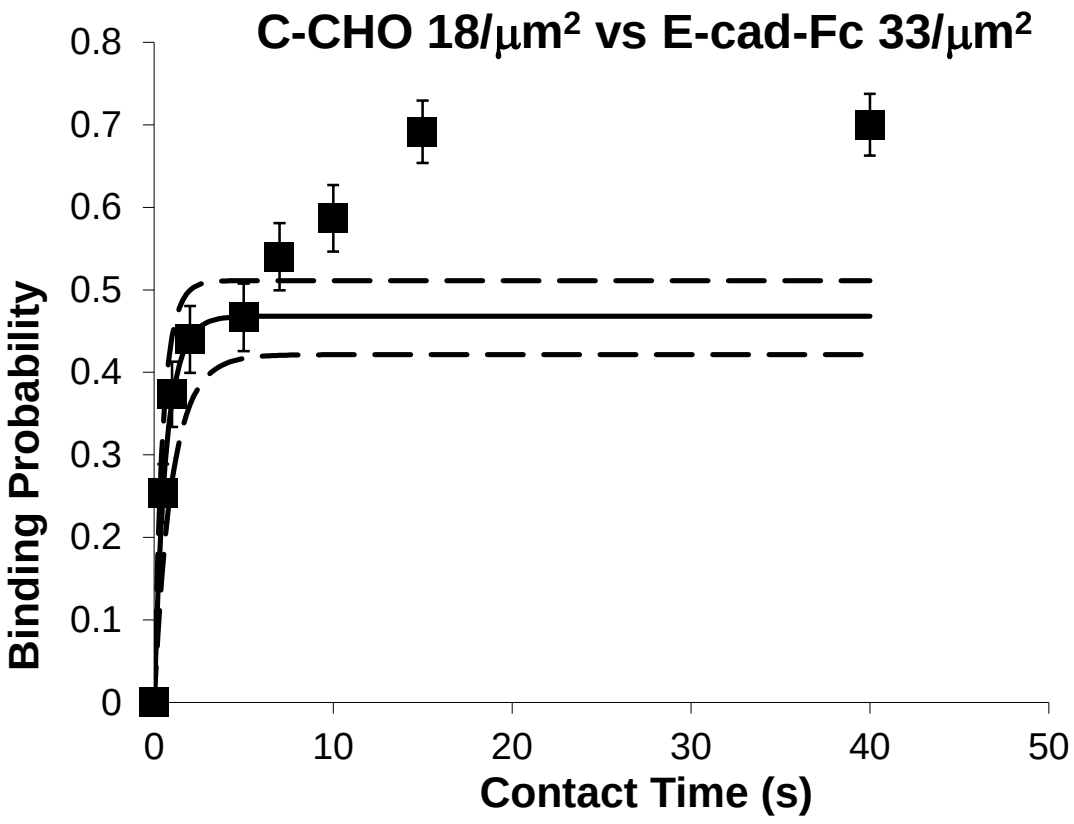
C-CHO 18/μm² vs E-cad-Fc 33/μm²
Binding Probability
0.8
0.7
0.6
0.5
0.4
0.3
0.2
0.1
0
0
10
20
30
40
50
Contact Time (s)

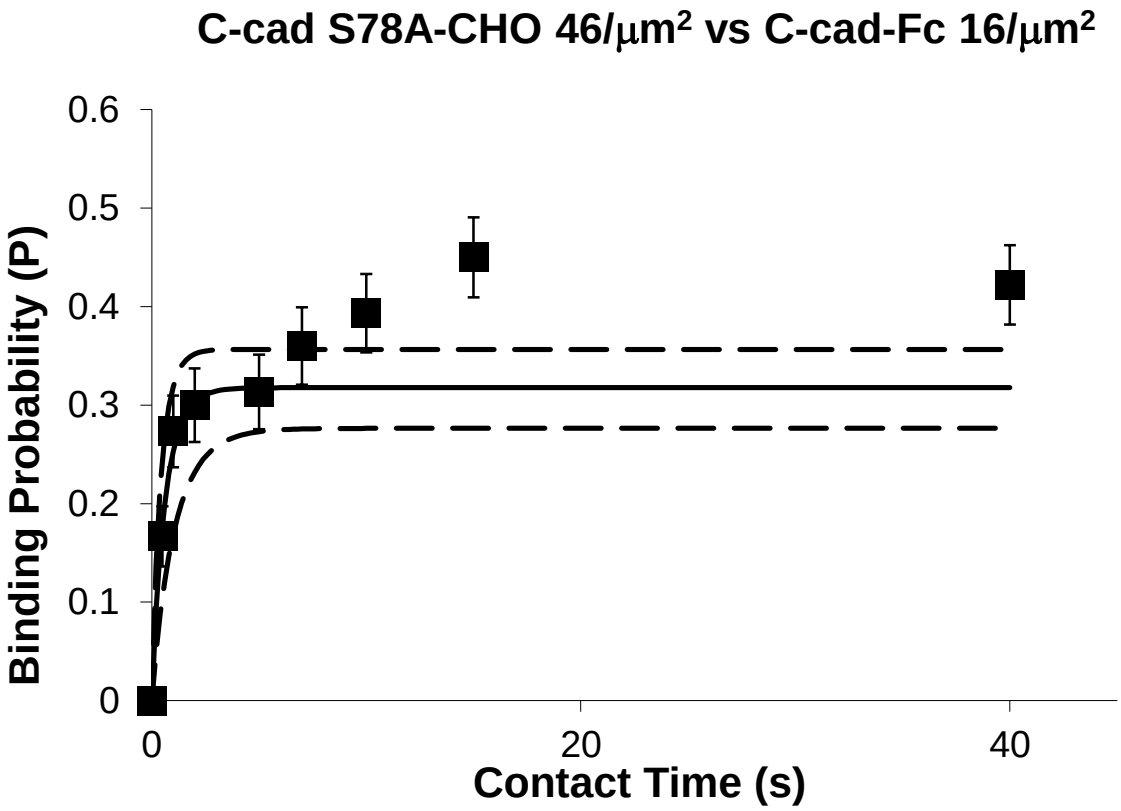
C-cad S78A-CHO 46/μm² vs C-cad-Fc 16/μm²
Binding Probability (P)
0.6
0.5
0.4
0.3
0.2
0.1
0
0
20
40
Contact Time (s)

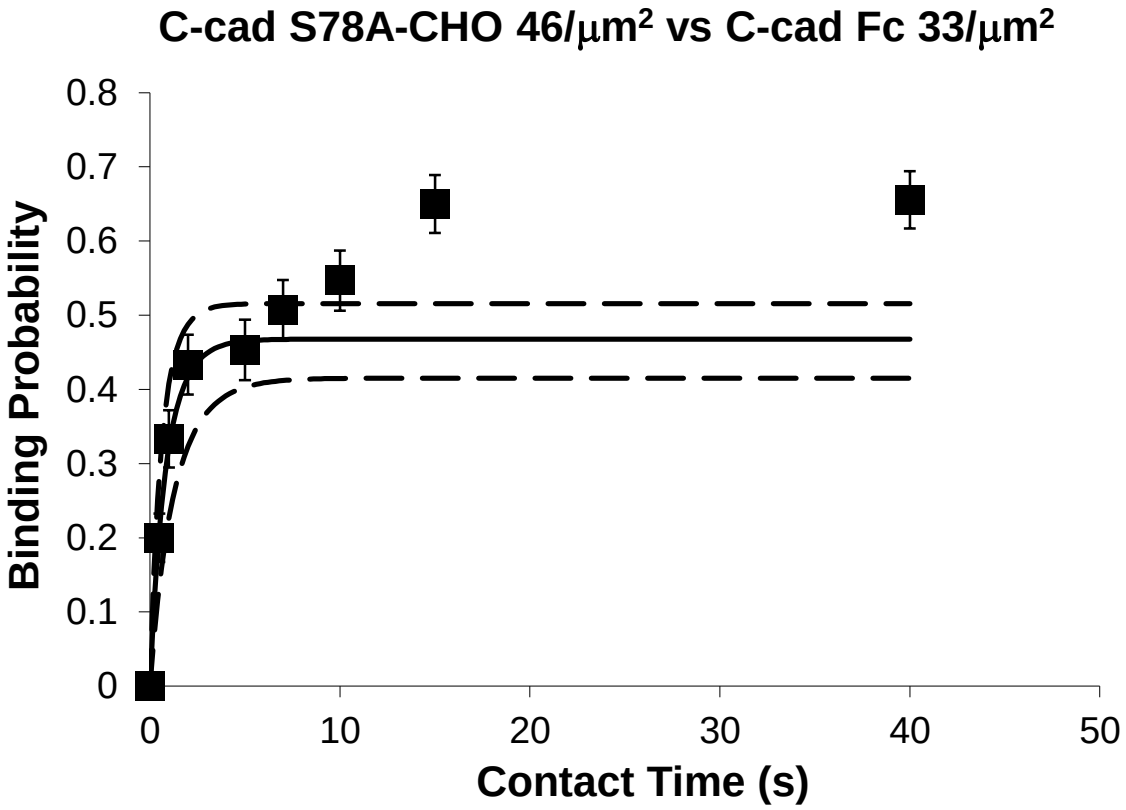
C-cad S78A-CHO 46/μm² vs C-cad Fc 33/μm²
Binding Probability
0.8
0.7
0.6
0.5
0.4
0.3
0.2
0.1
0
0
10
20
30
40
50
Contact Time (s)

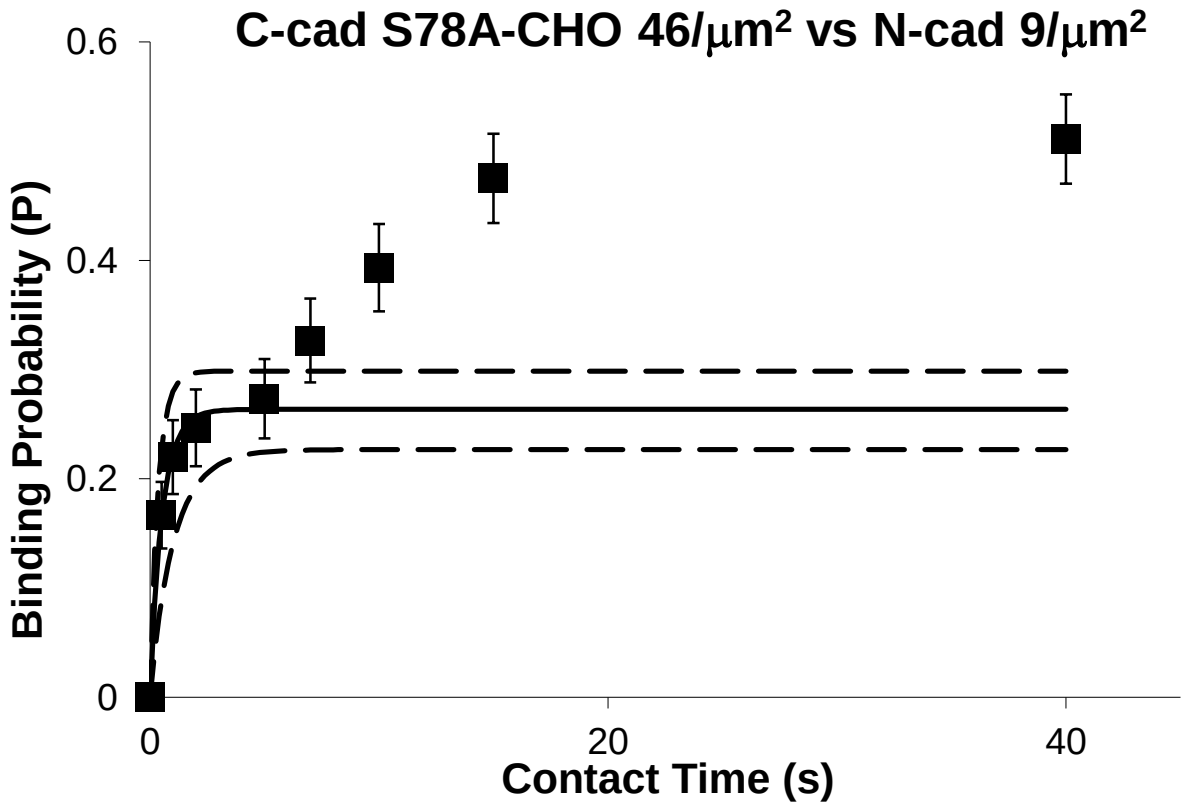
C-cad S78A-CHO 46/μm² vs N-cad 9/μm²
Binding Probability (P)
0.6
0.4
0.2
0
0
20
40
Contact Time (s)

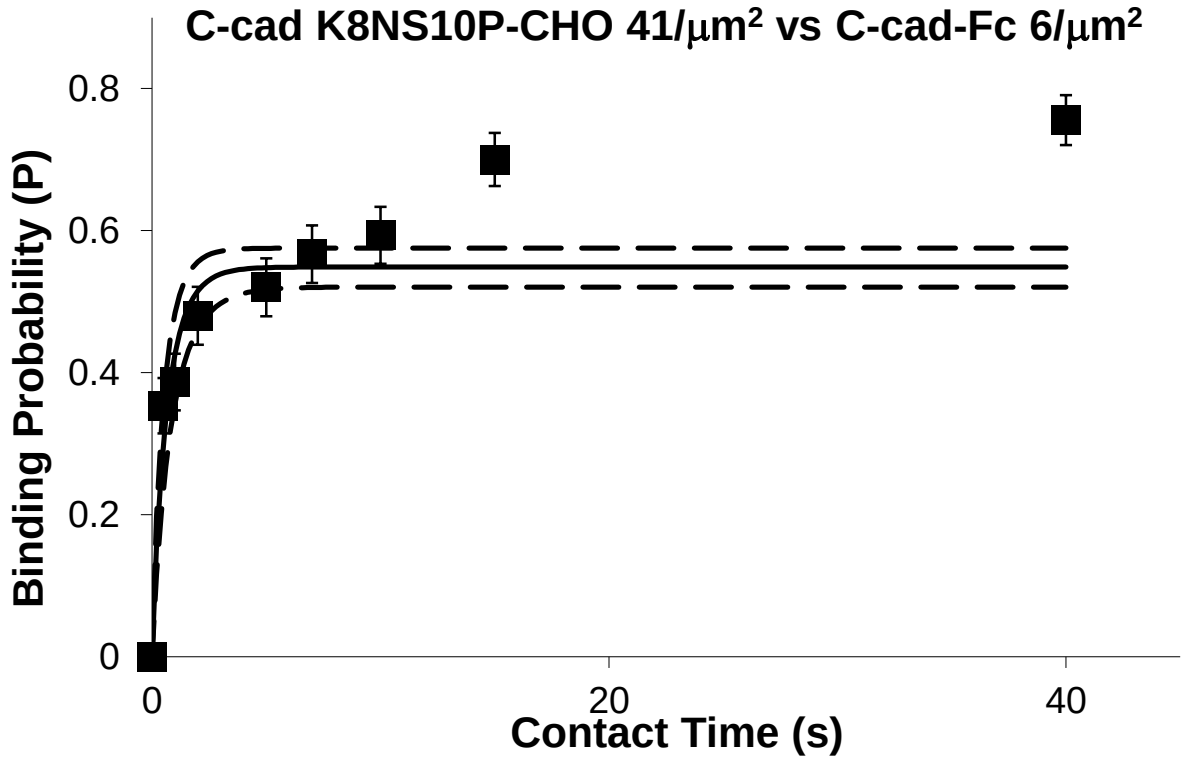
C-cad K8NS10P-CHO 41/μm² vs C-cad-Fc 6/μm²
Binding Probability (P)
0.8
0.6
0.4
0.2
0
0
20
40
Contact Time (s)

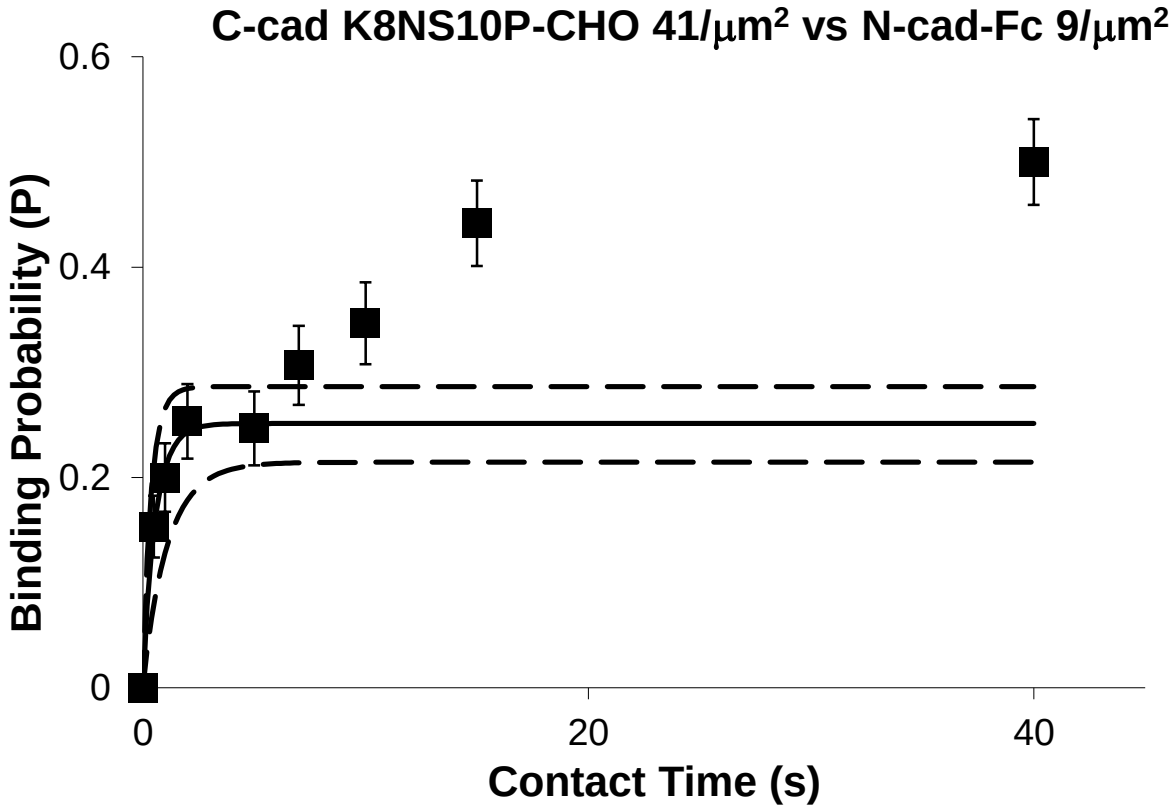
C-cad K8NS10P-CHO 41/μm² vs N-cad-Fc 9/μm²
Binding Probability (P)
0.6
0.4
0.2
0
0
20
40
Contact Time (s)

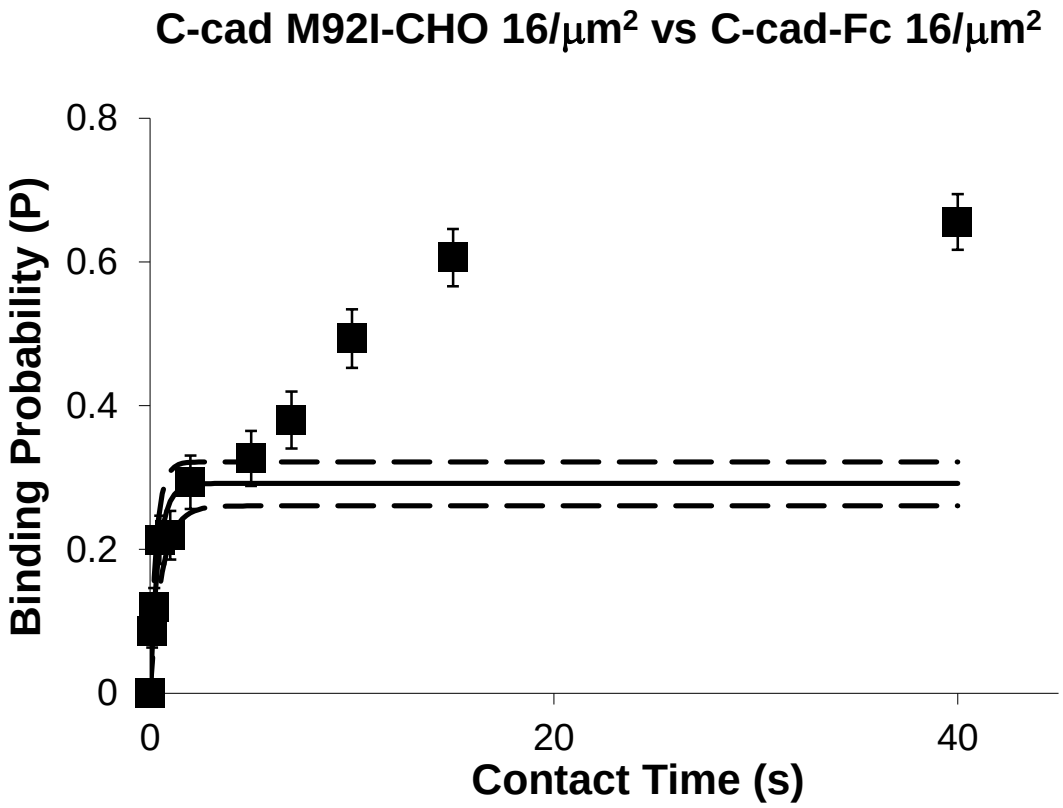
C-cad M92I-CHO 16/μm² vs C-cad-Fc 16/μm²
Binding Probability (P)
0.8
0.6
0.4
0.2
0
0
20
40
Contact Time (s)

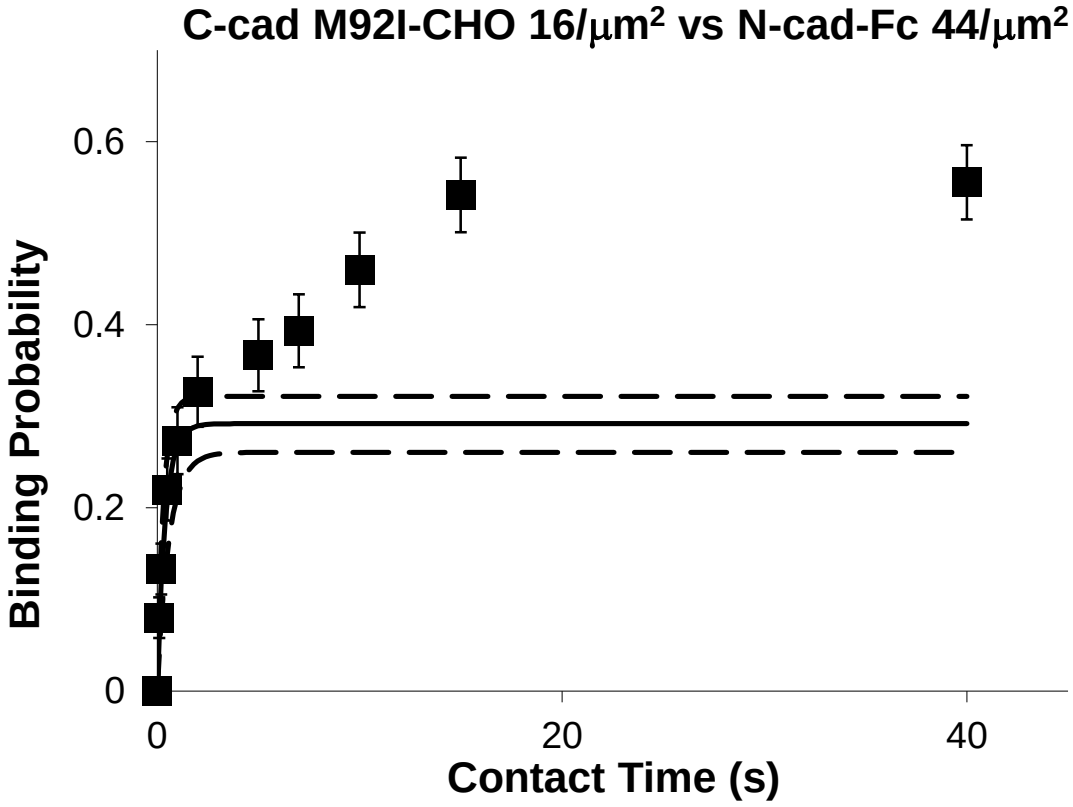
C-cad M92I-CHO 16/μm² vs N-cad-Fc 44/μm²
Binding Probability
0.6
0.4
0.2
0
0
20
40
Contact Time (s)

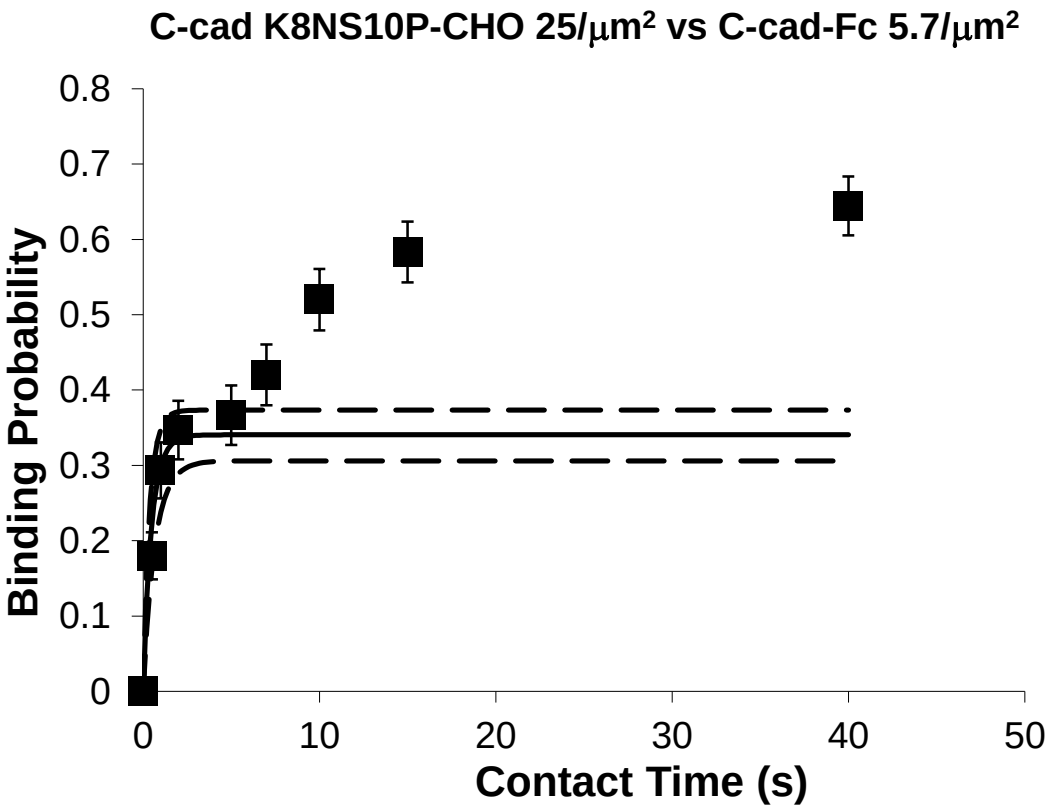
C-cad K8NS10P-CHO 25/μm² vs C-cad-Fc 5.7/μm²
Binding Probability
0.8
0.7
0.6
0.5
0.4
0.3
0.2
0.1
0
0
10
20
30
40
50
Contact Time (s)

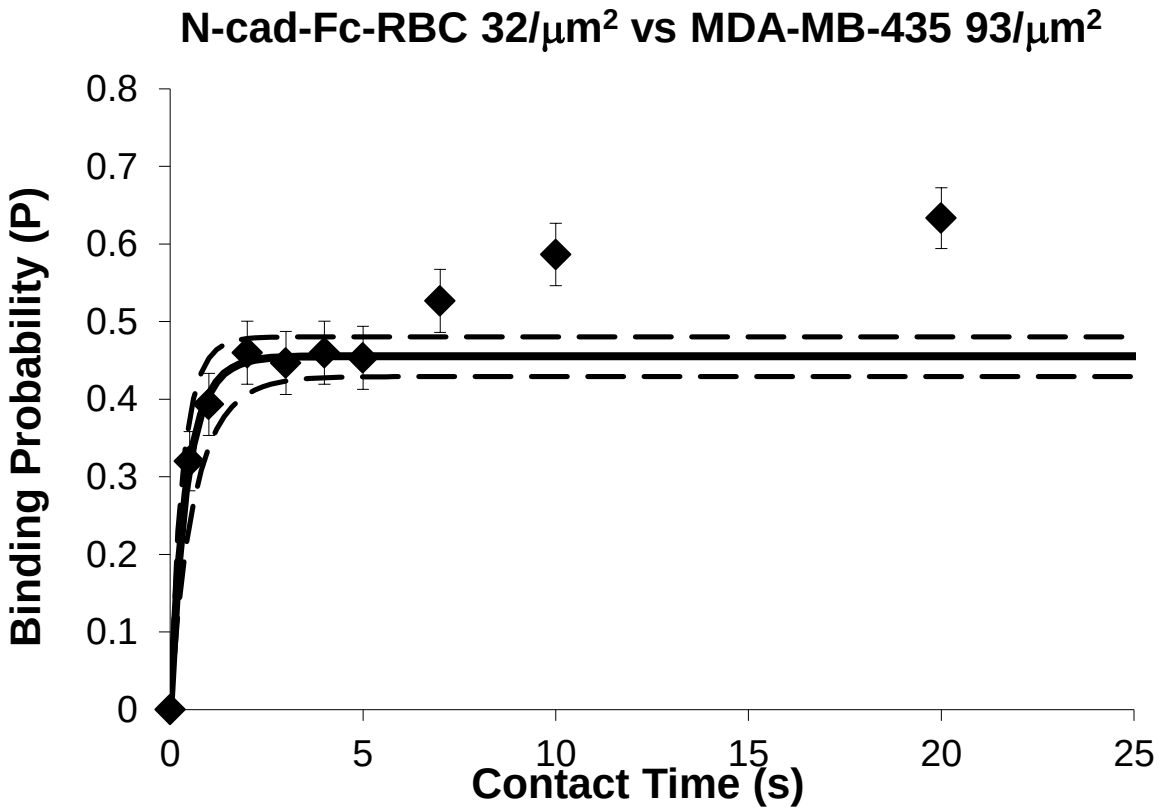
N-cad-Fc-RBC 32/μm² vs MDA-MB-435 93/μm²
Binding Probability (P)
0.8
0.7
0.6
0.5
0.4
0.3
0.2
0.1
0
0
5
10
15
20
25
Contact Time (s)

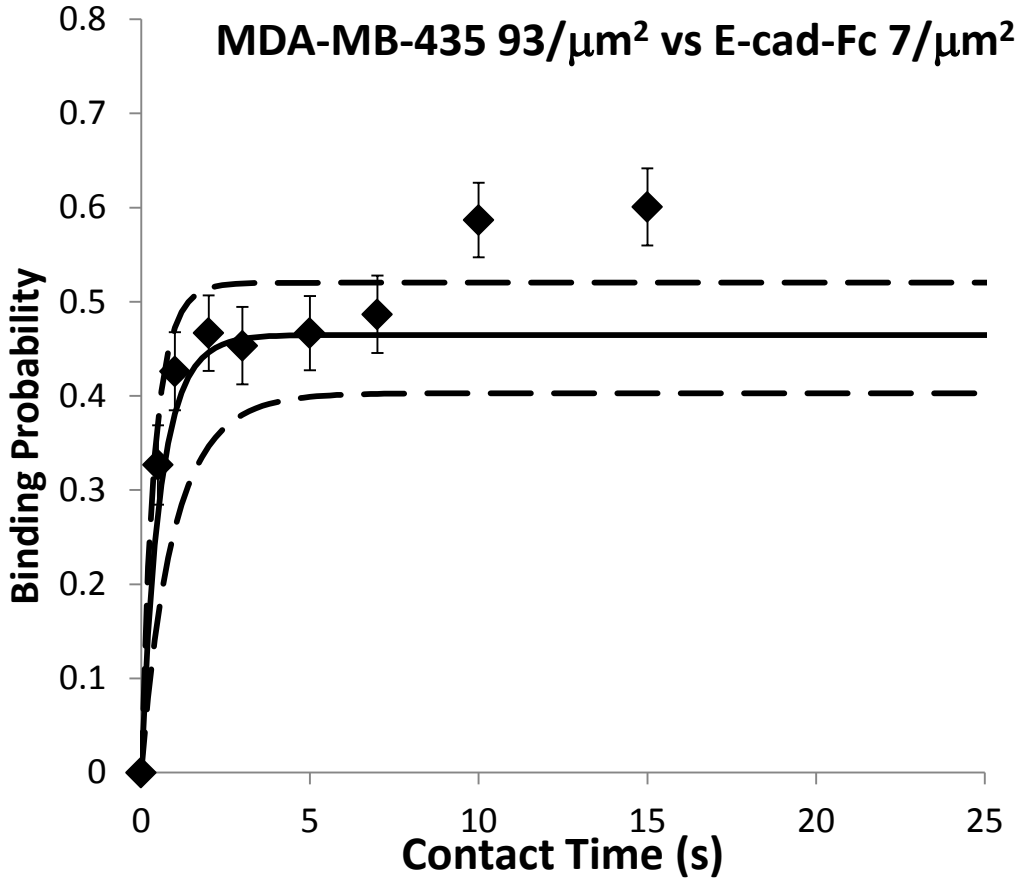
MDA-MB-435 93/μm² vs E-cad-Fc 7/μm²
Binding Probability
0.8
0.7
0.6
0.5
0.4
0.3
0.2
0.1
0
0
5
10
15
20
25
Contact Time (s)

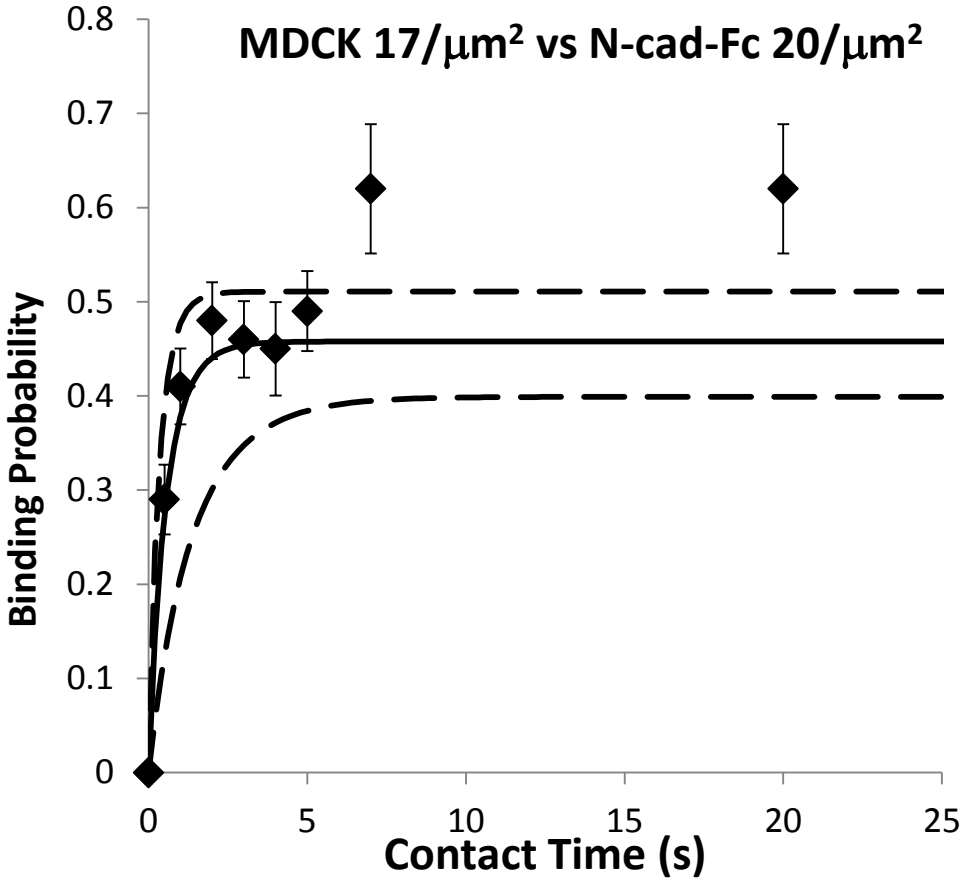
MDCK 17/μm² vs N-cad-Fc 20/μm²
Binding Probability
0.8
0.7
0.6
0.5
0.4
0.3
0.2
0.1
0
0
5
10
15
20
25
Contact Time (s)

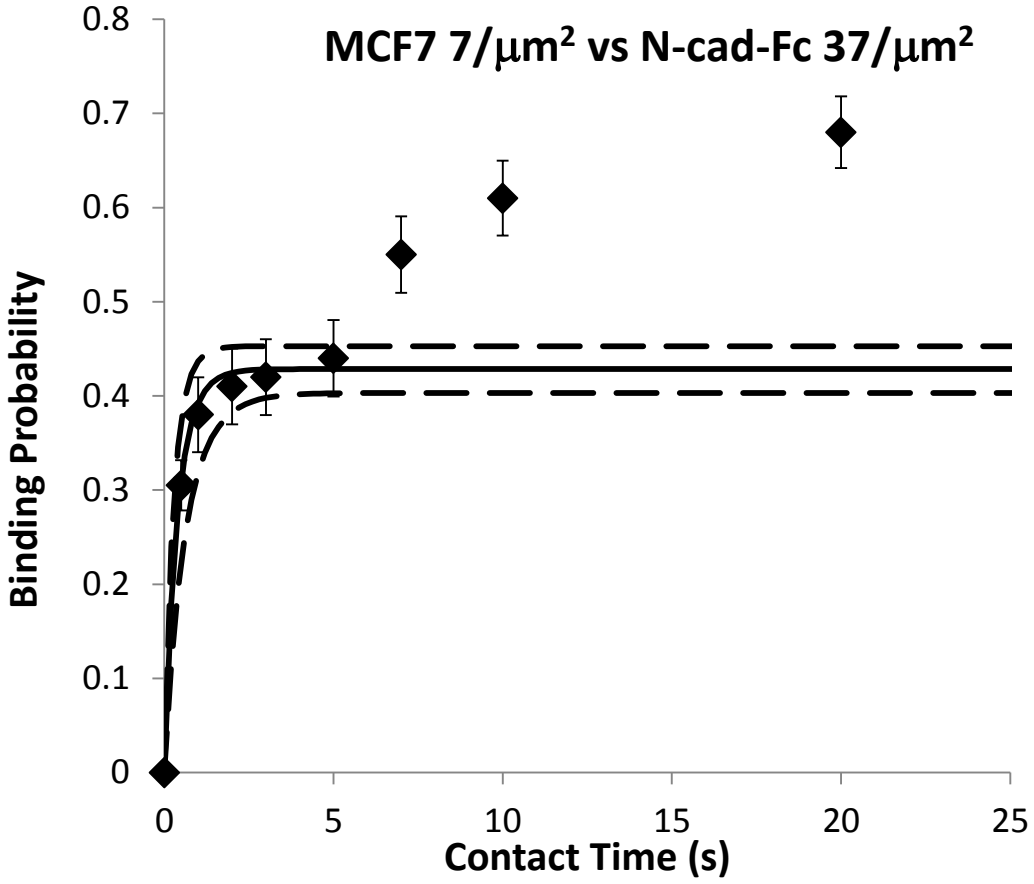
MCF7 7/μm² vs N-cad-Fc 37/μm²
Binding Probability
0.8
0.7
0.6
0.5
0.4
0.3
0.2
0.1
0
0
5
10
15
20
25
Contact Time (s)

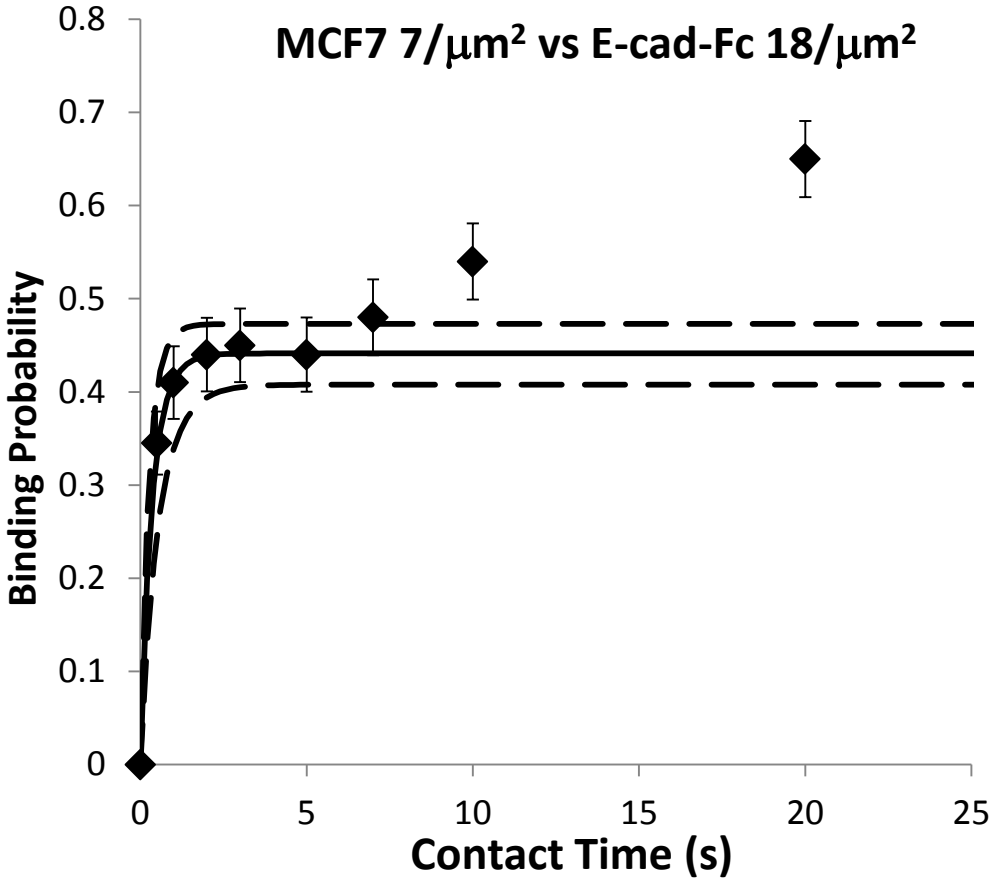
MCF7 7/μm² vs E-cad-Fc 18/μm²
Binding Probability
0.8
0.7
0.6
0.5
0.4
0.3
0.2
0.1
0
0
5
10
15
20
25
Contact Time (s)

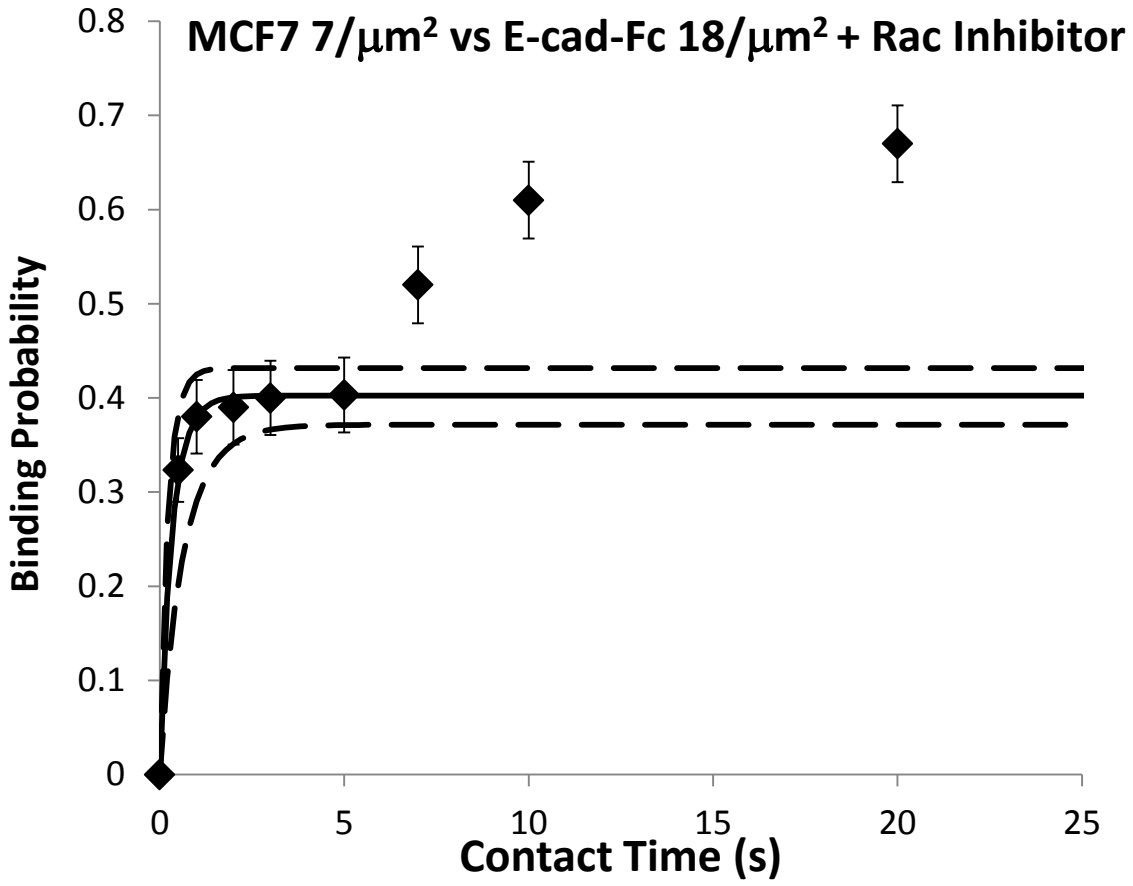
MCF7 7/μm² vs E-cad-Fc 18/μm² + Rac Inhibitor
Binding Probability
0.8
0.7
0.6
0.5
0.4
0.3
0.2
0.1
0
0
5
10
15
20
25
Contact Time (s)

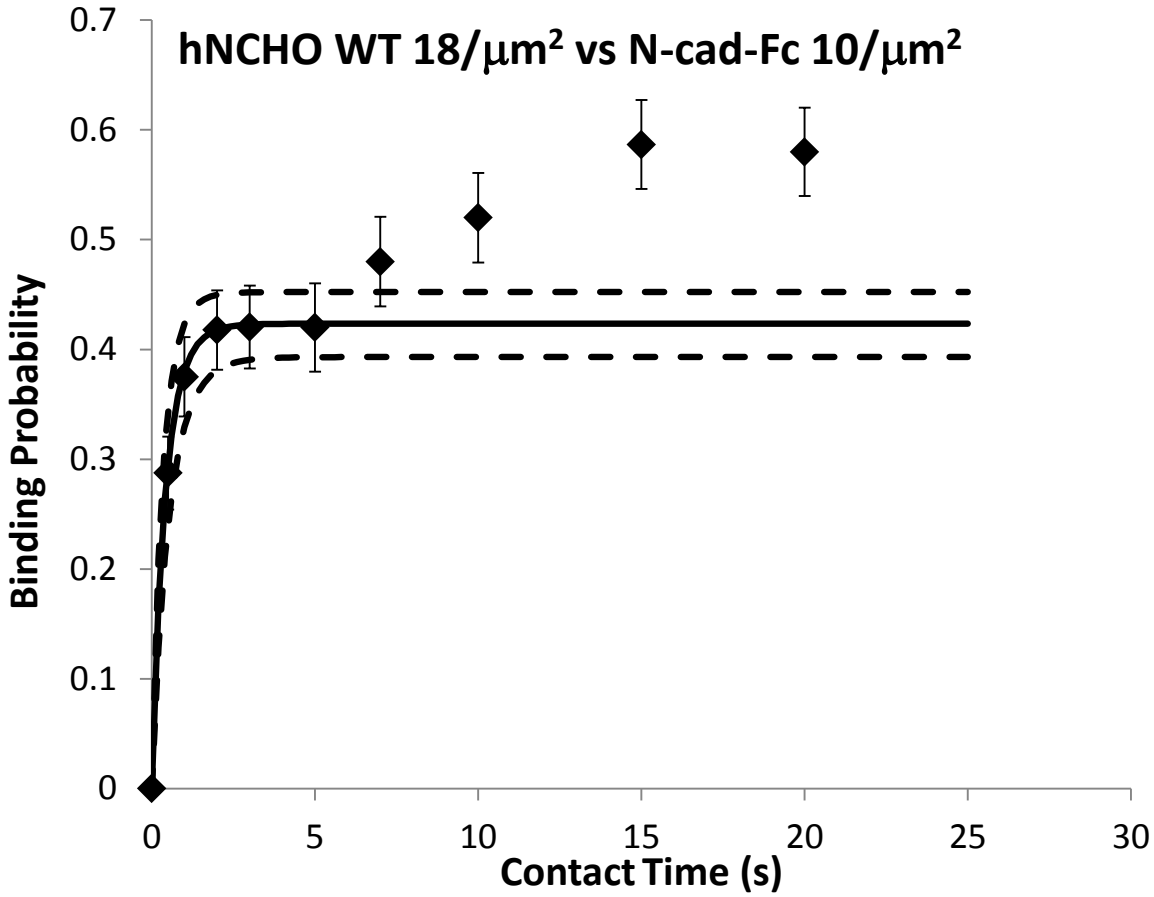
hNCHO WT 18/μm² vs N-cad-Fc 10/μm²
Binding Probability
0.7
0.6
0.5
0.4
0.3
0.2
0.1
0
0
5
10
15
20
25
30
Contact Time (s)

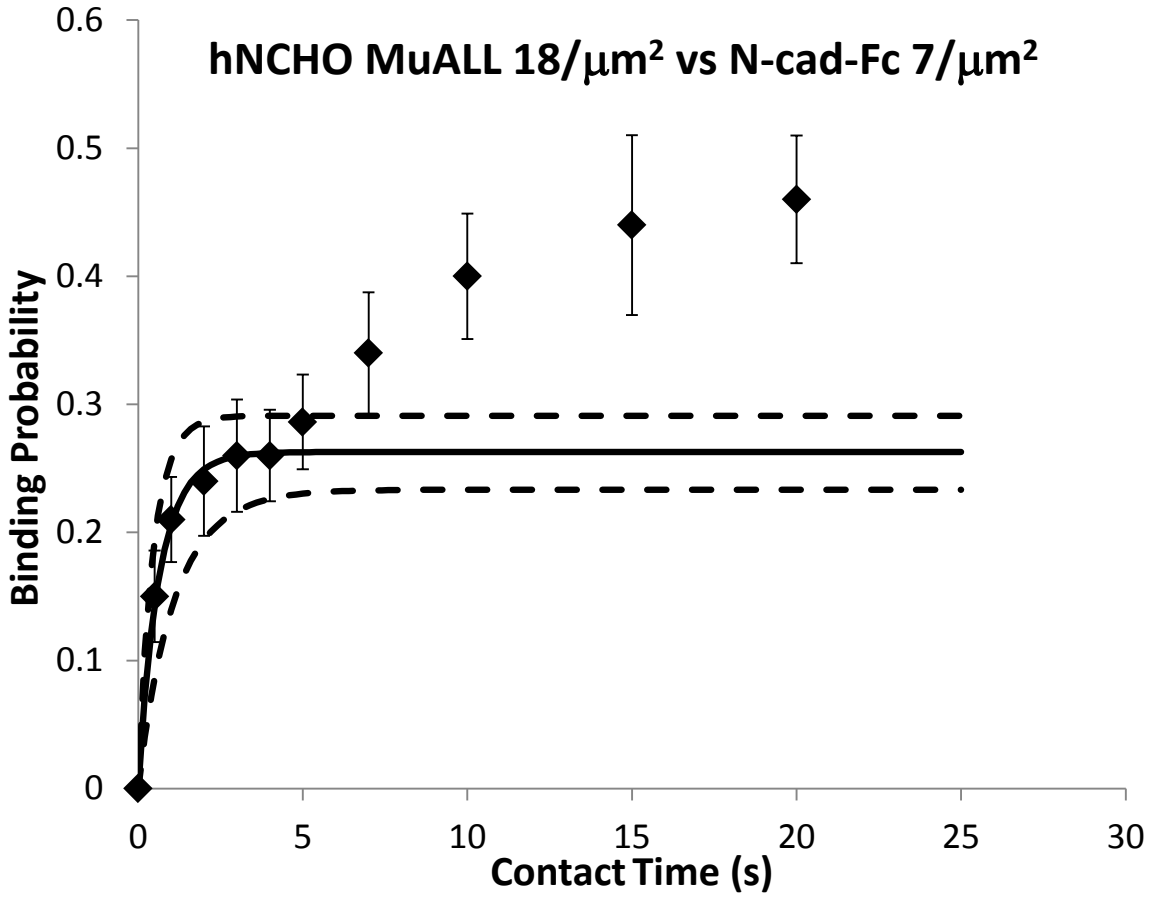
hNCHO MuALL 18/μm² vs N-cad-Fc 7/μm²
Binding Probability
0.6
0.5
0.4
0.3
0.2
0.1
0
0
5
10
15
20
25
30
Contact Time (s)

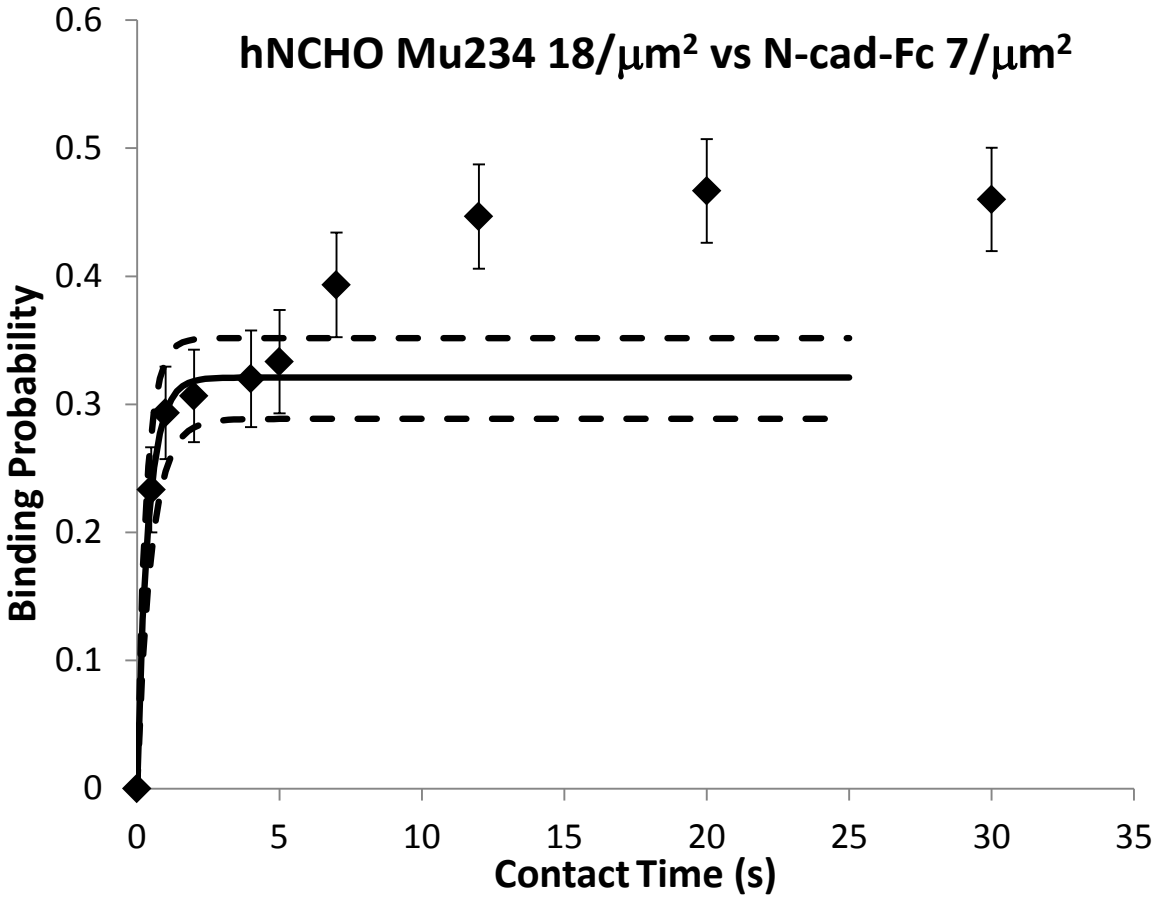
hNCHO Mu234 18/μm² vs N-cad-Fc 7/μm²
Binding Probability
0.6
0.5
0.4
0.3
0.2
0.1
0
0
5
10
15
20
25
30
35
Contact Time (s)

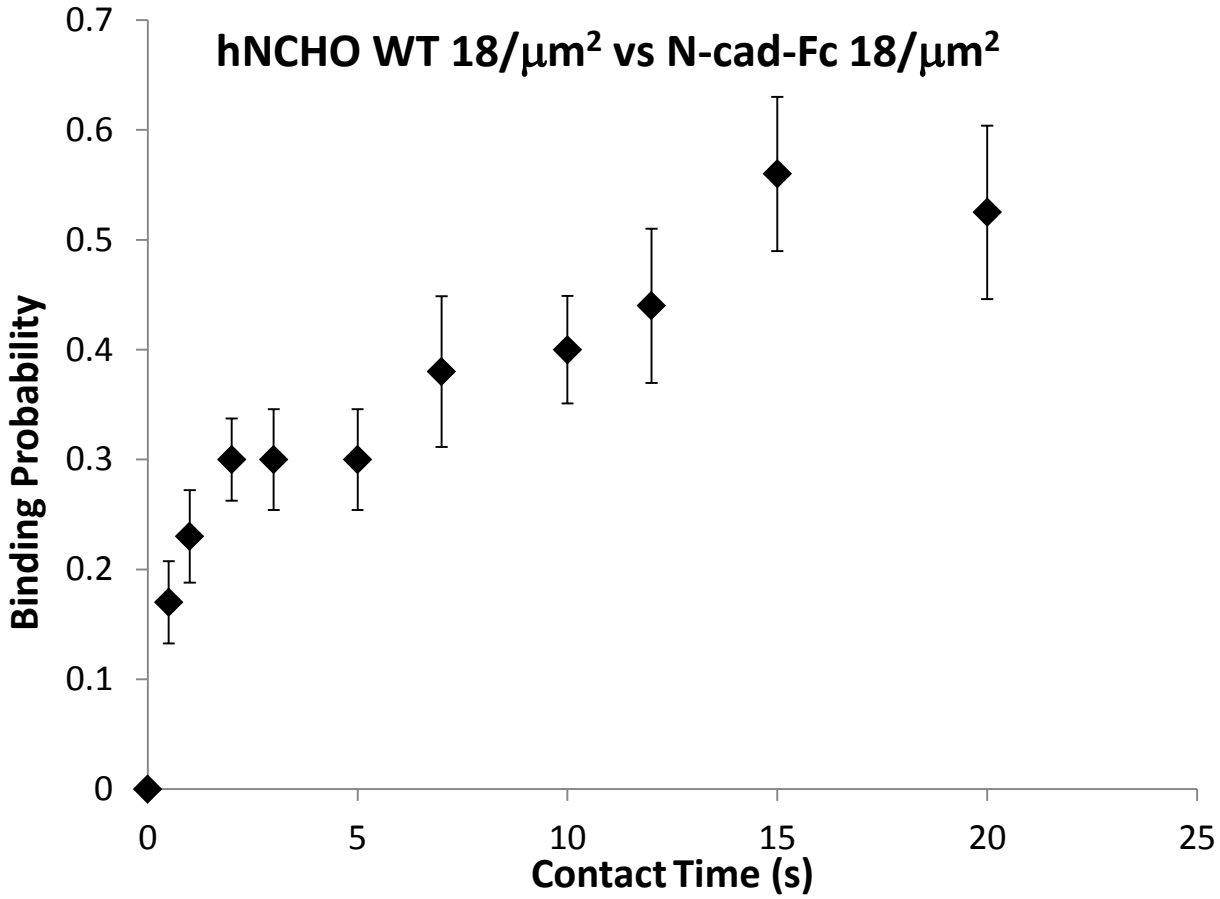
hNCHO WT 18/μm² vs N-cad-Fc 18/μm²
Binding Probability
0.7
0.6
0.5
0.4
0.3
0.2
0.1
0
0
5
10
15
20
25
Contact Time (s)

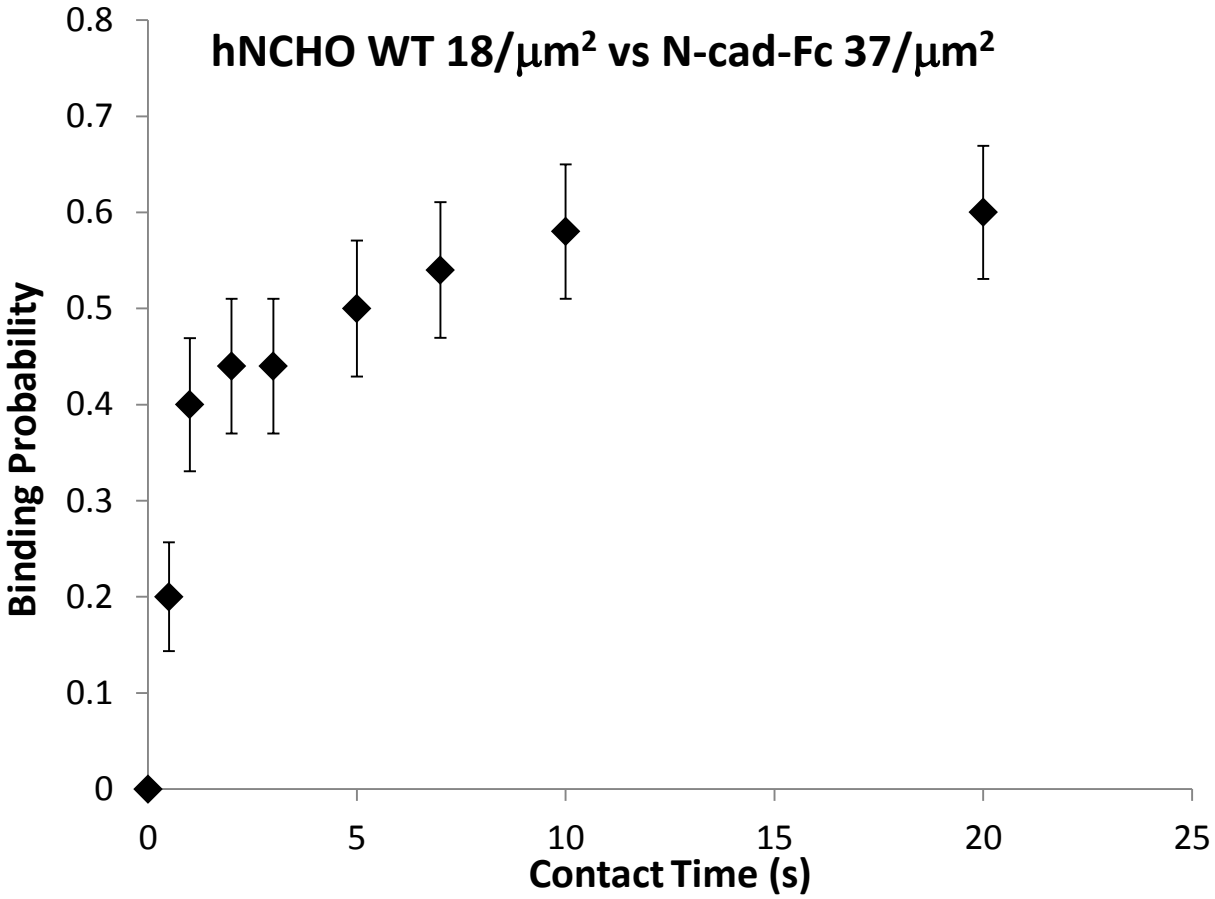
hNCHO WT 18/μm² vs N-cad-Fc 37/μm²
Binding Probability
0.8
0.7
0.6
0.5
0.4
0.3
0.2
0.1
0
0
5
10
15
20
25
Contact Time (s)

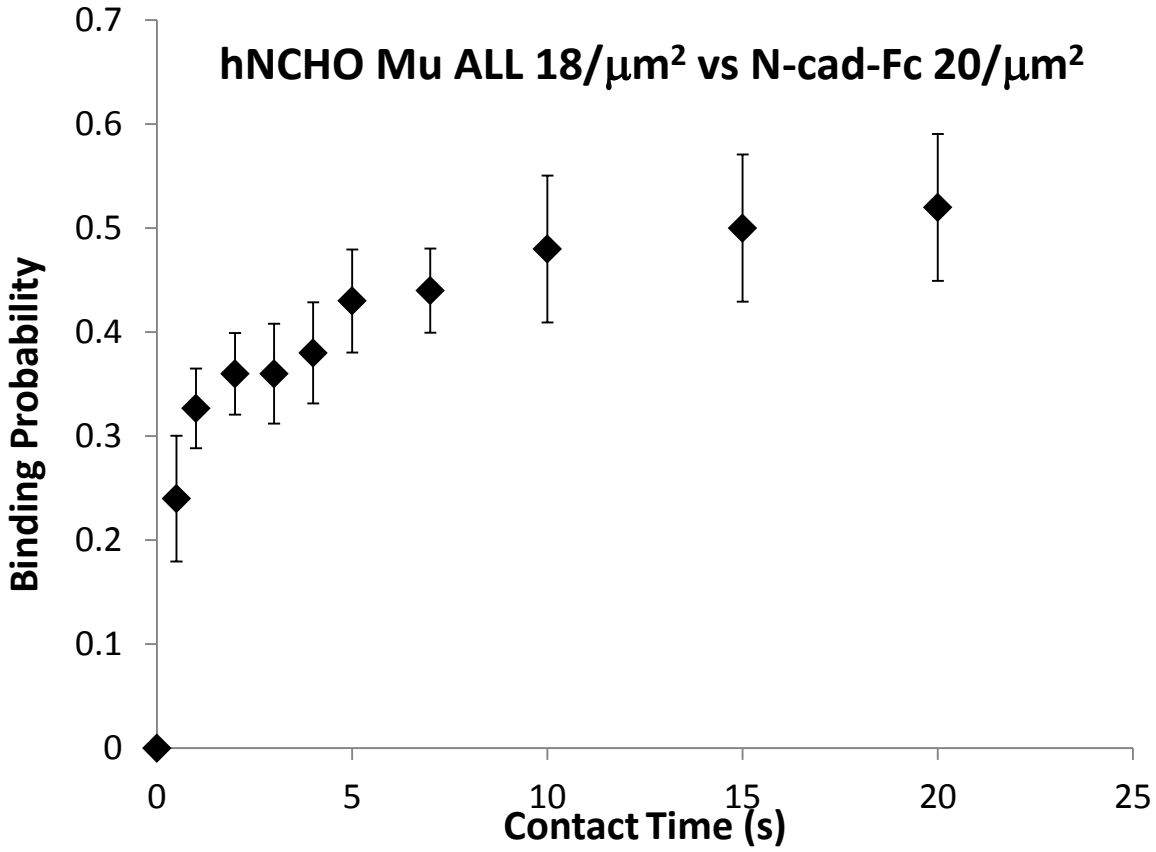
hNCHO Mu ALL 18/μm² vs N-cad-Fc 20/μm²
Binding Probability
0.7
0.6
0.5
0.4
0.3
0.2
0.1
0
0
5
10
15
20
25
Contact Time (s)

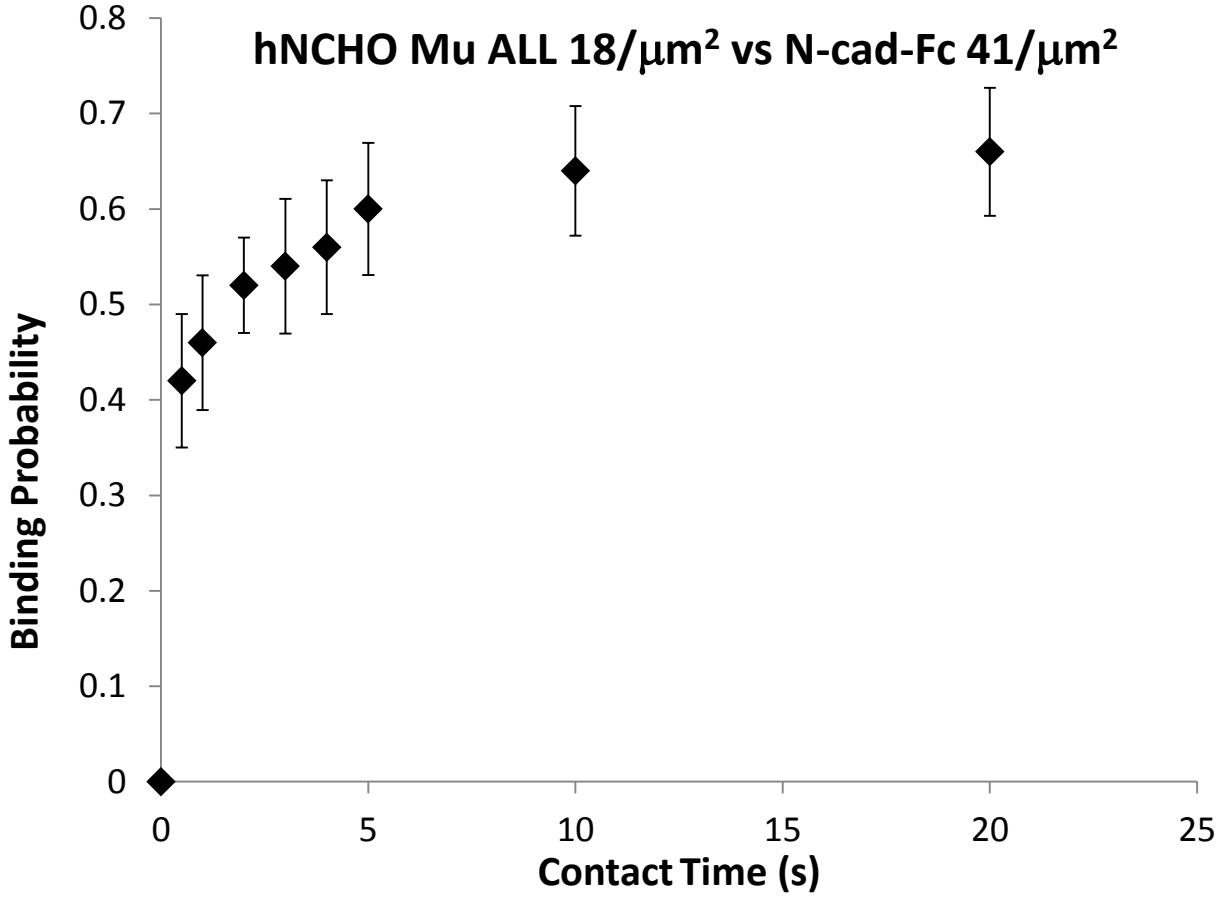
hNCHO Mu ALL 18/μm² vs N-cad-Fc 41/μm²
Binding Probability
0.8
0.7
0.6
0.5
0.4
0.3
0.2
0.1
0
0
5
10
15
20
25
Contact Time (s)

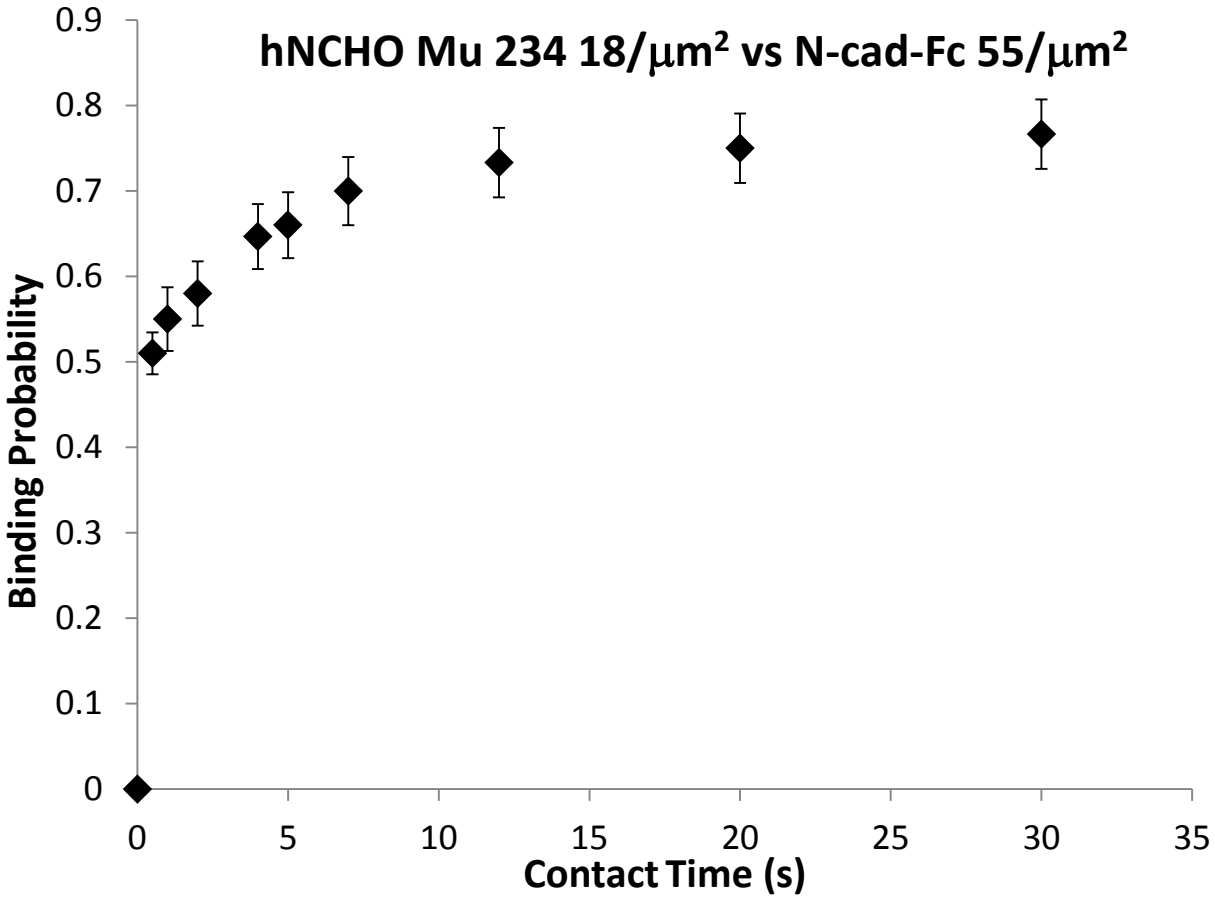
hNCHO Mu 234 18/μm² vs N-cad-Fc 55/μm²
Binding Probability
0.9
0.8
0.7
0.6
0.5
0.4
0.3
0.2
0.1
0
0
5
10
15
20
25
30
35
Contact Time (s)

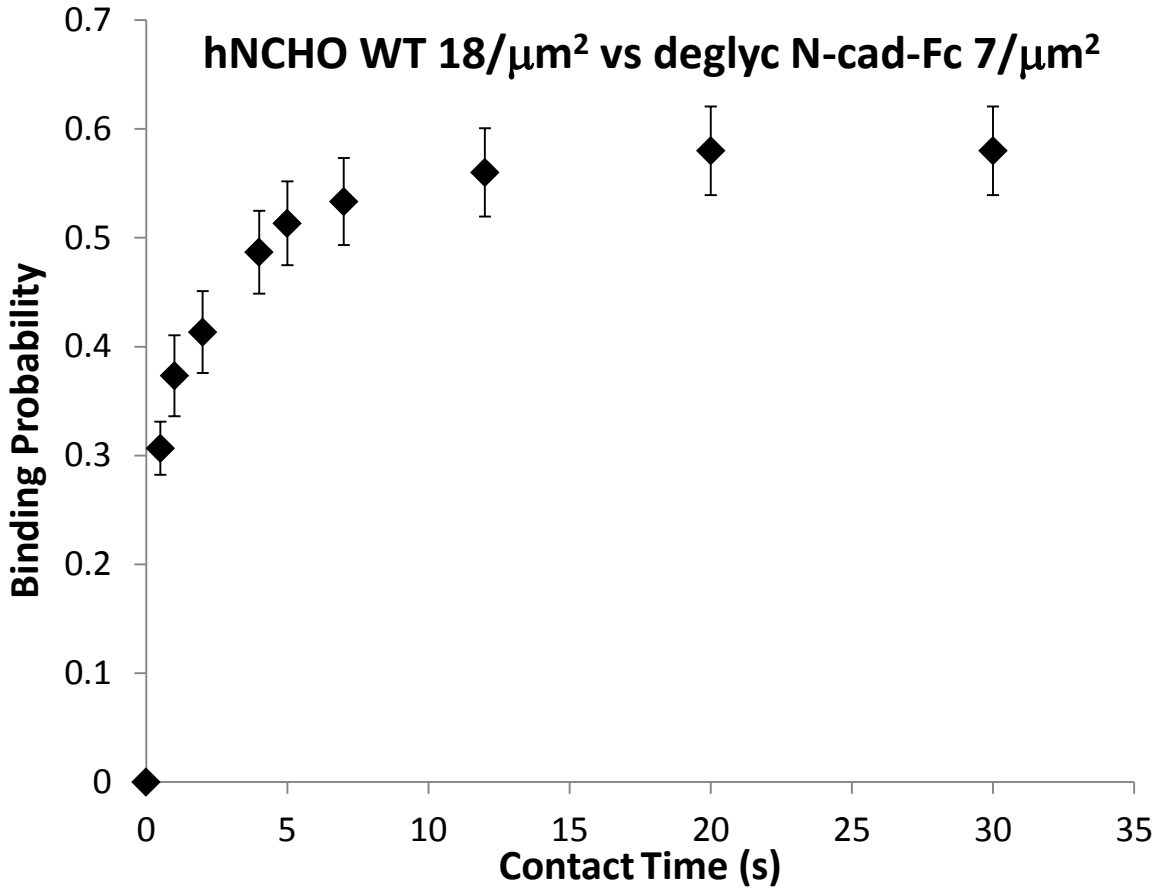
hNCHO WT 18/μm² vs deglyc N-cad-Fc 7/μm²
Binding Probability
0.7
0.6
0.5
0.4
0.3
0.2
0.1
0
0
5
10
15
20
25
30
35
Contact Time (s)

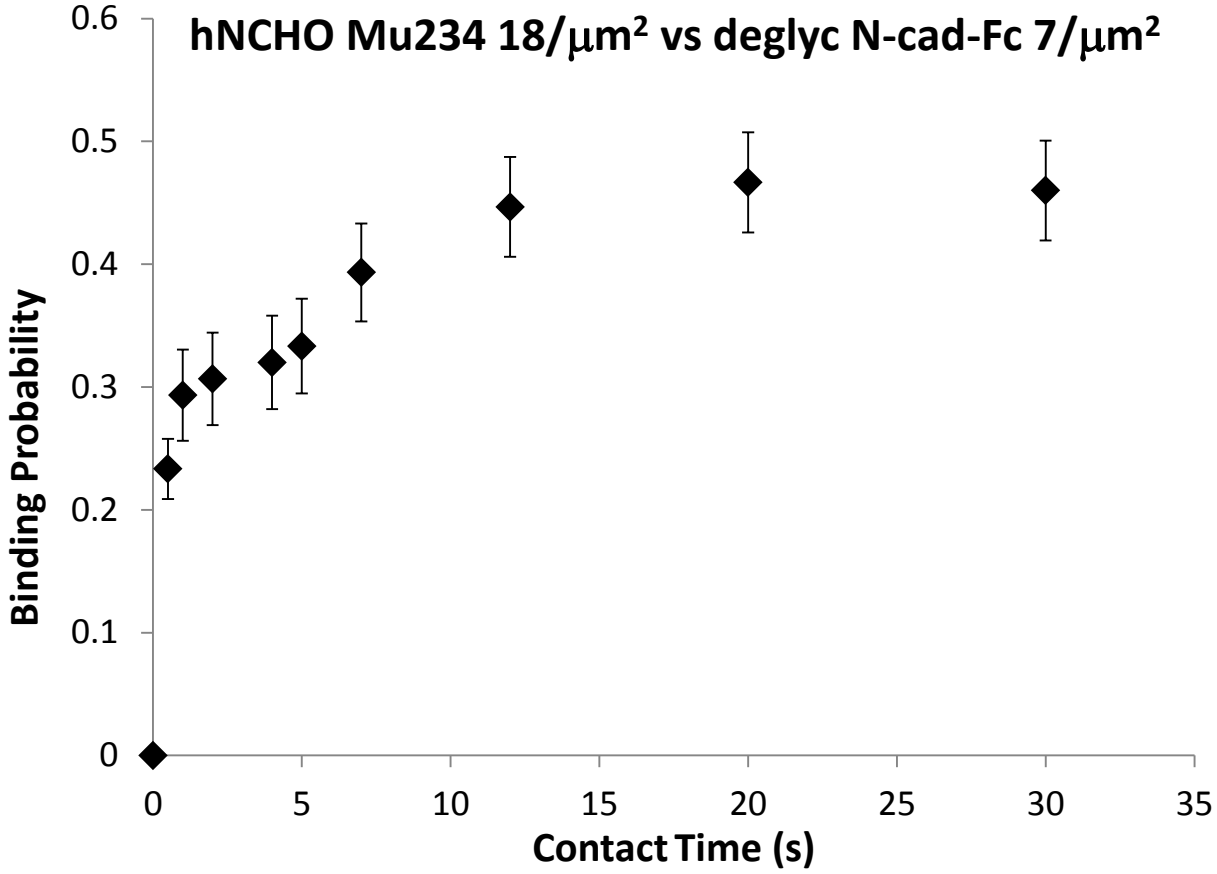
hNCHO Mu234 18/μm² vs deglyc N-cad-Fc 7/μm²
Binding Probability
0.6
0.5
0.4
0.3
0.2
0.1
0
0
5
10
15
20
25
30
35
Contact Time (s)

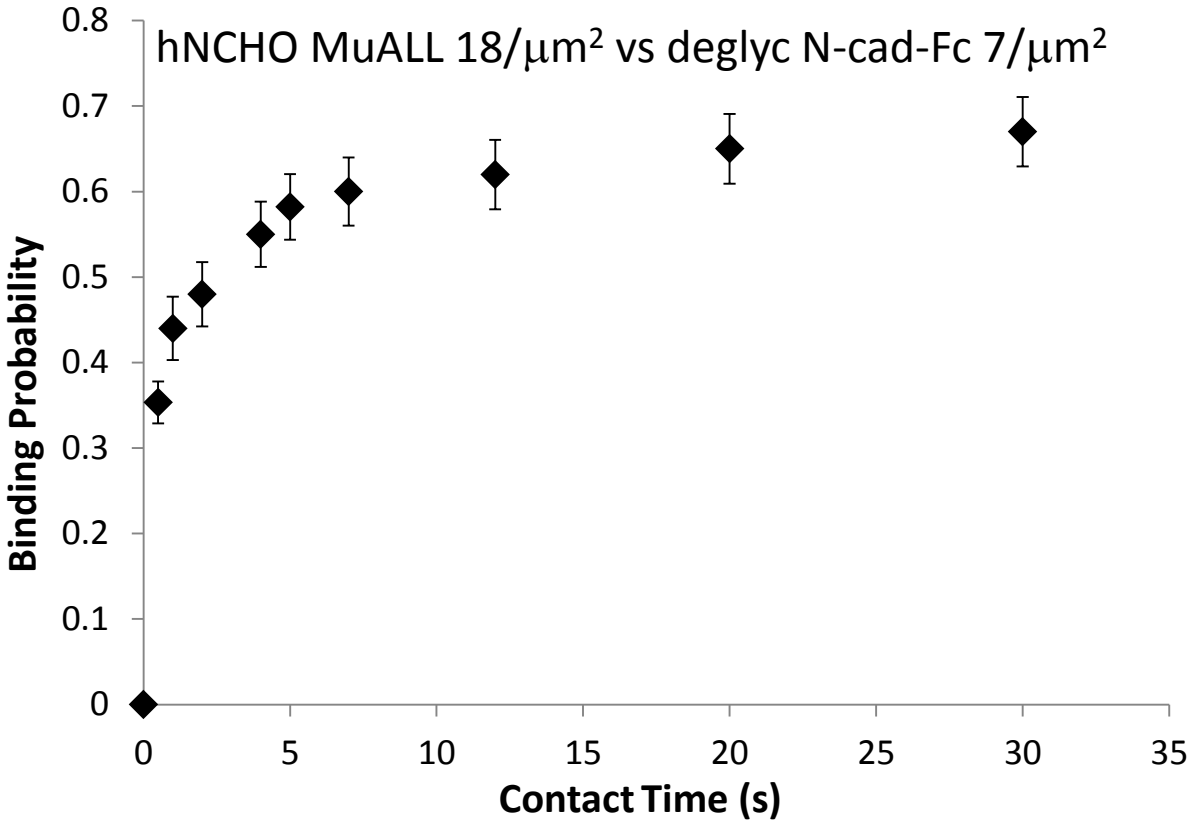
hNCHO MuALL 18/μm² vs deglyc N-cad-Fc 7/μm²
Binding Probability
0.8
0.7
0.6
0.5
0.4
0.3
0.2
0.1
0
0
5
10
15
20
25
30
35
Contact Time (s)

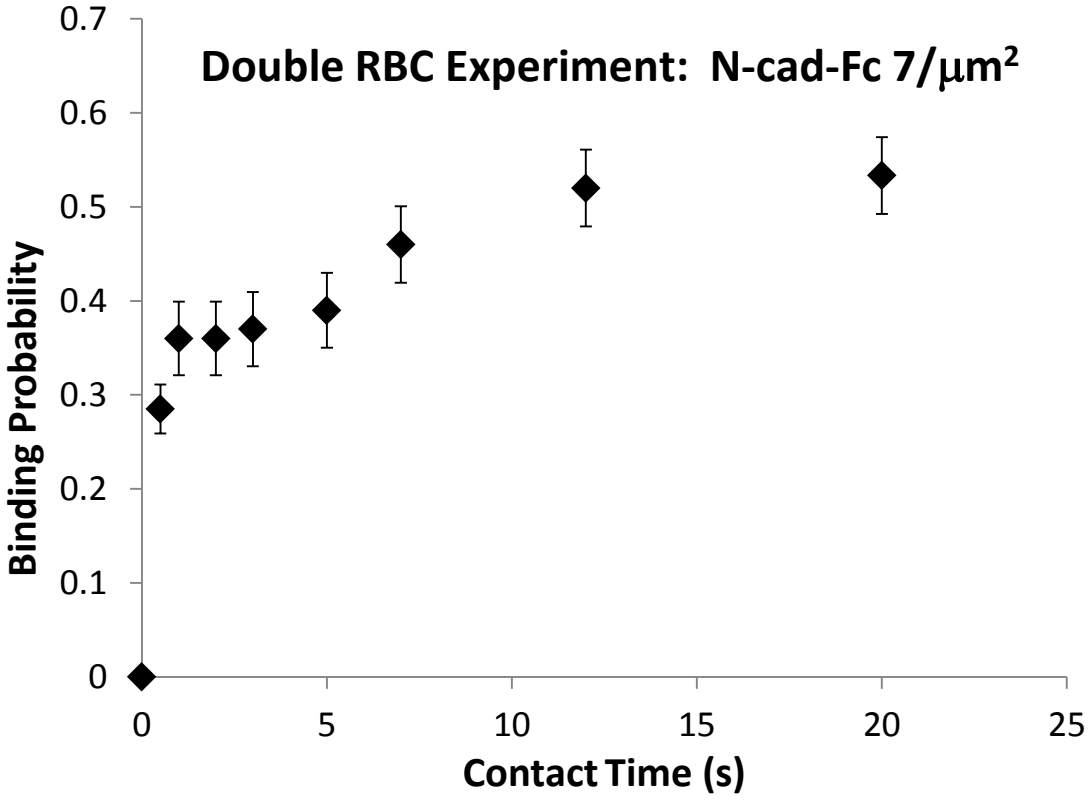
Double RBC Experiment: N-cad-Fc 7/μm²
Binding Probability
0.7
0.6
0.5
0.4
0.3
0.2
0.1
0
0
5
10
15
20
25
Contact Time (s)

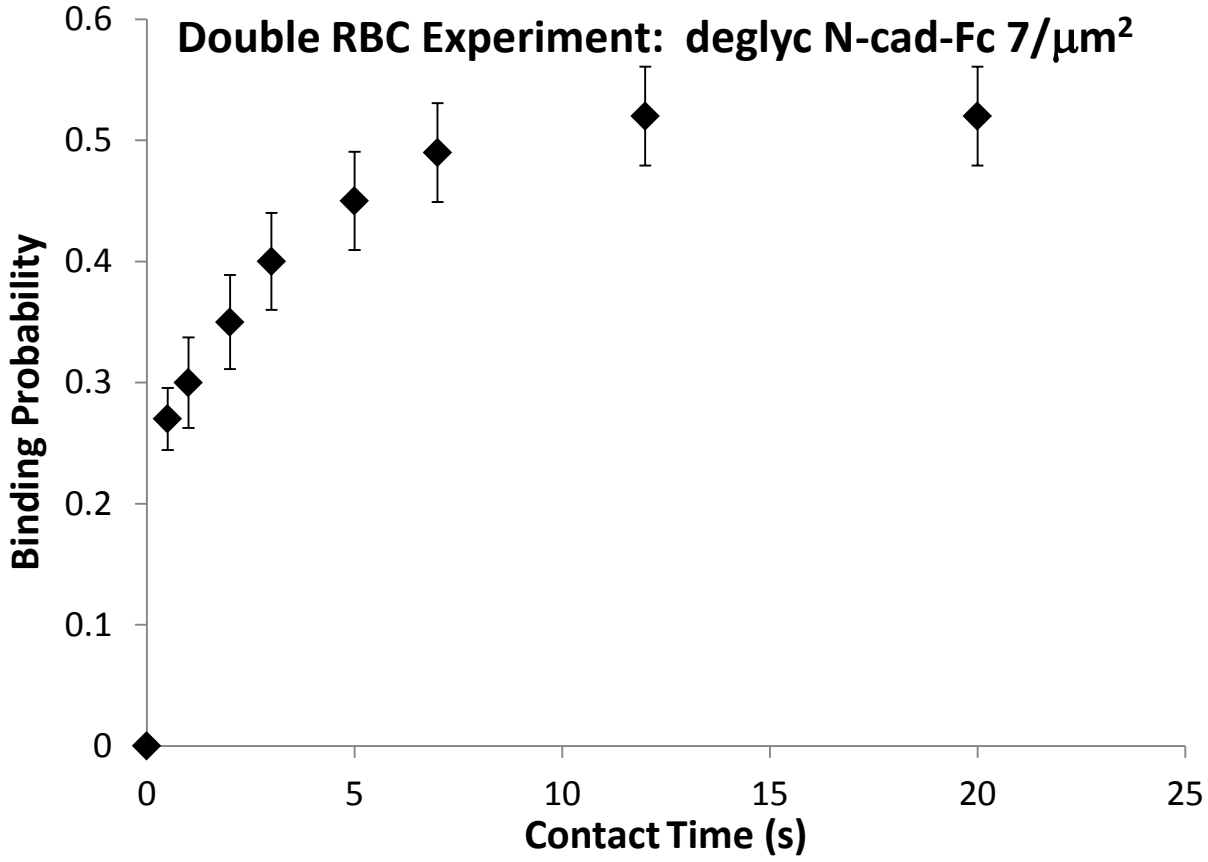
Double RBC Experiment: deglyc N-cad-Fc 7/μm²
Binding Probability
0.6
0.5
0.4
0.3
0.2
0.1
0
0
5
10
15
20
25
Contact Time (s)

Table A.1 Kinetic Parameters for Fits

Cell Protein	Protein on CHO Cell Density (μm^{-2})	RBC Protein	Protein on RBC Density (μm^{-2})	Ka (x 10^{-4} μm^2)	koff (1/s)
*N-cadherin	15	N-cadherin-Fc	69	1.9±0.3	1.1±0.4
*N-cadherin	17	N-cadherin-Fc	178	1.3±0.2	1.0±0.3
*N-cadherin	15	N-cadherin-Fc	33	2.8±0.5	1.1±0.4
*C-cadherin	18	C-cadherin-Fc	10	11±2	0.6±0.2
*C-cadherin	18	C-cadherin-Fc	20	8.0±0.9	0.5±0.1
*E-cadherin	16	E-cadherin-Fc	14	4±1	0.7±0.3
*E-cadherin	16	E-cadherin-Fc	57	3.0±0.4	1.0±0.3
*E-cadherin	16	E-cadherin-Fc	44	3.3±0.5	1.0±0.3
*N-cadherin,1	15	C-cadherin-Fc	103	1.9±0.2	0.4±0.1
*N-cadherin,1	15	C-cadherin-Fc	49	1.9±0.2	0.7±0.2
*N-cadherin,1	15	C-cadherin-Fc	221	1.0±0.2	0.6±0.2
*N-cadherin,1	15	C-cadherin-Fc	19	3.2±0.7	0.8±0.4
C-cadherin,1	14	N-cadherin-Fc	38	3.5±0.2	1.3±0.3
*N-cadherin	16	E-cadherin-Fc	49	2.8±0.3	1.9±0.7
*N-cadherin	16	E-cadherin-Fc	33	2.6±0.4	1.2±0.5
*C-cadherin	18	E-cadherin-Fc	20	3.5±0.6	0.9±0.4
*C-cadherin	18	E-cadherin-Fc	33	3.3±0.5	1.3±0.4
*C-cadherin S78A	46	C-cadherin-Fc	16	1.7±0.3	1.4±0.6
*C-cadherin S78A	46	C-cadherin-Fc	33	1.3±0.2	1.0±0.3
*C-cadherin S78A	46	N-cadherin-Fc	9	2.3±0.4	1.7±0.8
*C-cadherin K8NS10P	41	C-cadherin-Fc	6	10.3±0.8	1.2±0.3
*C-cadherin K8NS10P	41	N-cadherin-Fc	9	2.5±0.4	1.6±0.8
*C-cadherin M92I	16	C-cadherin-Fc	16	4.2±0.5	2.3±0.7
*C-cadherin M92I	16	N-cadherin-Fc	44	1.9±0.2	1.9±0.6
*C-cadherin K8NS10P	25	C-cadherin-Fc	5.7	10.4±0.2	1.2±0.5
E-CHO	16	E-cadherin-Fc	14	3.86±0.97	0.69±0.34
N-CHO	16	E-cadherin-Fc	33	2.64±0.41	1.21±0.47
MDA-MB-435	93	N-cadherin-Fc	32	0.7±0.06	1.93±0.29
MDA-MB-435	93	E-cadherin-Fc	7	1.2±0.2	1.46±0.28
MDCK	17	E-cadherin-Fc	7	3.6±0.2	1.65±0.30
MDCK	17	N-cadherin-Fc	20	2.5±0.2	1.49±0.42
MCF7	7	E-cadherin-Fc	18	4.2 ± 0.2	2.4±0.4
MCF7	7	N-cadherin-Fc	37	2.7±0.1	2.2±0.4
MCF7(-Rac)	7	E-cadherin-Fc	18	4.3 ± 0.2	2.6±0.6
hN-CHO WT	18	N-cadherin-Fc	10	4.2 ± 0.4	2.0 ± 0.5
hN-CHO MuALL	18	N-cadherin-Fc	7	4.0 ± 0.5	1.4 ± 0.6
hN-CHO Mu234	18	N-cadherin-Fc	7	4.3 ± 0.4	2.2 ± 0.5

* Experiment Performed by Yuan-Hung Chien